Closed-Loop Control of HCCI Engine Dynamics

Bengtsson, Johan

2004

Document Version:
Publisher's PDF, also known as Version of record

Closed-Loop Control of HCCI Engine Dynamics

Johan Bengtsson

Automatic Control

Closed-Loop Control of HCCI Engine Dynamics

Closed-Loop Control of HCCI Engine Dynamics

Johan Bengtsson

Department of Automatic Control
Lund Institute of Technology
Lund, November 2004

Department of Automatic Control
Lund Institute of Technology
Box 118
SE-221 00 LUND
Sweden

ISSN 0280–5316
ISRN LUTFD2/TFRT--1070--SE

Printed in Sweden by Media-Tryck.
Lund 2004

Acknowledgments

This thesis would not have been possible without the help from many people. It is therefore a great pleasure to have the opportunity to express my gratitude for all the help and support I have received during this work. First of all I would like to thank my advisor Rolf Johansson for his guidance and for many stimulating discussions. His enthusiasm and profound knowledge of numerous disciplines together with generous sharing of time has contributed substantially to this thesis. I am also profoundly indebted to my other co-workers and co authors, especially Petter Strandh from the Division of Combustion Engines at Lund Institute of Technology, Lund University, which this work has been performed in collaboration. I would also like to thank Magnus Gäfvert for stimulating cooperation, and Per Tunestål and Bengt Johansson from the Division of Combustion Engines at Lund Institute of Technology, Lund University, colleagues in the GIHR project.

I would like to thank Mathias Haage, Tomas Olsson and Anders Robertsson and Klas Nilsson for all the work and fun we have had in Robotics Lab.

I would like to thank all the people who worked, or have worked, at the department during these five years. The nice atmosphere at the department is due to the staff and many thanks go out to all of them. I would like to thank my former roommate Bo Lincoln for valuable discussions during the years. Staffan Haugwitz have always had time for playing board games.

I would like to thank Matrin Kjaer and Karl-Erik Årzén for valuable comments on the manuscript.

This work have been performed as a part of the GIHR (Grön bIl HoRisontell) contract. I would like to thank VINNOVA, the Swedish Agency for Innovation System, Volvo Technical Corporation, Scania and Volvo Car which funded the work.

Finally, I would also like to thank family and friends for their encouragement and for fulfilling my life with good time.

Papers

This thesis is mainly based on the following papers, referred in the text by their Roman numerals, some material is updated, together with new introduced results.

I. Strandh, P., M. Christensen, J. Bengtsson, R. Johansson, A. Vressner, P. Tunestål, and B. Johansson: “Ion current sensing for HCCI combus-

tion feedback." SAE Technical Paper 2003-01-3216, 2003.

II. Bengtsson, J., P. Strandh, R. Johansson, P. Tunestål, and B. Johansson: "Closed-loop combustion control of homogeneous charge compression ignition (HCCI) engine dynamics." *International Journal of Adaptive Control and Signal Processing*, **18**, pp. 167–179, 2004.

III. Bengtsson, J., P. Strandh, R. Johansson, P. Tunestål, and B. Johansson: "Control of homogeneous charge compression ignition (HCCI) engine dynamics." In *Procedings of American Control Conference*, pp. 4048–4053, Boston, Massachusetts, 2004.

IV. Bengtsson, J., P. Strandh, R. Johansson, P. Tunestål, and B. Johansson: "System identification of homogenous charge compression ignition (HCCI) engine dynamics." In *IFAC Symp. Advances in Automotive Control (AAC04), Salerno, Italy, April 19-23, 2004*.

V. Strandh, P., J. Bengtsson, R. Johansson, P. Tunestål, and B. Johansson: "Cycle-to-cycle control of a dual-fuel HCCI engine." SAE Technical Paper 2004-01-0941, 2004

VI. Bengtsson, J., M. Gäfvert, and P. Strandh: "Modeling of HCCI engine combustion for control analysis." In *Conference in Decision and Control (CDC 2004)*, 2004.

VII. Bengtsson, J., P. Strandh, R. Johansson, P. Tunestål., and B. Johansson (2005): "Variable valve actuation for timing control of a homogeneous charge compression ignition engine." *draft submitted to SAE world Congress 2005*. Detroit, USA.

Other publications

Work that has not been included in this thesis but was performed during the Ph.D. studies

Adaptive Cruise Control

Bengtsson, J.: "Adaptive cruise control and driver modeling." Licentiate thesis ISRN LUTFD2/TFRT--3227--SE. Department of Automatic Control, Lund Institute of Technology, Lund, Sweden, 2001.

Bengtsson, J., R. Johansson, and A. Sjögren: "Modeling of driver's longitudinal behavior." In Johansson and Rantzer, Eds., *Nonlinear and Hybrid Systems in Automotive Control*, pp. 41–58. Springer Verlag, London, 2002.

Bengtsson, J., R. Johansson, and A. Sjögren: "Modeling of drivers longitudinal behavior." In *2001 IEEE/ASME International Conference on Advanced Intelligent Mechatronics (AIM'01)*, 2001. Como, Italy.

Visual servoing

Bengtsson, J., A. Ahlstrand, K. Nilsson, A. Robertsson, M. Olsson, A. Heyden, and R. Johansson: "A robot playing scrabble using visual feedback." In *6th Int. IFAC Symposium on Robot Control (SYROCO 2000)*. Vienna, Austria, 2000.

Bengtsson, J., M. Haage, and R. Johansson: "Variable time delays in visual servoing and task execution control." In *2nd IFAC Conference on Mechatronic Systems*. Berkeley, CA, 2002.

Olsson, T., J. Bengtsson, A. Robertsson, and R. Johansson: "Visual position tracking using dual quaternions with hand-eye motion constraints." In *IEEE Int. Conference on Robotics and Automation*, pp. 3491–3496. Taipei, Taiwan, 2003.

Olsson, T., J. Bengtsson, R. Johansson, and H. Malm: "Force control and visual servoing using planar surface identification." In *IEEE Int. Conference on Robotics and Automation*, pp. 4211–4216. Washington D.C., USA, 2002.

Other

Bengtsson, J. and S. Solyom: "ABS and anti-skid on a Lego car." Technical Report LUTFD2/TFRT --7609-- SE. Automatic Control, Lund Institute of Technology, Sweden, 2004.

Contents

Nomenclature

α	Combustion timing in crank angle after TDC	20
α_{50}	Crank angle where 50% of the energy has been released	21
α_{50}^{net}	Crank angle where 50% of the net energy has been released	76
α_{max}^{p}	Crank angle for the peak pressure	76
$\alpha_{max}^{p,c}$	Crank angle where pressure increase due to combustion has reached its maximum level	77
$\alpha_{50}^{p,c,v}$	Crank angle where pressure increase due to combustion has reached half its maximum level	77
α_{max}^{dQ}	Crank angle for the peak heat release rate	76
α_{50}^{MFB}	Crank angle where 50% of the charge has burned	78
α_{SOC}	Crank angle for Start Of Combustion	20
γ	Specific heat ratio, c_p/c_v	24
θ	Crank angle	
κ	Polytropic exponent in the relation pV^{κ} =constant	78
λ	Air/fuel ratio, relative to stoichiometric air/fuel ratio	183
CAD	Crank Angle Degree	20
CI	Compression Ignition	17
c_p	Specific heat at constant pressure	24
c_v	Specific heat at constant volume	23
CVA	Canonical Variable Algorithm	95
EGR	Exhaust Gas Recirculation	17
EVC	Exhaust Valve Closing	136
EVO	Exhaust Valve Opening	136
FTM	Fast Thermal Management	49
FuelMEP	Fuel Mean Effective Pressure	184
h_c	Heat Transfer Coefficient	24

HCCI	Homogeneous Charge Compression Ignition	14
IVC	Inlet Valve Closing	136
IVO	Inlet Valve Opening	136
$IMEP_g$	Gross Indicated Mean Effective Pressure	183
$IMEP_n$	Net Indicated Mean Effective Pressure	183
LPP	Location of Peak Pressure	76
LQG	Linear Quadratic Gaussian	138
MFB	Mass Fraction Burned	69
MOESP	Multi-variable Output-Error State sPace model algorithm	95
MON	Motored Octane Number	31
MIMO	Multiple-Input, Multiple-Output system	93
MISO	Multiple-Input, Single-Output system	93
MPC	Model Predictive Control	138
n	Engine speed	25
NO_x	Oxides from nitrogen (sum of NO and NO_2)	18
p^c	Pressure increase due to combustion	77
PI	Proportional Integral controller	53
PIC	Peripheral Interface Controller	53
PID	Proportional Integral Derivative controller	137
P_{in}	Inlet pressure	113
PD	Proportional Derivative controller	53
PFI	Port Fuel Injection	51
PRBS	Pseudo Random Binary Sequence	97
PRF	Primary Reference Fuel	38
PM	Particular Matter from the exhaust gas	18
Q_{hr}	Heat released due to combustion	21
Q_{ht}	Heat transfered to combustion chamber walls	24
R	Gas constant	23
R_f	Fuel ratio between two fuels	97
RON	Research Octane Number	31
SI	Spark Ignition, Spark Ignited	17
SNR	Signal-to-Noise Ratio	28

TDC	Top Dead Center	20
T_{in}	Inlet temperature	113
VVA	Variable Valve Actuation	48
VVT	Variable Valve Timing	48
W_f	Injected fuel energy	113

1

Introduction

The Homogeneous Charge Compression Ignition (HCCI) principle uses a lean premixed air-fuel mixture that is compressed with high compression ratio, resulting in simultaneous auto-ignition in the whole combustion chamber. The HCCI engine principle is a fairly new engine principle, in respect to the well known spark ignition and compression ignition engine principles [Christensen *et al.*, 1997]. The first work in HCCI was presented in the late seventies, but it was not until the late nineties it became a significant research area. The benefit with HCCI is the promise of low emissions of nitrogen oxides together with fairly high efficiency, similar to that of CI engines. As the HCCI principle lacks features for direct control of the combustion phasing, control becomes a key issue in operating HCCI engines. HCCI combustion can be unstable and in some cases the instability can be very fast, as will be exemplified later in this thesis. In only a few engine cycles, the combustion phasing could change substantially, resulting in fast cylinder pressure increases. Hence, control on cycle-to-cycle basis is a desired feature, in order to have robust and reliable operation of an HCCI engine.

1.1 Contributions of the Thesis

Most of the work has been performed in collaboration with Petter Strandh at Division of Combustion Engines, Department of Heat and Power Engineering at Lund Institute of Technology, Lund University. Some of the contributions were a result of this collaboration and hence both are credited. In the list of contributions, the abbreviation JB stands for Johan Bengtsson and PS stands for Petter Strandh.

Ion current signal in HCCI–PS

For SI engines there exist combustion control based on a ion current signal. Previously it was believed that the HCCI engine offered no significant ion current signal. In Paper I, it is demonstrated that for $\lambda \in [2, 2.7]$, there is a detectable ion current signal, which could be used for estimation of the combustion phasing.

Proof of good correlation between combustion phasing estimates, in a HCCI engine, based on cylinder ion current and cylinder pressure–JB and PS

A first step toward using ion current for control was to show that the combustion phasing information from pressure transducer and from ion current sensor had high correlation. In Paper [I], it was shown that, the combustion phasing estimation based on ion current signal and the cylinder pressure signal had high correlation; The frequency content, especially the oscillations, between the two signals had high correlation.

HCCI feedback control based on ion current–JB and PS

In Papers [III, V], it was demonstrated that control of the combustion phasing using feedback control based on ion current was possible. It exhibited similar control performance as feedback control based on cylinder pressure.

Modeling of HCCI engine dynamics using system identification–JB

In Paper [IV], it was shown that low order linear dynamic models are sufficient to capture the dynamics of the combustion phasing with a high degree of accuracy at certain HCCI operation points. Also modeling of the cylinder pressure trace was performed with good accuracy.

Control of HCCI based on model based design–JB

Model based design has several desired features, for example, tuning of the controller can be performed without access to the process, stability and robust analysis may be performed. In paper [V, VII], different control strategies are applied, PID, LQG and MPC control, using the identified models of HCCI engine dynamics.

Physical modeling of HCCI for control–JB

There are at least two approaches for obtaining models; the system identification modeling approach and the physical and kinetic modeling approach. Today there exists several highly complex physical and kinetics models of HCCI combustion describing the reactions between different species, but these are not well suited for control design and evaluation

as the purpose of these models are not to capture the dynamic behavior of an HCCI engine. In Paper [VI], a dynamic model with low complexity of HCCI combustion was presented. The model was compared with other known models, one with lower complexity and one with higher complexity, and it was concluded that the presented model gave better result than the model of lower complexity.

Comparison of feedback alternatives from pressure signal–JB and PS

Cylinder pressure contains information about the combustion, but for control purposes it is desired to have a feedback variable that indicates the crank angle where the combustion occurred, the combustion phasing. There are several methods to obtain a feedback signal and in Paper [II] alternative feedback candidates were validated, and it was concluded that feedback directly based on heat release analysis was a robust candidate, and that feedback directly based on pressure had problem to detect the combustion phasing in all operating conditions.

2

Homogeneous Charge Compression Ignition (HCCI)

2.1 What is HCCI?

As the description Homogeneous Charge Compression Ignition (HCCI) indicates, a homogeneous or close to homogeneous mixture is ignited by compression. Therefore, HCCI can be described as a hybrid of the well-known Spark Ignition (SI)–also called Otto engine–and Compression Ignition (CI)–also called Diesel engine–principles. As in an SI engine, the fuel and air are blended into a homogeneous mixture. Instead of using a spark plug to ignite the mixture, the ignition starts as in a CI engine, where temperature of the mixture increases during the compression stroke and reaches a point of auto-ignition. In the cylinder, the combustion occurs close to globally and simultaneously in a homogeneous compression-ignited mixture [Onishi *et al.*, 1979]. Hence, there will be no flame propagation as in a SI engine. Since the combustion occurs globally, the mixture needs to be highly diluted in order to limit the rate of combustion. A mixture close to stoichiometry would have a very quick combustion rate, resulting in very high pressure rise. The combustion rate depends on concentrations and by diluting the mixture the combustion rate can be decreased. Even if the combustion occurs simultaneously, HCCI combustion still has a considerable combustion duration, but the duration is shorter than the duration in a SI or CI engine. The dilution can be achieved by excess air and/or with Exhaust Gas Recirculation (EGR). The homogeneous mixture can be achieved by mixing the fuel and air in the intake port, or by injecting fuel directly into the cylinder at a very early stage of the cycle in order to allow time for mixing.

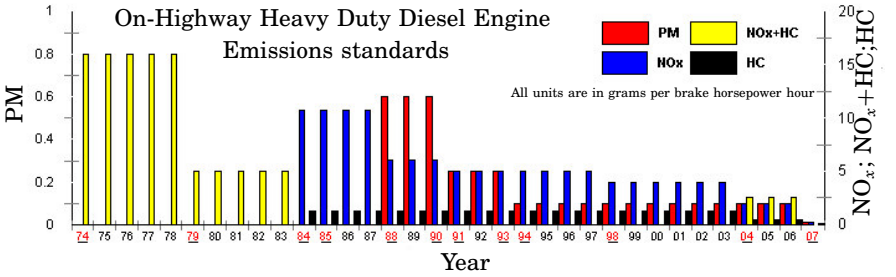

Figure 2.1 U.S. Environmental Protection Agency emissions standards Time-line (http://www.epa.gov/otaq/retrofit/overoh-all.htm).

2.2 Why HCCI?

The first HCCI publication was presented in the late seventies [Onishi *et al.*, 1979; Noguch *et al.*, 1979]. These studies were conducted on two-stroke engines. In the eighties it was shown that HCCI combustion could also be achieved on a four-stroke engine [Najt and Foster, 1983]. But it was not until the nineties that the area had grown to a large world wide research topic [Aoyama *et al.*, 1996; Ryan and Callahan, 1996; Christensen *et al.*, 1997; Hultqvist *et al.*, 1997; Christensen *et al.*, 1999]. One reason for the growth of interest is the high demands of the emission levels. In order to meet the upcoming EU and US strict emission legislations, new technology must be used [European Federation for Transport and Environment, 2004; U.S. Environmental Protection Agency, 2000]. Both particular matter (PM) and NO_x need to be significantly decreased (Fig. 2.1). In some regards, the HCCI principle incorporates the best features of both the SI and the CI engine principles. The mixture is homogenized, which minimizes the particulate emissions and the mixture is compression ignited using high compression ratios, without throttling losses and with shorter combustion duration, which leads to high efficiency.

The SI principle has low efficiency at part load, where the HCCI has good efficiency. The CI engine has similar efficiency as the HCCI engine, but the former generates soot particles and NO_x. Especially the NO_x emissions would be a problem in order to meet the upcoming emission legislation, as it can not be adequately reduced by a three-way catalyst. A NO_x reducing catalyst is today expensive. NO_x is mostly dependent on the temperature during the combustion [Heywood, 1988]. The low emissions of PM and NO_x in HCCI engines are a result of the diluted homogeneous mixture of fuel and air in addition to low combustion temperatures. The

low combustion temperature has two causes. Firstly, since the mixture is highly diluted the temperature increase due to combustion is moderate since the fuel must heat a large mass. Secondly, since the mixture is close to homogeneous there will not be as many hot zones as in a CI engine.

The HCCI engine principle is not limited to a certain fuel, instead it can be used for a wide range of fuels with different octane numbers [Fiveland *et al.*, 2001].

Does the HCCI principle have any poor features? Currently, there are some issues to be solved. One issue is that it can produce fairly high concentrations of unburned hydrocarbon, which needs to be taken care of by the catalyst. Another is that the promise of fairly high efficiency and low NO_x concentrations is difficult to fulfill when increasing the load. In order to run at high load the supercharging needs to be high in order to achieve a diluted charge, which will decrease the overall efficiency due to increased pumping losses. The pumping losses is the work transfer between the piston and the cylinder gases during the inlet and exhaust strokes.

Summarizing, HCCI is interesting because it promises low NO_x emissions and fairly high efficiency.

2.3 Why Control?

In contrast to the SI and CI principle the HCCI principle lacks features for direct control of the combustion phasing. In an SI engine the combustion is controlled by the spark plug and in a CI engine the combustion is controlled by direct fuel injection. An HCCI engine have none of these actuators, hence it is very sensitive to the initial conditions. After the initial conditions are set, there is no way to affect the combustion phasing. Without precise control of temperature, pressure and composition of the air/fuel mixture there may be misfire, too high peak pressure or too high pressure gradient ($dp/d\theta$), which could lead to damage of the engine and NO_x generation. It is necessary to be able to control the combustion phasing in order to have a large operating range. Even a small variation in the load can change the phasing from too early to too late combustion phasing. The HCCI combustion can also be unstable, resulting in successively earlier (or later) auto-ignition. In this case the wall temperature acts as a positive feedback and makes the combustion phasing drift away. A higher wall temperature gives an earlier combustion phasing resulting in an even higher wall temperature. Therefore, a fast combustion phasing control is necessary since it sets the performance limitations of the load control.

2.4 Combustion Phasing in HCCI

For an HCCI engine it is necessary to control the operating conditions so that the combustion phasing, α, occurs at a certain crank angle degree (CAD). The combustion phasing can be constant even if the combustion duration varies. As combustion phase expressed in CAD is not engine speed dependent, the combustion time in seconds is not as important to control as it is to control the combustion phase in CAD. Therefore ,the combustion phase will be expressed in CAD. Still, the kinetics evolve over time. The choice of CAD where the combustion should occur, mostly depends on the load. When the load increases, the combustion phasing needs to be shifted to a later CAD, since early combustion phasing (close to Top Dead Center TDC) gives high peak pressure and high temperature during the combustion. This will result in faster combustion and at high load very rapid combustion causes high mechanical strain on the engine, due to high peak pressure and high pressure gradients. The high pressure gradients cause strain on the engine components, as the pressure wave will reduce the thermal boundary layer at the walls adding positive feedback on the combustion phasing [Olsson, 2004]. The increased combustion temperature increases the heat losses and may lead to NO_x emissions. Hence, a short combustion duration at TDC is not always the best solution, even if it has good theoretical efficiency, as combustion at TDC may generate very high pressure rates and absolute pressure which could damage the engine.

What is the demand on a sensor used for feedback of combustion phasing? To answer that question we need to decide what we mean by combustion phasing. The combustion phasing could be defined by several criteria. It could be the crank angle where the maximum pressure during the engine cycle occurs. It could be defined as when the start of combustion (α_{SOC}) occurs. Another definition could be the time when a certain percentage amount of the fuel has been consumed. The CAD of the maximum pressure has the disadvantage that if the combustion occurs very late the maximum pressure can occur at TDC, even if the combustion occurs much later. Using α_{SOC} as a definition of the combustion phasing is not a good choice since auto-ignition is sensitive to temperature and concentrations of fuel/air in the mixture and the combustion often start around a similar CAD before we have reached the TDC in cases without misfire. But the duration of the combustion differs a lot. Therefore α_{SOC} does not give a good indication of the combustion phasing. Using the CAD where a certain percentage amount of the fuel has been burned as indication has benefits, as it is robust measurement at both early and late combustion phasing. But a low percentage such as 10% or 20% has similar problem as α_{SOC}, it does not give the phasing where the combustion rate is highest. How

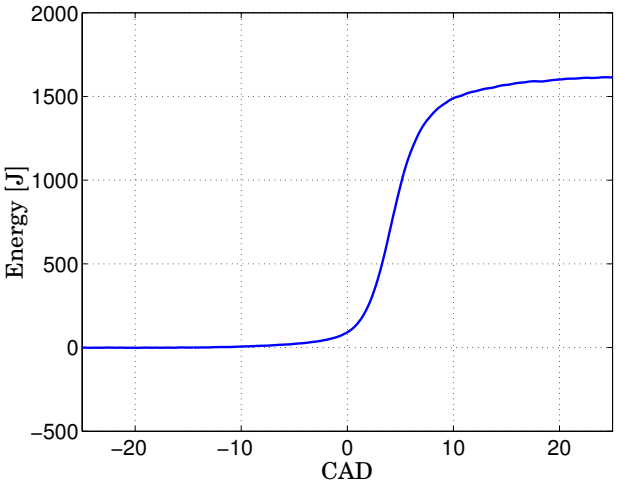

Figure 2.2 A heat release curve calculated from cylinder pressure.

much energy that has been released can be found by calculating the heat release, see Sec. 2.5 for the calculations. It is found that the heat release is fairly symmetric (Fig. 2.2). Hence the crank angle where 50% of the energy has been released is a good indication of the combustion phasing. It is the median of the combustion, where the combustion rate is highest. This gives a robust indication of the combustion phasing, a small error in 50% released energy result in a very small error of the phasing in CAD, since the slope of the energy rate is steep. Hence, for feedback it would be suitable to have a sensor which can be used for estimation of the crank angle where 50% energy has been released. This crank angle has sometimes been denoted as CA50 [Olsson *et al.*, 2001b], but in this thesis α_{50} will be used as α_{50} is better suited notation for mathematical expressions. 50% of the energy released is the same as 50% of the fuel burned, and in the future α_{50} is read as the crank angle of 50% burnt. A more detailed study of different feedback options is performed in Chapter 6.

2.5 Modeling of Heat Release

The method of monitoring the progression and completeness of the combustive reactions, and separating the effect of volume change, heat transfer and mass loss based on cylinder pressure is usually referred to as

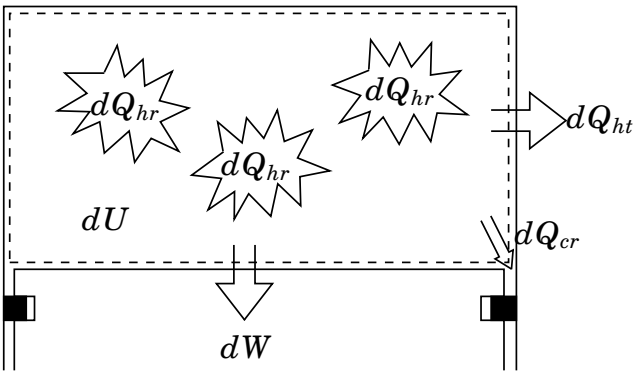

Figure 2.3 Energy balance for an open system with internal chemical heat release.

heat release analysis, and uses the first law of thermodynamics. A person familiar to thermodynamics might have objections to the use of the term *heat release*, as from a formal thermodynamics point of view, heat is transfered across system boundaries. But in the heat release analysis, it is also included a transformation of fuel energy into thermal energy [Heywood, 1988]. In heat release analysis, the time derivative of the enthalpy is calculated relative to some reference state of the cylinder charge.

The purpose of the heat release analysis is to find a method which can be used for calculation of an scalar combustion phasing variable, α, in real-time. The model complexity needs to be sufficiently low to allow sufficient time in every engine cycle for both calculation of combustion phasing and actuation time. Therefore, the model is a trade-off between low complexity and high accuracy. In order to keep the model complexity low, the heat release was modeled using a one-zone model. Hence, we assume that the temperature and the gas composition are global homogeneous in the whole cylinder. The model, based on the first law of thermodynamics, has been widely used and model properties have been described earlier in the literature [Gatowski *et al.*, 1984], [Heywood, 1988].

Consider the first law of thermodynamics for an open system:

$$dU = dQ - dW + h_{cr}\mathrm{dm}_{cr} \tag{2.1}$$

where, dU is the change of internal energy of the mass in the system; Q is the heat transported into the system; dW is the work performed; $\dot{h}_{cr}\mathrm{dm}_{cr}$ is the energy leakage due to inflow and outflow from crevice regions between the piston and the cylinder wall above the piston rings; h_{cr} is the enthalpy at cylinder condition when dm_{cr} differs from zero; dm_{cr}

is the mass flow into and out from the crevice region. The change of heat transported into the system dQ consists of the released energy from the fuel, dQ_{hr} and the heat transfered to the chamber walls, dQ_{ht}. Rewriting Eq. 2.1 using $dQ = dQ_{hr} - dQ_{ht}$ gives

$$dQ_{hr} = dU + dW + dQ_{ht} + h_{cr}\mathrm{dm}_{cr} \tag{2.2}$$

We would like to express the heat release in terms of pressure, p, volume, V, and temperature T. The first step is to rewrite the internal energy term as

$$dU = m\mathrm{du} + u\mathrm{dm} = mc_v\mathrm{dT} + u\mathrm{dm} \tag{2.3}$$

where, m is the charge mass; c_v is the specific heat at constant volume. By differentiating the ideal gas law, when assuming that the gas constant R is constant, dT can be expressed in p,V, and m

$$\begin{aligned} pV &= mRT & (2.4)\\ \mathrm{dp}V + p\mathrm{dV} &= mR\mathrm{dT} + \mathrm{dm}RT & (2.5) \end{aligned}$$

with p being pressure, V volume and R gas constant. Hence, dU can be written as

$$\begin{aligned} dT &= \frac{1}{mR}(\mathrm{dp}V + p\mathrm{dV}) - \frac{T}{m}\mathrm{dm} \Rightarrow & (2.6)\\ dU &= \frac{c_v}{R}(\mathrm{dp}V + p\mathrm{dV}) + u\mathrm{dm} - c_vT\mathrm{dm} & (2.7) \end{aligned}$$

The second step is to rewrite the work performed as

$$dW = p\mathrm{dV} \tag{2.8}$$

Using Eq. (2.7) and Eq. (2.8), Eq. (2.2) can be written as

$$\begin{aligned} dQ_{hr} &= \frac{c_v}{R}(\mathrm{dp}V + p\mathrm{dV}) + p\mathrm{dV} + dQ_{ht} + u\mathrm{dm} - c_vT\mathrm{dm} + h_{cr}\mathrm{dm}_{cr}\\ &= (1 + \frac{c_v}{R})p\mathrm{dV} + \frac{c_v}{R}V\mathrm{dp} + dQ_{ht} + u\mathrm{dm} - c_vT\mathrm{dm} + h_{cr}\mathrm{dm}_{cr} \end{aligned} \tag{2.9}$$

The crevice effect is modeled as a single volume at the cylinder pressure to simulate the piston/ring/cylinder-wall region. A mass balance gives

$$\begin{aligned} \mathrm{dm} &= -\mathrm{dm}_{cr} \Rightarrow & (2.10)\\ dQ_{hr} &= (1 + \frac{c_v}{R})p\mathrm{dV} + \frac{c_v}{R}V\mathrm{dp} + dQ_{ht} + (u - c_vT + h_{cr})\mathrm{dm}_{cr} & (2.11) \end{aligned}$$

For ideal gas the relation between c_v, c_p and R is

$$c_p = c_v + R \tag{2.12}$$

where c_p is the specific heat at constant pressure. Assuming that the changes are quantified per crank angle degree, we choose crank angle since our system will be crank angle based. Eq. (2.11) is then written as

$$\begin{aligned}\frac{dQ_{hr}}{d\theta} &= \frac{\gamma}{\gamma-1}p\frac{dV}{d\theta} + \frac{1}{\gamma-1}V\frac{dp}{d\theta} + \frac{dQ_{ht}}{d\theta} + (u - c_vT + h_{cr})\frac{dm_{cr}}{d\theta} \\ &= \frac{\gamma}{\gamma-1}p\frac{dV}{d\theta} + \frac{1}{\gamma-1}V\frac{dp}{d\theta} + \frac{dQ_{ht}}{d\theta} + \frac{dQ_{cr}}{d\theta}\end{aligned} \tag{2.13}$$

where γ is the specific heat ratio defined by

$$\gamma = \frac{c_p}{c_v} \tag{2.14}$$

The specific heat ratio γ, depends on gas composition and temperature. There is not a linear relationship between γ and temperature, [Heywood, 1988], but a simple and fairly accurate model is to assume a relationship as

$$\gamma(T) = a + bT \tag{2.15}$$

given that the enthalpy is related to the internal energy as

$$h = u + pv \tag{2.16}$$

The third term, the heat transfer rate to the combustion chamber walls, Q_{ht}, can be calculated from the relation

$$\frac{dQ_{ht}}{dt} = h_cA_w(T - T_w) \tag{2.17}$$

where h_c is the heat transfer coefficient, A_w is the chamber wall area, T_w is the mean wall temperature, and h_c can be estimated using Nusselt-Reynold numbers. The heat transfer coefficient is estimated by using result from [Woschni, 1967] who assumed a correlation of the form

$$\mathrm{Nu} = 0.0035 \cdot \mathrm{Re}^{0.8} \tag{2.18}$$

where Nu is the Nusselt number, Re is the Reynolds number. Then is h_c given by

$$\omega = 2.28\left(2Sn + 3.24 \cdot 10^{-3}C_2\left(\frac{V_d}{V_{IVC}}\right)\left(\frac{p - p_m}{p_{IVC}}\right)T_{IVC}\right) \tag{2.19}$$

$$h_c = 131C_1B^{-0.2}p^{0.8}T^{-0.55}\omega^{0.8} \tag{2.20}$$

where V_d is the displaced volume, V_{IVC} is the volume at inlet valve closing (IVC), p_m is the motored cylinder pressure, p_{IVC} is the pressure at IVC, T_{IVC} is the temperature at IVC, C_1 and C_2 are motor dependent constants, B is the cylinder bore, S is the stroke and n is the engine speed in revolutions per second.

The energy due to the crevice effect, Q_{cr}, can be modeled using the fact that the crevice regions are narrow. Therefore an appropriate assumption is that the aggregate crevice volume has the same gas temperature as the walls and the same pressure as the cylinder,

$$m_{cr} = pV_{cr}/RT_w \tag{2.21}$$

where T_w is the wall temperature. We rewrite the term which is multiplied with m_{cr} as

$$h_{cr} - u + c_v T = u^{cr} + p^{cr} v^{cr} - u + c_v T = u^{cr} - u + R(T^{cr} + \frac{T}{\gamma - 1}) \tag{2.22}$$

The difference $u - u^{cr}$, using $\gamma(T) = a + bT$, can then be expressed as

$$u^{cr} - u = \int_{T^{cr}}^{T} c_v dT = -\frac{R}{b} \ln\left(\frac{\gamma - 1}{\gamma^{cr} - 1}\right) \tag{2.23}$$

The heat transfer due to crevice effect, dQ_{cr}, can then be written as

$$dQ_{cr} = \frac{V_{cr}}{T_w}\left(T^{cr} + \frac{T}{\gamma - 1} - \frac{1}{b}\ln\left(\frac{\gamma - 1}{\gamma^{cr} - 1}\right)\right) dp \tag{2.24}$$

using Eq. (2.21) and Eq. (2.23). The crevice effect on the heat release is very small, a few percent of the total energy. Hence, crevice effects are often neglected in heat release calculations and at least in the case when the objective is to control the combustion, this simplification is justified.

2.6 HCCI Combustion

HCCI combustion differs from SI and CI combustion, since the combustion occurs globally and is very fast. Therefore, the time for the combustion needs to be controlled to avoid fast pressure rise, pressure oscillations and high maximum pressure. In Fig. 2.4, a pressure trace with corresponding heat release is shown. It can be observed that the combustion duration is short, the heat release of 10% to 90% burned is reached approximately around 5 CAD. This can be compared with SI, where the combustion duration is around 30-40 CAD, and CI, where the combustion duration is

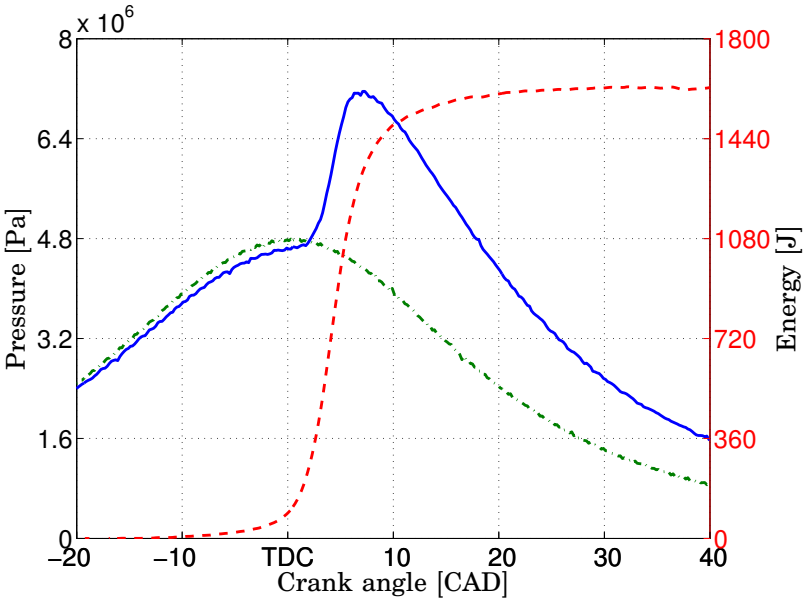

Figure 2.4 Cylinder pressure trace of a motored cycle (*dash-dotted*), burned cycle (*solid*) and the heat release of the burned cycle (*dashed*).

around 60-90 CAD [Heywood, 1988]. From the figure, the mixture effect on the pressure trace can also be observed. In the motored cycle the mixture consists of only air and in the burned cycle the mixture consisted of fuel and air. The mixtures have different ratio of specific heats, which results in that the pressure trace during the compression will differ for the two mixtures. The temperature for these two pressure traces were almost the same, since there were only three engine cycles between them and the engine was operated at 1200 rpm during the experiment. In Fig. 2.5, a p-V diagram of an engine cycle is shown. It can be observed that the pumping losses are small, this is due to that an HCCI engine is operated unthrottled. It can also be observed that the combustion phasing of this cycle occur not at TDC, but a few CAD after TDC. It is desired to maximize the work performed and therefore having the combustion to occur close to TDC. But combustion close to TDC will lead to high peak pressure, pressure oscillations and possibly damage to the engine and therefore a later combustion phasing was chosen. During the compression cycle and the expansion cycle after the combustion is finished, no chemical reactions

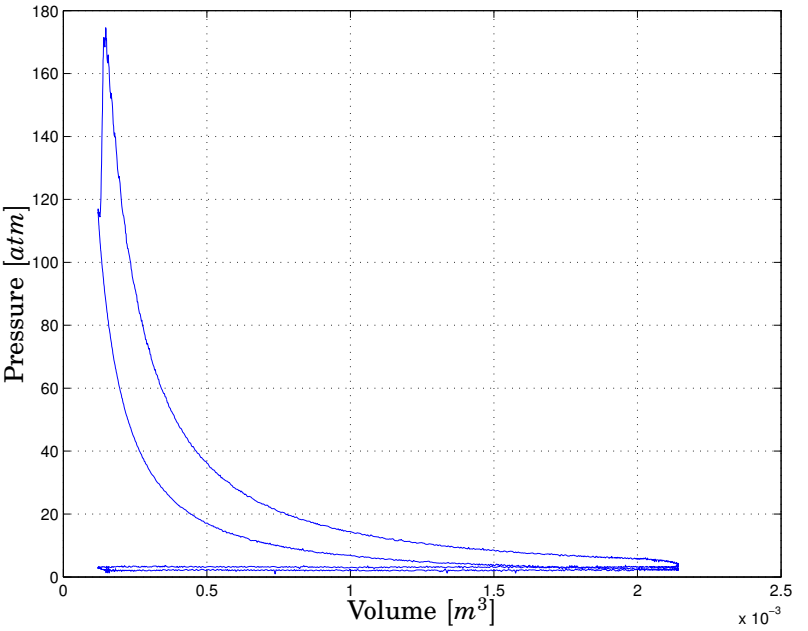

Figure 2.5 Pressure-volume curve of a full engine cycle.

take place and Eq. (2.9) is simplified to

$$0 = dQ_{hr} = \frac{c_v}{R} V dp + \frac{c_p}{R} p dV - dQ_{ht} \tag{2.25}$$

dQ_{ht} can be defined as

$$dQ_{ht} = aVdp + bpdV \tag{2.26}$$

for this certain type of process, where a and b are functions of temperature [Tunestål, 2001]. Eq. (2.25) is then rewritten as

$$\frac{dp}{p} = -\kappa \frac{dV}{V} \tag{2.27}$$

with

$$\kappa = \frac{\frac{c_v}{R} - b}{\frac{c_p}{R} - a}$$

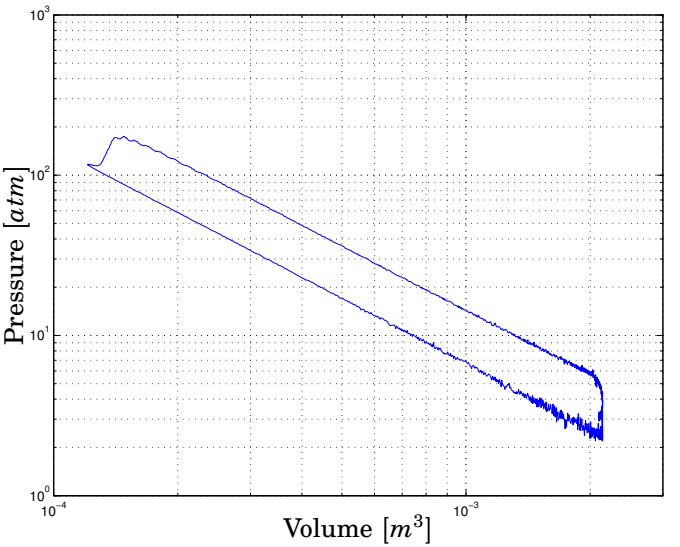

Figure 2.6 Logarithmic Pressure-volume curve of a full engine cycle.

Observe that κ differs from the ratio of specific heat, γ. A process that fulfills Eq. (2.6) is called a polytropic process and κ is called the polytropic exponent. With κ constant, Eq (2.27) can be rewritten as

$$pV^{\kappa} = C$$

where

$$C = p_0 V_0^{\kappa}$$

In Fig. 2.6 the same cycle as in Fig. 2.5 is shown, but now in logarithmic scale. The polytropic exponent can be observed in this figure and it seems to be constant during the compression cycle and in the expansion cycle when the combustion is finished. The pressure oscillations can also clearly be observed. Also an indication of the Signal-to-Noise Ratio, SNR, can be observed. At low pressure, below 5 atm, the SNR is low, but in the area where the combustion occurs the SNR is very high. The HCCI principle can be seen as a controlled engine *knock* principle. Knock is the name given to the noise which is transmitted through the engine structure when auto-ignition of the mixture only partly occurs. The engine knock in an HCCI engine differ from the ones in an SI engine, since there is no flame propagation. These knocks generate pressure oscillations that are very audible. The oscillations also destroy the boundary layer, resulting in higher heat losses. Even if the mixture would be completely

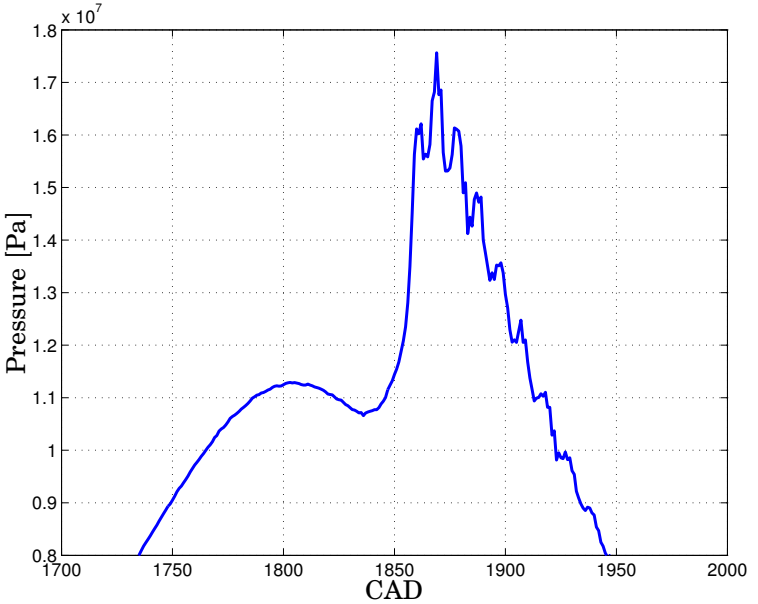

Figure 2.7 Pressure trace with oscillations

homogeneous, there would be knock since the temperature still would not be spatially uniform. For example, the cylinder wall has impact on the in-cylinder temperature. As the kinetics start the temperature becomes initial spatially almost uniform as a result of the temperature inversion of the reactivity, but regions having different chemical composition may exist [Griffiths and Whitaker, 2002]. This will lead to that the combustion will not be completely spatially uniform and knock may occur. There are also studies in order to predict when knock may occur [Yelvington and Green, 2003; Oakley *et al.*, 2001; Vressner *et al.*, 2003]. Fig. 2.7 shows an example of the pressure oscillations in an HCCI engine. Even if the cycle-to-cycle variations of an HCCI is lesser than for SI and CI principles, there still is a significant variation (Fig. 2.8). The variation depends on operating condition.

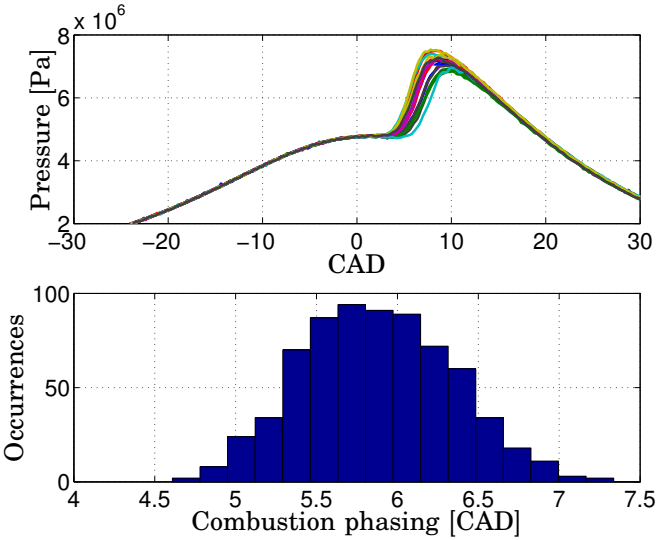

Figure 2.8 Cycle-to-cycle variations at open-loop control. Upper figure shows the pressure traces and the lower shows a histogram of the combustion phasing.

2.7 Emissions

Nitrogen Oxides

The NO formation is exponentially dependent on the temperature and in-cylinder combustion temperatures above 1800 K results in NO formation [Heywood, 1988; Christensen *et al.*, 1997]. HCCI combustion results in low combustion temperature, since the premixed mixture is highly diluted, and no or very low NO_x emissions are formed.

Hydrocarbons

The HC emissions are the result of incomplete combustion of the mixture. The emissions are a result of the low combustion temperature. The low temperature makes the HCCI combustion sensitive to flame quenching at the chamber walls and crevice regions. The levels of HC have effect on the overall engine efficiency [Christensen, 2002].

Carbon Monoxide

The source of CO is fuel that oxidizes late enough for the mixture to freeze before CO is further oxidized to CO_2. The formation of CO is temperature

dependent and a higher temperature will decrease the formation. CO formation decrease when the combustion phasing is advanced due to higher temperature and longer time for oxidation, but such conditions will result in increased NO_x formation [Christensen, 2002].

2.8 Efficiency

An HCCI engine is operated unthrottled and can use high compression ratio, which gives good fuel conversion efficiency. The HCCI combustion temperature is low, but even so there are significant heat losses due to combustion close to the chamber walls and due to the in-cylinder pressure oscillations. At high load the combustion phasing must be retarded in order to keep the in-cylinder temperature and pressure at acceptable levels. Late combustion phasing also have negative impact on the engine efficiency, since there will be loss in the performed work of the engine. The HCCI engine has an engine efficiency similar to the Diesel engine [Christensen, 2002].

2.9 Fuel Properties

An HCCI engine can be operated on a wide range of fuels, but the fuels have different properties which have significant effects on the operation range [Christensen *et al.*, 1997]. The fuel properties should be such that the engine can run in HCCI mode both at low and high load. Since the benefits with HCCI decrease at high load, the fuel could be used for SI operation. There are several studies on the characteristics of different fuels in an HCCI engine, to obtain a fuel which is suitable for HCCI [Tanaka *et al.*, 2003b; Dec and Sjöberg, 2004; Sjöberg and Dec, 2003; Jeuland *et al.*, 2004]. The octane numbers–Research Octane Number (RON) and Motor Octane Number (MON)–are used to characterize fuel for SI engines and cetane number to characterize fuel for CI engines. Whereas RON, MON and cetane may have no relevance to characterize HCCI combustion, it remains important to find effective characterizations of HCCI fuel properties. HCCI engines have requirements on the fuel that differ from other engines and a fuel specification of HCCI combustion should be developed. Fuels with similar octane number may have s different HCCI combustion, the formation of the fuel has significant effect on the combustion [Sjöberg and Dec, 2003]. In [Tanaka *et al.*, 2003b] a control scheme for controlling ignition delay, maximum dp and burn rate was proposed, but practically it can only be used to shorten ignition delay and faster burn rate. In HCCI

combustion the challenge is mostly to obtain the opposite, longer ignition delay and slower burn rate.

2.10 Scientific Challenges

The scientific challenges with HCCI are to control the combustion at a wide operation range and simultaneously have fairly high efficiency and low concentrations of NO_x, HC and CO. To fulfill these requirements, several barriers must be overcome before HCCI engines can reach production.

Deriving Dynamic Models of HCCI Combustion

There is a need of models suitable for control design. The HCCI combustion is very complex, even so a model useful for control design purposes needs to be dynamically accurate, yet preferably simple and not with hundreds of states. Full kinetic models of the HCCI combustion may be needed to understand the kinetics in the combustion. If accurate and dynamically precise, these models can be used for evaluation of the control performance and simulation of the combustion.

Sensor and actuator study

For commercial success, cheap sensors that can measure the combustion phasing, which are reliable and have long lifespan need to be found. Today's cylinder pressure transducers are too expensive and have too short life-span for production. At the moment, ion current sensors are not reliable in the whole operating range for HCCI. There are several possible actuators for controlling the HCCI dynamics and more studies are needed in order to show the actuators fully potential in controlling the HCCI dynamics.

Development of Direct Injection System for HCCI

If diesel is going to be used as fuel, there is a need to develop direct injection system, where homogeneous mixture can be obtained and still start the injection close to TDC. This is mostly a challenge in developing HCCI engines for heavy trucks in the short run.

Control of the Combustion Phasing

To control the combustion phasing in the whole HCCI mode range (i.e., for various loads, speeds and temperatures) is a challenge, as the HCCI principle lacks features for direct combustion phasing. A precise and fast control of combustion phasing is needed in order to fulfill good efficiency, load control and low emissions.

Control at High Load

A HCCI engine needs to be able to operate at a load range similar to the SI or CI engine principles. At high load the combustion rate is very high results in very high pressure increases, pressure oscillations and absolute pressure. This limits the efficiency and puts high structural demands on the engine. Research is needed to further understand how to slow the kinetics and achieve longer combustion duration.

Control of the Noise Level

The engine knock generates an audible manifestation which is commercially unacceptable. This issue is related to control at high load.

Control of Emissions

The level of the emissions need to be controlled, still with an acceptable overall efficiency. The exhaust temperature from HCCI combustion is low and development of oxidation catalysts for low-temperature exhaust are needed to meet the future emission standards for HC and CO.

Fuel Characterization for HCCI Combustion

The fuel has strong effects on the HCCI combustion and a classification of fuel effects on HCCI combustion is needed.

Cold-start

The HCCI engine has cold-start difficulties, the temperature of the mixture is not high enough to auto-ignite. Today the most practical approach is to start the engine in another standard operation mode as CI or SI and to switch to HCCI mode after warm-up.

3

Physical Modeling of HCCI Engine Dynamics

In homogeneous charge compression ignition (HCCI) engines the combustion phasing is determined by the autoignition properties of the air-fuel mixture in use. Small variations in the cylinder environment may greatly influence the combustion phasing [Hyvönen *et al.*, 2004]. In order to control engine operation it is therefore necessary to have good models and substantial understanding of the ignition and combustion process. This work aims at describing the major thermodynamic and chemical interactions in the course of an engine stroke and their influence on combustion phasing. The goal is to construct a simulation model that (qualitatively) reproduces HCCI engine operation for the purpose of synthesizing, analyzing, and evaluating various combustion phasing control strategies. This chapter is a feasibility study on requirements and choice of complexity level for a suitable model, and is to be regarded as a first step towards a complete model. The proposed model structure consists of a zero-dimensional cylinder model, combined with a reduced chemical kinetic model to describe the ignition process. Experiments on a real engine with dual fuels and inlet air temperature control have been conducted to collect information on the phenomena to reproduce and to compare to simulated results.

Experiments

The experimental setup consisted of a heavy duty Volvo diesel engine, Table 3.1, and the set-up will in more detail be described in Sec. 5.1. In the experiments, the fuel ratio, R_f, of the dual fuels ethanol and n-heptane, fuel energy per cycle, Q_{in}, inlet air temperature, T_{in}, and the engine speed, n, were changed according to Table 3.2. By changing the injected fuel energy per cycle the load is changed and $Q_{in} = 1000$ J corresponds to

Table 3.1 Engine specifications.

Operated cylinders	6
Displaced Volume	2000 cm^3
Bore	131 mm
Stroke	150 mm
Connecting Rod Length	260 mm
Number of Valves	4
Compression Ratio	18.5:1
Fuel Supply	port fuel injection

Table 3.2 Experimental conditions

T_{in} [°C]	100–115	100	100	100
$n[rpm]$	1200	1000–1500	1200	1200
$Q_{in}[J]$	1400	1400	1000–1500	1400
R_f [vol%]	0.93	0.93	0.93	0.892–1.0

a FuelMEP (Fuel Mean Effective Pressure, see Sec. A.2) of 5 bar and $Q_{in} = 1500$ J corresponds to a FuelMEP of 7.5 bar. As the engine was naturally aspirated this corresponds to that λ, air/fuel ratio, varied from 6.2 to 4.1. Only low load experiments in open loop were performed, when the engine temperature was at steady state. At each operating point, data of 500 cycles were collected. The mean value of these 500 cycles was thereafter used in comparison with the result from the model.

3.1 Model

HCCI combustion is often achieved without a complete homogeneous mixture. But in order to derive a control-relevant model, we might firstly proceed by assuming that the mixture is homogeneous, thus allowing a single-zone cylinder model. Such assumption may be justified by laser-diagnostic measurements [Richter *et al.*, 2000]. To reproduce the effects relevant for combustion phasing control it is required that the autoignition model captures the effects on ignition delay (induction time) of varying

species concentrations, temperature trace, and fuel quality. Several alternative approaches are possible for modeling the instant of autoignition for fuels. Large models, e.g. [Sjöberg and Dec, 2003] (PRF fuels, 857 species, 3,606 reactions, CHEMKIN/LLNL), have been used to model complete combustion. In addition to ignition prediction, such models are also aimed at describing intermediate species and end product composition. Reduced chemical kinetics models, e.g. [Tanaka *et al.*, 2003a] (PRF fuels, 32 species, 55 reactions, CHEMKIN), have also been proposed, where reactions with little influence on the combustion have been identified and removed. For simulation of multi-cycle scenarios it is necessary to keep the model complexity low in order to arrive at reasonable simulation times. An attractive and widespread alternative is to use the Shell model [Halstead *et al.*, 1977], which is a lumped chemical kinetics model using only five representative species in eight generic reactions. This model is aimed at prediction of autoignition rather than describing the complete combustion process. Compression ignition delay may also be described by empirical correlations, such as the *knock integral* condition

$$\int_{t=0}^{t_i} \frac{dt}{\tau} = 1 \tag{3.1}$$

where t_i is the instant of ignition and τ is the estimated ignition time (ignition delay) at the instantaneous pressure and temperature conditions at time t, often described by Arrhenius type expressions [Heywood, 1988]. A drawback is that dependence on species concentrations is normally not regarded. An integral condition with concentration dependence was used in [Shaver *et al.*, 2003; Shaver *et al.*, 2004] in a similar study for propane fuel, where also autoignition models based on very simple reaction mechanisms were evaluated. Alternatives to physical or physical based models are to use system identification to obtain models or to use empirical look-up tables. The latter gives very little physical insight, and require substantial efforts to calibrate. In this work, the Shell model was chosen to describe the process of autoignition. A static model is then used to describe the major part of the actual combustion and corresponding heat release. The result from the Shell model is compared with result from an integrated Arrhenius rate threshold model.

Cylinder Model

The cylinder gas dynamics are described by the first law with volume-pressure work

$$\delta Q_{HR} = (1 + \frac{c_v}{R}) p \mathrm{dV} + \frac{c_v}{R} V \mathrm{dp} + \delta Q_{HT} \tag{3.2}$$

where p is the cylinder pressure, V the volume, R_u the universal gas constant, $c_v = c_p - R_u$ the specific heat capacity, and n the molar substance amount contained in the cylinder. The time derivatives of Q_{HR} and Q_{HT} denote rates of heat released by the combustion process and heat flowing from the wall.

Gas Properties

The gas is described as a mixture of dry air and fuel, and the combustion products are nitrogen, carbondioxide and water. Specific heat for each species i is described by NASA polynomial approximations of JANAF data

$$c_{p,i}(T) = \frac{R_u}{M_i} \sum_{j=1}^{5} a_{i,j} T^{j-3} \tag{3.3}$$

where M_i is the molar mass of species i and T is the cylinder temperature. The mixture specific heat is then

$$c_p(T) = \frac{1}{n} \sum_i n_i M_i c_{p,i}(T) \tag{3.4}$$

where n_i is the mole of species i.

Shell Autoignition Model

The Shell autoignition model for hydrocarbon fuels [Halstead *et al.*, 1977], $C_a H_b$, is based on a general eight-step chain-branching reaction scheme with lumped species: The hydrocarbon fuel RH, radicals $\bar{R}$, intermediate species Q, and the chain branching agent B.

$$RH + O_2 \xrightarrow{k_q} 2\bar{R} \quad \text{(initiation)} \tag{3.5}$$

$$\bar{R} \xrightarrow{k_p} \bar{R} + \text{products and heat} \quad \text{(propagation cycle)} \tag{3.6}$$

$$\bar{R} \xrightarrow{f_1 k_p} \bar{R} + B \quad \text{(propagation forming } B\text{)} \tag{3.7}$$

$$\bar{R} + Q \xrightarrow{f_2 k_p} \bar{R} + B \quad \text{(propagation forming } B\text{)} \tag{3.8}$$

$$\bar{R} \xrightarrow{f_3 k_p} \text{out} \quad \text{(linear termination)} \tag{3.9}$$

$$\bar{R} \xrightarrow{f_4 k_p} \bar{R} + Q \quad \text{(propagation forming } Q\text{)} \tag{3.10}$$

$$2\bar{R} \xrightarrow{k_t} \text{out} \quad \text{(quadratic termination)} \tag{3.11}$$

$$B \xrightarrow{k_b} 2\bar{R} \quad \text{(degenerate branching)} \tag{3.12}$$

Autoignition is described by integrating the time variations of species concentrations from the beginning of the compression stroke.

$$\frac{d[\bar{R}]}{dt} = 2\left\{k_q[RH][O_2] + k_b[B] - k_t[\bar{R}]^2\right\} - f_3 k_p[\bar{R}] \tag{3.13}$$

$$\frac{d[B]}{dt} = f_1 k_p[\bar{R}] + f_2 k_p[Q][\bar{R}] - k_b[B] \tag{3.14}$$

$$\frac{d[Q]}{dt} = f_4 k_p[\bar{R}] - f_2 k_p[Q][\bar{R}] \tag{3.15}$$

$$\frac{d[O_2]}{dt} = -g k_p[\bar{R}] \tag{3.16}$$

The species $\bar{R}$, Q, and B are not considered in thermodynamic computations for the gas mixture. The stoichiometry is approximated by assuming a constant CO/CO_2 ratio, ν, for the complete combustion process, with oxygen consumption $g = 2[a(1-\nu) + b/4]/b$ mole per cycle. The heat release from combustion is given by

$$\frac{dQ_{HR}}{dt} = k_p q V[\bar{R}] \tag{3.17}$$

where q is the exothermicity per cycle for the regarded fuel. The propagation rate coefficient is described as

$$k_p^{-1} = \frac{1}{k_{p,1}[O_2]} + \frac{1}{k_{p,2}} + \frac{1}{k_{p,1}[RH]} \tag{3.18}$$

To capture dependence of induction periods on fuel and air concentrations the terms f_1, f_3, and f_4 are expressed as

$$f_i = f_i^{\circ}[O_2]^{x_i}[RH]^{y_i} \tag{3.19}$$

Rate coefficients and rate parameters k_i and f_i° are then described by Arrhenius rate coefficients

$$k_i = A_i \exp\left[\frac{E_i}{R_u T}\right], \quad f_i^{\circ} = A_i \exp\left[\frac{E_i}{R_u T}\right] \tag{3.20}$$

Calibrated parameters for a number of fuels, including a set of Primary Reference Fuels (PRF), are found in the literature [Halstead *et al.*, 1977]. PRFx is a mixture of n-heptane and iso-octane, where the octane number x is defined as the volume percentage of iso-octane. Parameters for PRF90 were used in the simulations. Autoignition was defined as the crank angle where the explosive phase of combustion starts.

Integrated Arrhenius Rate Threshold

The Arrhenius form can be used to determine the rate coefficient describing a single-step reaction between two molecules [Thurns, 1996]. The single-step rate integral condition is based on the knock integral with

$$K_{th} = \int_{\theta_{\mathrm{IVC}}}^{\theta} 1/\tau \; d\theta/w \tag{3.21}$$

$$1/\tau = A \exp(E_a/(R_u T))[\mathrm{Fuel}]^a [O_2]^b \tag{3.22}$$

where θ is the crank angle and θ_{IVC} is the cank angle of the inlet valve closure. The integral condition describes a generalized reaction of fuel and oxygen and this is an extreme simplification of the large number of reactions that take place during combustion. The empirical parameters A, E_a, a, b and K_{th} are determined from experiments. Values for n-heptane and iso-octane from [Thurns, 1996] was used in the comparison below. Autoignition was defined as the crank angle where the integral condition has reached the threshold K_{th}.

Combustion

When autoignition is detected by the Shell model or the Integrated Arrhenius Rate Threshold, the completion of combustion is described by a Wiebe function [Vibe, 1970].

$$x_b(\theta) = 1 - \exp\left[-a(\frac{\theta - \theta_0}{\Delta\theta})^{m+1}\right] \tag{3.23}$$

where x_b denotes the mass fraction burnt, θ is the crank angle, θ_0 start of combustion, $\Delta\theta$ is the total duration, and a and m adjustable parameters that fix the shape of the curve. The heat release is computed from the rate of x_b and the higher heating value of the fuel.

Heat Transfer

Heat is transfered by convection and radiation between in-cylinder gases and cylinder head, valves, cylinder walls, and piston during the engine cycle. In this case the radiation is neglected. This problem is very complex, but a standard solution is to use the Newton law for external heat transfer

$$\frac{dQ_W}{dt} = h_c A_W (T - T_W) \tag{3.24}$$

where Q_W is the heat transfer by conduction, A_W is the wall area, T_W is the wall temperature, and the heat-transfer coefficient, h_c, is given by the Nusselt-Reynold relation by Woschni [Woschni, 1967].

$$h_c = 3.26 B^{-0.2} p^{0.8} T^{-0.55} (2.28 S_p)^{0.8} \tag{3.25}$$

Table 3.3 Simulation conditions

T_{in} [°C]	100–115	100	100	100
$n[rpm]$	1200	1000–1500	1200	1200
$Q_{in}[J]$	1400	1400	1000–1500	1400

where S_p is the mean piston speed and B is the bore.

Simulations

The described models were implemented and simulated in Matlab™ for single engine cycles with given initial gas mixtures and states. Cylinder specifications were set according to Table 3.1 and simulation conditions according to Table 3.3.

3.2 Results

Experiments were carried out to investigate the influence on combustion phasing from inlet temperature, engine speed, fuel energy, and fuel ratio. There are several alternatives how to calculate the combustion phasing and in this work the combustion phasing is calculated as the crank angle where 50% of the fuel has burned, α_{50}, [Bengtsson *et al.*, 2004]. The phasing effects on α_{50} were studied by varying the corresponding variables from a nominal operating condition of $T_{in} = 373$ K, $Q_{in} = 1400$ J, $n = 1200$ rpm, and $R_f = 0.93$ vol% as described in Table 3.2. The acquired pressure, reconstructed temperature traces, and reconstructed heat release [Gatowski *et al.*, 1984] for the nominal condition are shown in Fig. 3.1.

Fig. 3.2 shows pressure trace, temperature trace, and heat release for a simulation of a nominal operating point of $T_{in} = 373$ K, $Q_{in} = 1400$ J, $n = 1200$ rpm for PRF90 fuel. The dynamics of the ignition model is illustrated by the species concentrations in Fig. 3.3. Note that the concentrations of $\bar{R}$, Q, and B are frozen as the Shell model is switched for the Vibe combustion model. As earlier described the autoignition was defined as the crank angle where the explosive phase of the combustion phase and it can be observed that approximately 10% of the fuel has been burned at this crank angle. This is some few percentage above what was measured of burned fuel in the experiment at the point where the ignition started.

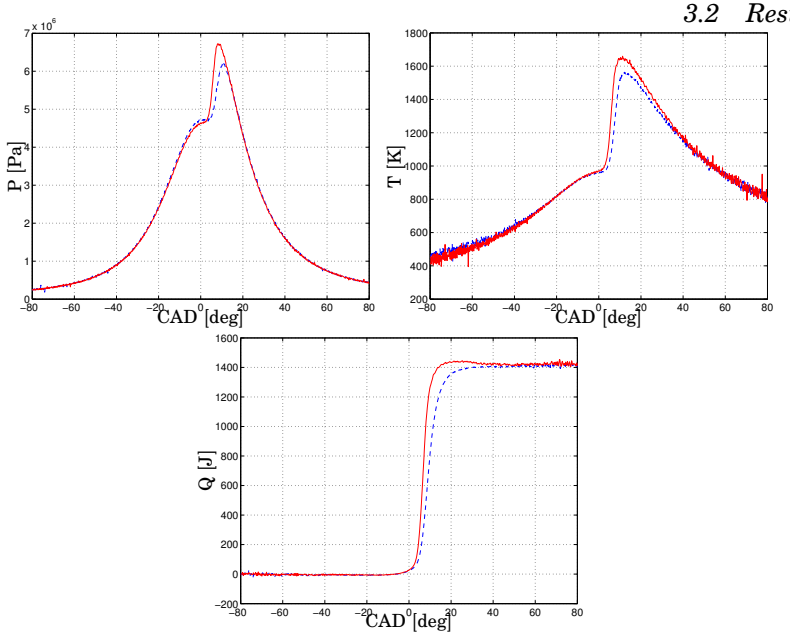

Figure 3.1 Pressure trace (left), temperature trace (middle), and heat release (right) from experiment at T_{in} = 373 K, Q_{in} = 1400 J, n = 1200 rpm (*solid*) and n = 1500 rpm (*dashed*).

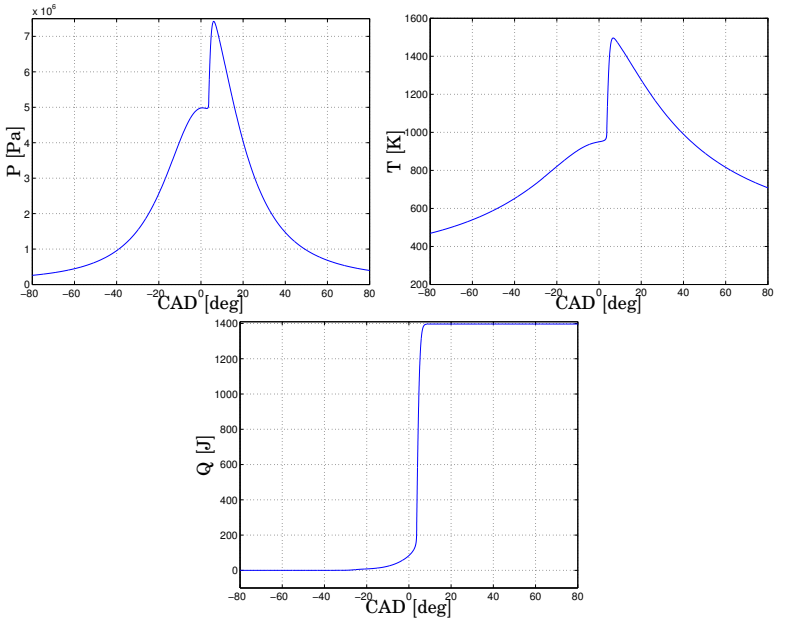

Figure 3.2 Pressure trace (left), temperature trace (middle), and heat release (right) of simulation at nominal conditions, T_{in} = 373 K, Q_{in} = 1400 J, n = 1200 rpm for PRF90 fuel.

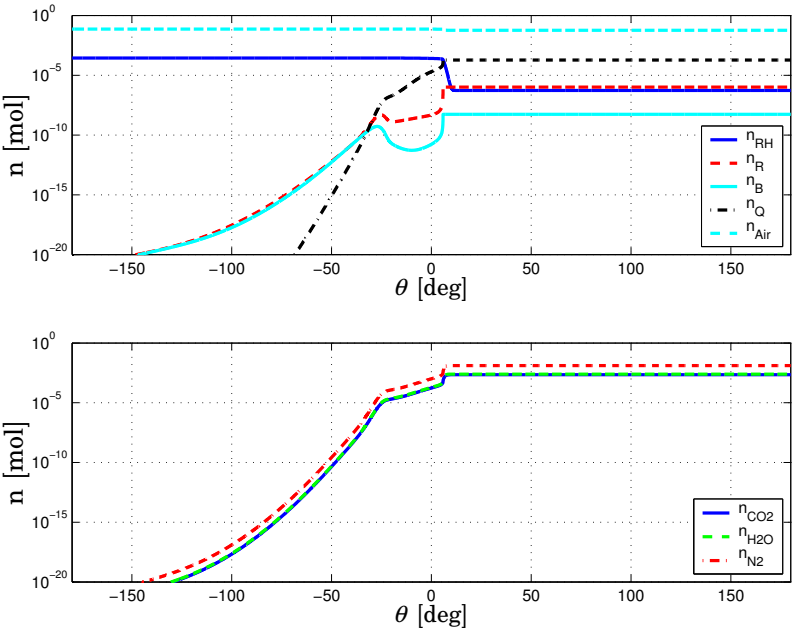

Figure 3.3 Concentrations of gas species from Shell model ignition dynamics for nominal conditions, $T_{in} = 373$ K, $Q_{in} = 1400$ J, $n = 1200$ rpm for PRF90 fuel.

Phasing effects on α_{50} from variations of inlet temperature, fuel energy and engine speed according to Tables 3.2 and 3.3 are summarized in Fig. 3.4. It can be noted that the Shell model gives quite accurate estimation of the phasing for the temperature and the engine speed sweep. The model is slightly less accurate when changing the load, but still gives the correct trend.

Results from simulations using the integrated Arrhenius model are also shown in Figure 3.4. This method gives good results for load variations. The results for speed variations are less accurate at higher speeds. However, the model fails at variations of the inlet temperature.

In order to compare the ignition prediction accuracy of these low complexity models with more refined ones, results from homogeneous calculations using detailed chemical kinetics are included in Figure 3.4. Here, detailed chemistry for an ethanol/n-heptane mixture was obtained through the Planet mechanism for PRF fuels. For more details on the physical and chemical modeling, see references [Amnéus, 2002; Ahmed *et al.*, 2003]. From Figure 3.4 it can be observed that the Shell model gives similar results of prediction of α_{50} as the Planet mechanism for inlet temperature

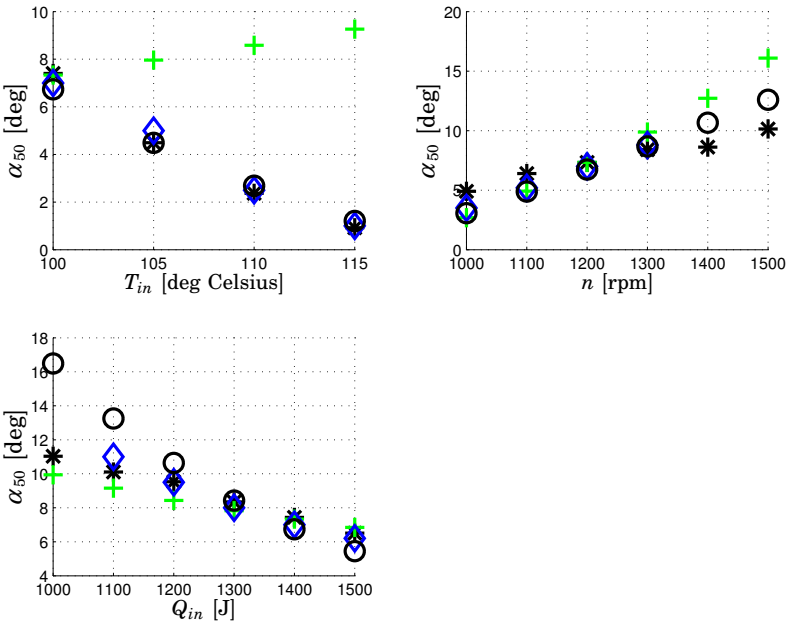

Figure 3.4 Effects on combustion phasing of variations from nominal conditions, $T_{in} = 373$ K, $Q_{in} = 1400$ J, $n = 1200$ rpm. The experimental results are marked as '*', the Shell model results with 'o', the Arrhenius Rate Integral results with '+', and the Planet mechanism with '◇'.

variations. This observation is also true for the speed variations. But in the case of load variation the Planet mechanism gives significantly better result.

3.3 Discussion

The results indicate that the proposed model may be used for studies on feedback strategies for ignition control. Qualitative phasing behavior is correctly reproduced at variations in inlet temperature, engine speed, and load.

The simulation model was only crudely calibrated and the quantitative results are expected to improve with calibration. The Shell-model parameters of [Halstead *et al.*, 1977] are from experiments on a rapid compression machine. Preliminary attempts with manual tuning of the parameters have shown to yield better agreement with the ignition pro-

cess in a heavy-duty engine.

The proposed model performed better than the integrated Arrhenius model in the comparisons. It should be noted that the results were obtained with nominal PRF90 parameters from the literature. The latter model has an advantage of having few parameters and engine specific calibration is likely to be easier. As in [Thurns, 1996], the integral expression can also include explicit temperature dependence, which also was included in [Shaver *et al.*, 2004]. It may then be possible to improve the results for temperature variations. In the prediction of α_{50}, the Shell model gave almost similar behavior as the detailed chemistry Planet mechanism, indicating that low complexity models can be used on feedback strategies for ignition control.

Presently, the model contains single-cylinder behavior for single-cycle simulations in steady-state only. It is of interest to study transient effects over multiple cycles. This requires the inclusion of gas-exchange models, wall heat dynamics, etc.

The Shell autoignition model is only applicable for single-component fuels. Therefore, no simulation results are presented to show the phasing effects of varying the fuel ratio. A possible extension of the model is to include multi-component fuels. Parameters for a number of PRF fuels are available in the literature [Halstead *et al.*, 1977]. These may be used to describe fuel quality variations, with restrictions to a limited set of fuel ratios. However, ignition control using dual fuels is a less practical approach, as it requires new infrastructure and the consumer would need to refuel two fuels. Instead, the current trend is to use variable valve phasing for which the proposed model is straightforwardly applicable in its current form.

The experiments were performed in open-loop at low load conditions. The applicability of a model calibrated from low load experiments at high load conditions need to be further investigated. For high-load experiments it is necessary to apply closed-loop control of combustion phasing.

3.4 Summary and Concluding Remarks

The results presented indicate that a fairly low complex autoignition model may be used to predict phasing behavior of HCCI engines at low load. The Shell model used for detecting autoignition of HCCI combustion gives qualitative correct reproduced phasing behavior at variations in inlet temperature, engine speed and load. The suggested model has a decent ratio between complexity and accurate prediction of the combustion phasing in HCCI.

4

Sensors and Actuators for HCCI Control

In this thesis, control was an objective all from the beginning and there were few limitations of which sensors should be used. The HCCI combustion depend on for example temperatures, pressures and engine speed. Therefore, sensors are vital in control of HCCI engines. The combustion phasing signal is the most important measurement, but other sensors measuring the state of the engine are also important. For example, the temperature of the exhaust gas gives indication of state of the engine. The sensor measuring the combustion phasing need to have high bandwidth as it measure the ongoing combustion, and the combustion phasing is preferably used for cycle-to-cycle control. The actuator must be capable of cylinder individual control of the engine in a large operating range. This chapter discusses the sensors available today and actuators for HCCI feedback control.

4.1 Sensors

The sensors may be divided into two classes, the ones which are used for measuring the on-going combustion and the ones which measure the result of the combustion and the engine state, measuring on cycle-to-cycle basis or slower. The sensor demands differs, both from a bandwidth and environmental point of view and hence the division. The purpose for measuring the on-going combustion is to estimate the combustion phasing, α, which is needed to control the HCCI combustion.

Combustion Phasing Sensors

Combustion phasing sensors provide feedback on the current combustion lapse. The sensor technologies for combustion phasing have not been thor-

oughly investigated by the author, as only some of the various technologies have been used.

Piezo-Electric Pressure Transducer The transducer works by emitting an electronic signal proportional to the deflection of a diaphragm when exposed to cylinder pressures. The transducer is able to measure changes in the pressure, but not absolute measurement. Absolute measurement can be obtained by estimation of the offset. The transducer has a wide frequency response and is linear over a large range. The pressure transducer could measure the full cylinder pressure trace or only the peak pressure. A peak pressure sensor traditionally measures the pressure through the cylinder block, resulting in distortion of the phase. Still, it can approximately estimate the peak pressure. Today there exist several low-cost piezo transducers [Sellnau *et al.*, 2000; Shimasaki *et al.*, 2004]. The accuracy of these low-cost sensors is probably sufficient for feedback control of HCCI combustion phasing.

Optical Pressure Transducer Measuring the light intensity reflected from a metal diaphragm. The sensing element of the pressure transducer is essentially a Fabry-Pérot type optical interferometer. The geometry and material of the transducer are selected in order to obtain a linear relationship between the deflection of the diaphragm and the applied pressure. Currently, the optical pressure transducers are less accurate than the best piezo-electric pressure transducers [Roth *et al.*, 2002].

Ion Current An alternative to the use of the pressure transducers is to use the electronic conductive properties for the reaction zone. The phenomenon is called ion current for which no expensive sensor is needed, instead a standard spark plug can be used [Gillbrand *et al.*, 1987; Reinmann, 1998; Eriksson *et al.*, 1997]. The basic principle of ion current sensing is that a voltage is applied over an electrode gap inserted into the actual gas volume (combustion chamber). In a non-reacting charge, no ion current through the gap will be present. In a reacting (burning) charge, however, ions that carry an electrical current will be present. This means that the ion current reflects the conditions in the gas volume. A standard spark plug can be used as sensor, having the benefits of low cost, long lifetime and a straight forward mounting in comparison with pressure transducer. The drawbacks with ion current sensing is that it gives only local information, but if the charge is homogeneous a local measurement is sufficient. The ion current signal is dependent on the fuel properties and operating conditions. Today, ion current measurement is mostly used for misfire and knock detection in SI engines [Reinmann, 1998]. The common belief so far has been that ion current levels are not measurable for

the highly diluted HCCI combustion. However, recent studies show that it is not the dilution level in itself but the actual fuel/air equivalence ratio which is an important factor for the signal level [Franke, 2002; Strandh *et al.*, 2003].

Sound Sensor Sound sensors today used in SI engines for knock detection could possibly also be used for detecting the combustion phasing. But today, there exist no sound sensor that fulfill the high demands which HCCI engine control require from the sensor. It has to be able to give a robust detection of the combustion phasing at different operating conditions, for example todays sound sensors have difficulties when operating at low load.

Engine State Sensors

Sensors measuring the result of the combustion and engine state, has not the demand of very high bandwidth and tough environment conditions as the ones measuring the on-going combustion. It is desirable that the bandwidth is sufficient for cycle-to-cycle sampling. But several sensors such as temperature and emission sensors can not fulfill this requirement.

Pressure Sensors Pressure transducers measuring the pressure at different locations in the engine system, typically pressures in the range of 1-3 bar. The standard type is piezo-resistive, which does not need any charge amplifier and is mounted in a current loop.

Temperature Sensors Temperature is measured using thermocouple. There exists several thermocouples having different operating conditions and bandwidth. Whereas the bandwidth of todays temperature sensors has increased, they can still not measure on a cycle-to-cycle basis. Hence, such sensor can not be used for in-cycle measurements.

Engine crank sensor Engine speed is measured using an encoder. The encoder could be optic, magnetic or capacitive.

4.2 Actuator Alternatives

In control of HCCI engine, several means to actuate the combustion phasing have been suggested [Olsson *et al.*, 2001b; Agrell *et al.*, 2003; Christensen *et al.*, 1999; Martinez-Frias *et al.*, 2000]:

- Dual fuels
- Variable valve actuation

- Variable compression ratio
- Thermal management

They all fulfill the requirement of fast actuation which is needed to control the combustion phasing, but all have their benefits and drawbacks.

Dual Fuels

The idea of using dual fuels is to use two fuels with different auto-ignition properties. The system will have a main fuel with a high octane number and a secondary fuel with low octane number [Olsson *et al.*, 2001b]. This feature can then be used to control the combustion phasing in HCCI as blending the two fuels at different fuel ratio changes the auto ignition properties. When the combustion phasing needs to be advanced, the fuel ratio of the secondary fuel amount is increased resulting in an earlier combustion phasing. When the secondary fuel (low octane number) starts reacting, it will also advance the reacting of the primary fuel with high octane number, resulting in a simultaneous combustion of the two fuels [Tanaka *et al.*, 2003b]. For cylinder individual control of the combustion phasing, each cylinder must have two injectors. The benefit with dual fuels is that it provides an accurate control without any large engine modifications. No expensive system or modifications are needed, only two traditional injectors. One drawback is that it requires carrying and refueling two fuel tanks. Whereas the amount of the secondary fuel being consumed would be minimal, the tank could be refueled only at the maintenance intervals. Ideally, the secondary fuel would be produced on board. A second drawback is that the two fuels used might not be the ones which today are supplied at a gasoline station and new infrastructure for the fuels is needed.

Variable Valve Actuation

Variable valve actuation (VVA)—also called variable valve timing (VVT)—can be used to changed the compression ratio of the engine. As the compression ratio strongly affects the combustion phasing, control can be achieved over a wide range of operating conditions. An HCCI engine using VVA has typically a high compression ratio and can obtain lower compression ratios by delaying the closing of the intake valve during the compression stroke. A full flexible VVA also has the benefit that it can change the temperature and composition of the incoming charge by rebreathing the residual gases from the previous cycle into the cylinder. With a full VVA system the timing for the inlet valve opening, IVO, inlet valve closing, IVC, exhaust valve opening, EVO and exhaust valve closing, EVC can be changed. Today there exists several fully flexible

VVA systems, which are either electro-mechanic [Pischinger *et al.*, 2000], electro-magnetic [Theobald *et al.*, 1994] or electro-hydralic [Law *et al.*, 2001]. One of the most advanced VVA system in production cars is today the BMW valvetronic system [Flierl *et al.*, 2001], which is electro-mechanic. The drawback is that for HCCI combustion phasing control, fully cylinder-individual VVA systems are needed, which today still are expensive and complex. Use of VVA for control of HCCI is a growing interest and there are both modeling and experimental results [Agrell *et al.*, 2003; Babajimopoulos *et al.*, 2003; Milovanovic *et al.*, 2004; Shaver *et al.*, 2004].

Variable Compression Ratio

The variable compression ratio (VCR) can be used to control combustion phasing by increasing the compression ratio and the charge temperature after compression. With a higher charge temperature, the charge auto-ignites at lower temperature and earlier in terms of crank angle. VCR can be achieved by several different methods. One method is to tilt the upper part of the engine block, the monohead. A hydraulic motor, controlled by an electronic valve turns the eccentric shaft [Haraldsson *et al.*, 2002]. Another method is to mount a plunger in the cylinder head whose position can be varied to change the compression ratio [Christensen *et al.*, 1999]. The two mentioned methods are just two of todays existing methods of obtaining VCR. The drawbacks are that VCR system currently does not allow cylinder individual control, which is necessary to obtain good combustion phasing control, and that they are expensive and complex.

Thermal Management

Fast Thermal management, FTM, can be used to control the temperature of the mixture at the beginning of compression stroke [Haraldsson *et al.*, 2004]. The temperature strongly affects the combustion phasing, resulting in a wide range of operating conditions, and Martinez-Frias et al. demonstrated that thermal management could be used for HCCI control [Martinez-Frias *et al.*, 2000]. A method to achieve fast thermal management control of the inlet temperature is using a source of cold ambient air and a source of hot recovery-heated air. By controlling the valves of the two air flows, cycle-to-cycle control of the inlet temperature can be achieved. The benefit of this method is that it does not require major engine modifications or use of fuel additives. The drawback is that the engine system has to be fitted with a heater.

4.3 Summary and Concluding Remarks

In this chapter available sensors and actuator alternatives for controlling an HCCI engine were presented. In this thesis, dual fuel and VVA were used as a means to control the combustion phasing. The dual-fuel approach has the benefit of not require major engine modification and provides accurate control, even if there is wall wetting and possible fuel splash. The engine was also equipped with a VVA system, which is a solution more suited for production, as it does not require the consumer to refuel two fuels or any other new infrastructure.

5

Experimental Set-up

For this thesis, experiments were performed on two engines: a multi-cylinder Volvo D12C and a single cylinder Volvo TD100. Originally, both engines were Diesel engines, but they were modified to use port fuel injection, PFI, and to run in HCCI operation. The same data acquisition system was used for both engines and the data sampling was crank angle based. A sample of the in-cylinder combustion sensor was taken at each 0.2 crank angle degree. This resulted in a system where the number of samples and crank angle value were independent of the operating point. This is a feature which is valuable both for the control and study of the HCCI concept. The multi-cylinder Volvo D12C was used for control studies and the one-cylinder Volvo TD100 engine was used for in-cylinder combustion sensor evaluation and control studies.

The goal with the experimental set-up was to provide several means to control in a large range of operating conditions and to this purpose appropriate sensors and actuators are needed. The actuators and sensors used are described in this chapter. In order to control the inlet temperature, an intercooler and a heater was added to the engine. An intercooler works as a large heat exchanger which removed heat from the intake charge air. One way to change the gas mixture was to use Exhaust Gas Recirculation, (EGR) measured by the percentage of the total intake mixture which is recycled exhaust. Hence, a long route EGR system including cooler was added to the engine.

5.1 Multi Cylinder Volvo D12C Engine

The engine was a modified turbo-charged Volvo D12C engine with a displaced volume of 12 liters. Originally, the engine was a Diesel engine, but the original injection system was removed and replaced by a low-pressure, sequential port fuel injection system.

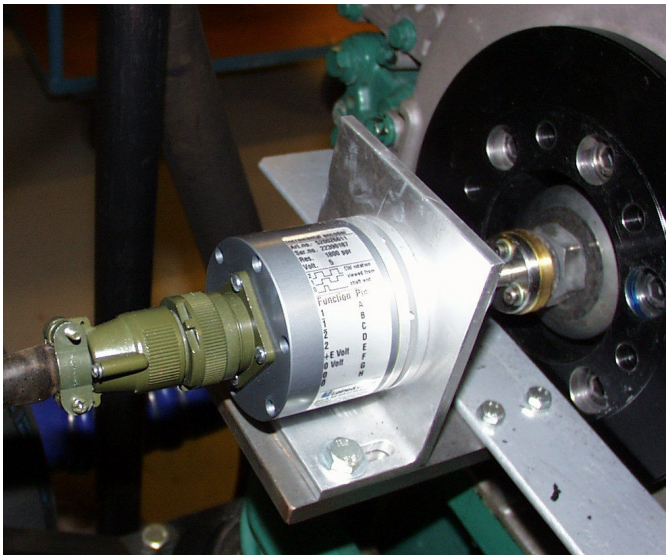

Figure 5.1 The encoder mounted on the front of the engine.

Table 5.1 Multi cylinder D12C engine specifications.

Operated cylinders	6
Displaced Volume	2000 mm^3
Bore	131 mm
Stroke	150 mm
Connecting Rod Length	260 mm
Number of Valves	4
Compression Ratio	18.5:1
Fuel Supply	PFI

The engine has four valves per cylinder heads, two inlet ports and two exhaust ports and the geometric properties for the engine are summarized in Table 5.1. An encoder was mounted on the crankshaft sending five pulses per crank-angle degree (Fig. 5.1). These pulses were used by the dual-fuel injection system to know when to start the injection and by the data acquisition system. Engine speed was governed by an electrical motor with the capability both for braking and motoring. The electrical motor had the effect of 355kW and was produced by ABB.

In the beginning of this project, only the engine existed and during this project the control and measurement system were built. The set-up was developed in close cooperation with Petter Strandh at Division of Combustion Engines and Petter is the major contributor on the aspects of design of the set-up and the data acquisition and actuation program.

Air Management System

The engine was equipped with a Variable Geometry Turbo (VGT) which made it possible to adjust the boost pressure. The VGT was changed manually. It also had an intercooler and an inlet air heater for controlling inlet air temperatures. Figure 5.2 shows a schematic outline of the engine and the air management system. The electrical heater, with capacity of 35 kW, was controlled by a PI controller. The intercooler and EGR cooler were stainless steel water/air heat exchangers. The intercooler and EGR cooler was controlled by PD controllers.

Dual Fuel Injection System

The engine was equipped with a dual-fuel system. Two injectors were mounted just upstream of the inlet port of each cylinder. This configuration resulted in: the two fuels and air were mixed and the fuel amount could be individually adjusted for each cylinder and for each fuel. The dual fuels used were ethanol and a fifty-fifty mixture of n-heptane and ethanol. The use of a mixture instead of pure n-heptane was to improve precision of the control. The dual fuels give research octane number (RON) ratings from 53 up to 106. The fuel injection system operated according to the same principles as a commercial port fuel injection system in a passenger car. The fuel is held at constant pressure in relation to the intake manifold pressure to maintain a constant fuel pressure drop across the injector. The injector opened once per every engine cycle with a differential pressure around 3 bar. Then, the injected fuel amount was dependent on the duration of the fuel injector being activated. The twelve injectors, two for each cylinder, were controlled by one PIC processor each. PIC stand for Peripheral Interface Controller and these low cost processors are used in many applications where small, programmable processing is useful. The PIC processors controlled the injectors via fiber optic cables. The fuel injection cycle begins at the top dead center gas exchange. The start of injection and injection duration must be programmed to the PIC before this point, in order to achieve cycle-to-cycle control.

Variable Valve Actuation System

During the project the engine also was equipped with a Variable Valve Actuation (VVA) system driven by the cam shaft. The system used is

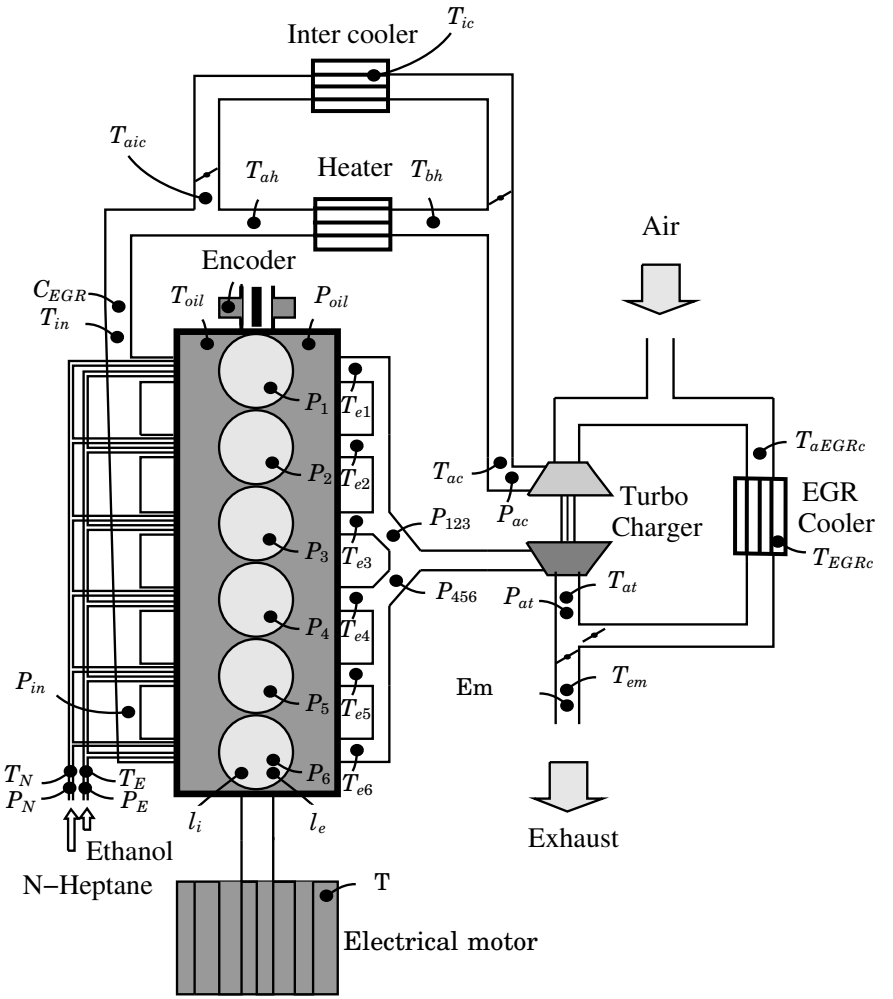

Figure 5.2 The Volvo D12C engine set-up

usually referred as a *lost motion system* as the maximum valve timing is determined by the cam lobes and earlier valve time closing can be regarded as a lost movement. The system was driven by the cam shaft and works by allowing the inlet valve to be closed ahead of the cam curve. It was, however, not possible to close the inlet valve later than the cam curve. The inlet valves were operated by use of hydraulics. The cam shaft pushed on a hydraulic cylinder which in turn supplied oil to a second

hydraulic cylinder which was used to move the inlet valve. There was an electronically controlled valve in between the two hydraulic cylinders. If the electronic valve was activated, oil could be transfered between the two hydraulic cylinders. If the electronic valve was inactive no oil was supplied to the second cylinder. If the intake valve was lifted and the electronic valve was deactivated, the inlet valve will be closed and thus resulting in an earlier closing of the intake valve. The VVA system was a commercial electro-hydraulic system for research.

Sensor Locations

The objective was to control the HCCI combustion. As HCCI operation is very dependent on the temperature, pressure, air-fuel mixture, several sensors are needed to obtain desired operating conditions. It is important to control the inlet temperature, in order to have a large operating range as the cycle-to-cycle control actuators has limited effect on the combustion phasing. To this purpose control of the heater, the inter cooler and the EGR cooler were needed and hence several sensor measuring suitable temperatures were needed. The engine wall temperature is today very difficult to measure and instead the exhaust temperatures and oil temperatures were measured. These measurements give indication of the slow trend of the engine wall temperature changes. The engine was equipped with an VGT and hence several pressure measurements were of interest. Not all of the sensors had direct control application, instead the purpose was to monitor the engine state. The measured signals are summarized in Table 5.2 and Fig. 5.2 shows the location of the gauges.

Table 5.2: Measured signals

Signal	Description
P_1	Cylinder pressure cylinder 1
P_2	Cylinder pressure cylinder 2
P_3	Cylinder pressure cylinder 3
P_4	Cylinder pressure cylinder 4
P_5	Cylinder pressure cylinder 5
P_6	Cylinder pressure cylinder 6
T_{e1}	Outlet temperature cylinder 1
T_{e2}	Outlet temperature cylinder 2
T_{e3}	Outlet temperature cylinder 3
T_{e4}	Outlet temperature cylinder 4
T_{e5}	Outlet temperature cylinder 5

Table 5.2: (continued)

Signal	Description
T_{e6}	Outlet temperature cylinder 6
P_{123}	Outlet pressure for cylinder 1,2 and 3
P_{456}	Outlet pressure for cylinder 4,5 and 6
T_{at}	Temperature after turbo
P_{at}	Pressure after turbo
T_{em}	Emission temperature
Em	Emissions
T_{EGRc}	EGR cooler temperature
T_{aEGRc}	Temperature after EGR cooler
P_{ac}	Pressure after compressor
T_{ac}	Temperature after compressor
T_{bh}	Temperature before heater
T_{ah}	Temperature after heater
T_{ic}	Intercooler temperature
T_{aic}	Temperature after intercooler
C_{EGR}	EGR concentration
T_{in}	Inlet temperature
P_{in}	Inlet pressure
T_N	Temperature of N-heptane
P_N	Pressure of Ethanol
T_E	Temperature of N-heptane
P_E	Pressure of Ethanol
T_{oil}	Oil temperature
P_{oil}	Oil pressure
l_i	Inlet valve lift cylinder 6
l_e	Exhaust valve lift cylinder 6
T	Engine torque

The types of pressure, temperature and valve lift sensors used:

Cylinder pressure transducer The cylinder pressure was measured with a piezo-electric pressure transducer. The pressure transducers used in the experiments were water-cooled Kistler 7061B pressure

transducers. The calibrated pressure range for the transducer was 0–250 bar and the natural frequency was 45 kHz [Kistler 7061 B, 2004]. The transducers were mounted in a bored pipe, where the transducers were flush mounted. This is important as otherwise the resonance frequency in the pipe will affect the pressure measurements and degrade the resolution of the measurements. An example on the pipes length effect on the resolution can be found at p. 480 in [Egeland and Gravdahl, 2002].

Pressure transducer The pressure transducers measuring the pressure outside the cylinders, for placement see Fig. 5.2, were Keller PAA-21S. Two types with different measuring range were used. Range was 0-5 bar or 0-10 bar [Keller PAA-21S, 2004]. The pressure transducers measured the absolute pressure.

Temperature sensor Thermocouples of type K from Pentronic were used in the experiments [Pentronic, 2004]. The Thermocouples measured the absolute temperatures.

Engine crank sensor The engine crank encoder was an incremental encoder from Leine & Lindes [Linde, 2004]. The encoder had the resolution of 1800 pulses per revolution.

Valve lift sensor For measuring the valve lift of the inlet and exhaust valves, a Hall element was used.

5.2 Measurement Aspects

The signal-to-noise (SNR) ratio gives indication on how much influences the noise have on the measurements. The single most important measurements are the cylinder pressure which is directly used for estimation of the combustion timing α. In Fig. 2.6, a visual indication on the SNR and its variation for the cylinder pressure is given. The SNR is calculated using the energy of the signal, y, and the noise, v.

$$SNR = \frac{e_{yy}}{e_{vv}} \tag{5.1}$$

$$e_{yy} = \sum y(k)y(k) \tag{5.2}$$

$$e_{vv} = \sum v(k)v(k) \tag{5.3}$$

In Table 5.3 SNR for cylinder pressure, inlet pressure, and inlet temperature at different operating conditions and crank angles, at IVC, TDC and peak pressure. Notice that even in the case that the engine is natural

Table 5.3 Signal-to-Noise Ratio

	P_{cyl} (1.0 bar)			P_{cyl} (2.4 bar)			P_{in}	P_{in}	T_{in}	T_{in}
Pos.	IVC	TDC	PP	IVC	TDC	PP	1.0bar	2.4bar	45°C	100°C
SNR	58.8	1.1e5	3.9e5	305	7.4e5	2.5e6	2.9e4	4.1e5	1.4e5	5.0e5

aspirated (1.0 bar) the SNR is 58.8. The combustion starts around TDC and at that point the SNR is 1.1e5 or more. The operational engine speed varied from 600 to 2000 rpm. Typical maximum engine speed for an heavy duty engine is around 2000 rpm. A sample of the cylinder pressure sensor is taken every 0.2 CAD or 5 times for each CAD. Then the sampling frequency in the case of 2000 rpm is

$$F_s = 2000 \cdot \frac{360}{60} \cdot 5 = 60\text{kHz} \tag{5.4}$$

Data Acquisition and Control Cards

The used data acquisition and control cards were:

Microstar DAP 5400a/627 The Microstar DAP 5400a/627 is a fast parallel sampled data acquisition card for real-time application under Linux or Windows. It had 16 analog inputs and 8 separate 1.25 MHz AD-converters with 14 bits resolution. The cylinder pressure data acquisition was controlled by an encoder connected to the crank shaft of the engine. The resolution of the encoder was 1800 pulses per revolution, resulting in that a cylinder pressure sample was taken at every encoder pulse, i.e., every 0.2 crank angle degree. As soon as one cylinder passed EVO, pressure data were transferred from the AD card to the main program. The cylinder pressure only used six of the channels. The other channels were also used, but the signals changed through the experiment. The inlet temperature often occupied one of the spare channels, resulting in that the inlet temperature was sampled both with the Microstar card and the HP logger.

HP 3852A The HP logger sampled the various temperatures and pressure and the engine torque. The logged data were sent to the main program. The sampling rate of the logger was 0.4 Hz. The logger actuated the voltage level to the intercooler and the EGR cooler.

NI 6014 The NI 6014 is a multifunction analog, digital, and timing card. In the experiments, it was used to actuate the voltage level for the heater. This was done once per each engine cycle.

Exhaust gas analysis The exhaust gas analysis system was from Boo instrument providing software and system integration. The system consisted of: A flame ionization detector from JUM Engineering for measuring the HC level in the emissions; A chemoluminescence detector for of measuring NOx level in the emissions, the detection principle relying on that fact that mixing NO with ozone produces a light-emitting reaction; Three SICK-MAIHAK analyzers were used to measure the CO, CO_2 and O_2 level in the emissions. The exhaust gas analysis system was also used to estimate the air/fuel ratio.

Control Architecture

The engine was controlled by combined data acquisition and engine control system. The engine control system ran on a standard PC (Pentium 4 2.4 GHz) with GNU/Linux operating system. The distribution used was Red Hat 8. The main program was written in C++. The combustion timing controller was designed in Simulink and converted to stand alone C-code using the automatic code generation tool of Real Time Workshop. Then, the C-code was compiled to an executable program communicating with the main program. FIFO pipes[1] were used for the communication between the combustion timing controller and the main program. This feature gave a system where controllers were easily implemented and put into operation. The controllers could also be replaced on-line without restart of the system. This property saved a lot of time when new controllers were tested. The heater and the two cooler controllers were implemented directly in C++. In order to assure good real-time performance, the data saving on disk was run as a separate thread with low priority.

All data coming from various sensors around the engine were collected in the main program (Fig. 5.3). These data included various temperatures and pressures collected via a data logger, sampling at low sampling rate, various temperatures and cylinder pressures collected via a Microstar DAP, sampling at fast sampling rate, and exhaust emissions data from the emission system sampling at low sampling rate. The program used four threads: Main thread, which collected the cylinder pressure and perform the control; Logger tread, which collected data from the data logger; Emission treads, which collect data from the emission system; Saving tread, which was active when the data were saved. The firing order for the cylinders was [1 5 3 6 2 4]. An engine cycle is 720 crank angle degrees with combustion cycle every 120 crank angle degree.

Even if the main program had several threads, the fuel control was sequential and the steps could be summarized as:

[1]Pipe is an interprocess communication (IPC) method which you can use to link C programs and C++ programs with each other

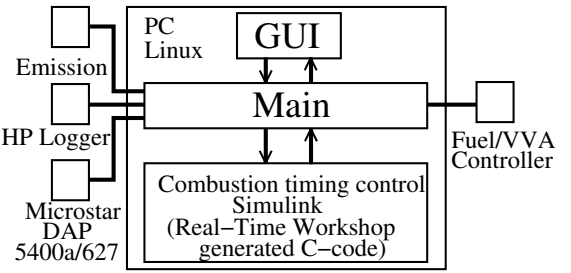

Figure 5.3 Schematic view of the data acquisition and control system

1. The cylinder pressure data were sampled by a Microstar 5400A/627 data acquisition processor. As soon as one cylinder passed Exhaust Valve Opening, pressure data were transferred from the AD card to the main program. As a result, a pressure segment was sent every 120 crank angle degree, the segmentations being shown in Fig. 5.4. The pressure segment consists of pressure data for all six cylinders. When six segments were received, the total pressure trace for the engine cycle was received. The segmentation size was chosen as a trade-off between having sufficient cylinder pressure data in order to be able to do simple heat release calculations as early as possible and guaranteeing enough time for sampling of cylinder pressure.
2. When a new pressure segment was available in the main program, a simplified rate of heat release calculation was performed on the cylinder next in fire order, where control inputs such as combustion timing α, peak pressure and pressure gradient were sent to the combustion timing controller.
3. The combustion time control signal, i.e., the output from the dual fuel or VVA controller, was then sent back to the main program and the fuel injector was programmed with a new fuel setting. The fuel injection cycle began at the TDC gas exchange point (TDC_{GE}). In order to have true cycle-to-cycle control, the injection duration had to be determined and programmed prior to TDC_{GE} which was achieved.

Conditional upon limits for cylinder peak pressure and pressure gradient, the main program had an engine check feature that could cut the fuel injection immediately.

To summarize, the input variables which could be controlled in the set-up, were the inlet temperature, inlet pressure, engine speed, injected fuel

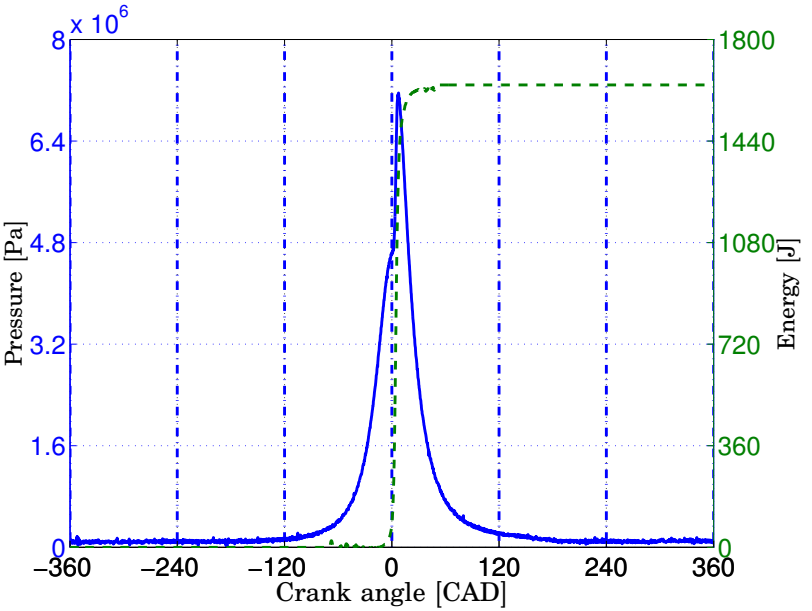

Figure 5.4 A typical pressure and heat release curve with the segmentation (*dash-dotted*), pressure curve (*solid*) and the heat release curve (*dashed*).

energy, fuel ratio between dual fuels and the effective compression ratio using VVA. Some of these variables interact. For example, the VGT can be used to change the inlet pressure, but also the temperature affect the inlet pressure. By changing the effective compression ratio with VVA also the λ value was effected. This kind of interactions complicated the control. The fuel ratio and the total injected fuel energy also interacted, in the sense that when the total energy was increased, the transient behavior of the λ depended on the fuel ratio. It could move to earlier or later timing. It depended on the heat of vaporization value of the mixture. A schematic view of the control structure is shown in Fig 5.5.

5.3 Single Cylinder Volvo TD100 Engine

The engine was a modified turbo-charged Volvo TD100 engine. Originally, the engine was a Diesel engine, but the original injection system was removed and replaced by a low-pressure, sequential port fuel injection system. The engine was an in-line six cylinder engine, modified to operate

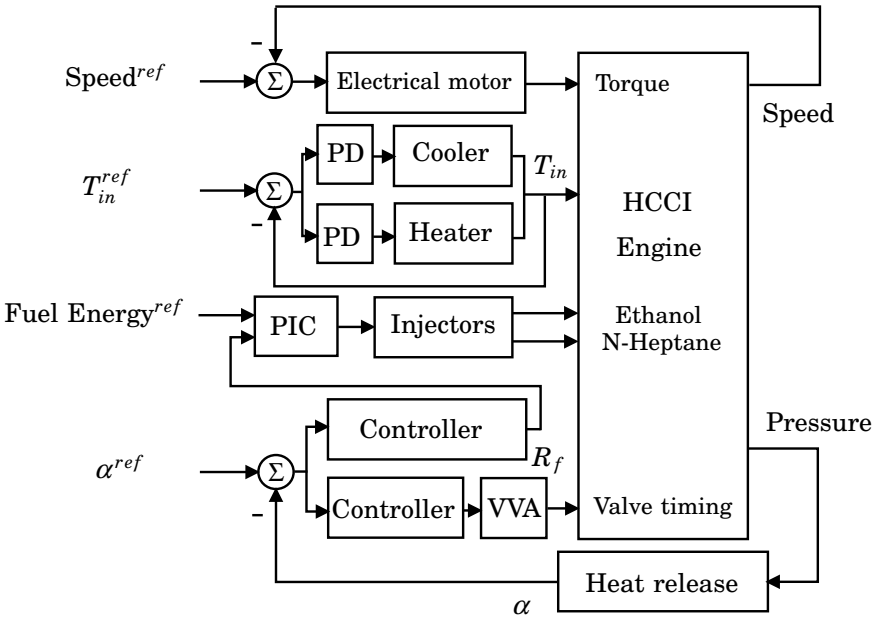

Figure 5.5 Block diagram of the control structure

on one cylinder. It is operated on cylinder 6, which is the cylinder closest to the flywheel. The other five cylinders were motored. The engine had two-valve cylinder heads, one inlet port, one exhaust port and the geometric properties for the engine being summarized in Table 5.4. An encoder was mounted on the crankshaft sending five pulses per crank angle degree. These pulses were used by the dual fuel injection system to monitor the start of injection and by the data acquisition system. Engine speed was governed by an electrical motor with the capacity for both braking and motoring.

Previously, this engine was used in several projects but, then, with an other data acquisition system.

Air Management System

The engine was equipped with an inlet air heater and long route EGR. The engine was operated with natural aspiration. Figure 5.6 shows a schematic outline of the engine and the air management system. The electrical heater, with a capacity of 10 kW, was controlled by a PI controller.

Table 5.4 Single cylinder engine specifications.

Displaced Volume	1600 cm^3
Bore	120.65 mm
Stroke	140 mm
Connecting Rod Length	260 mm
Number of Valves	2
Compression Ratio	15.5:1
Fuel Supply	PFI

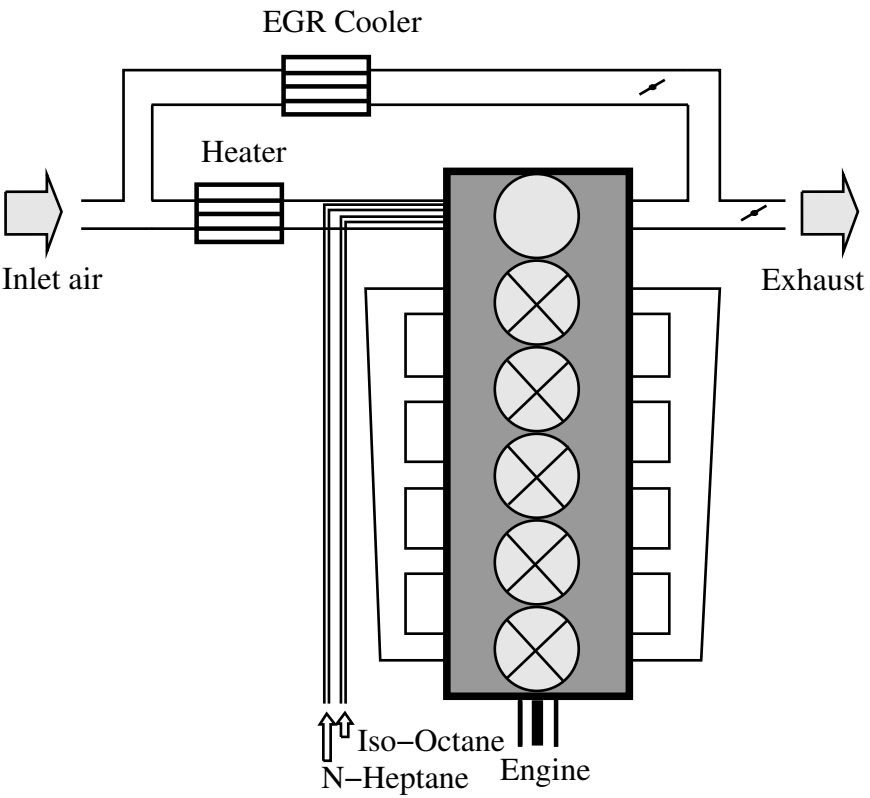

Figure 5.6 The Volvo TD100 engine set-up

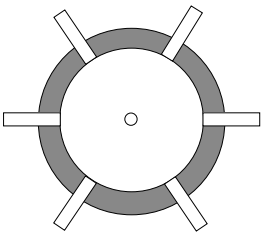

Figure 5.7 The spacer and the placement of the 7 modified spark plugs and the pressure transducer. The seventh spark plug is the normal center position of a spark plug in a SI engine.

Dual Fuel Injection System

The engine had a identical dual fuel injection system as the Volvo D12C engine. The only difference was that Iso-Octane was used instead of Ethanol.

Sensors

Experiments with a conventional spark plug with and without its side electrode removed were performed. The spark plug was used as an ion sensor, and it was mounted in the spacer placed between the cylinder head and engine block. The spacer had 6 evenly spaced radial 14mm fittings, which accommodated modified spark plugs (Fig. 5.7). The idea with a spacer was Andreas Vressner's, Ph.D. student at Division of Combustion Engines, who at the time also ran ion current experiment on the engine. The only modification of the spark plugs was the removal of the side electrode. The experiments without the spacer were performed both with standard spark plugs and with modified spark plugs. Figure 5.8 shows the principal layout of the measuring system. A DC voltage (U) of 85 V was applied across the electrode gap. The ion current was sampled by measuring the voltage over a resistance (R) of 100 kΩ, inserted in the electrical circuit. Since the signal current level was low, in the order of one μA or lower, it was amplified before the A/D conversion was made. The amplifier had a gain of 23 and a bandwidth of 330 kHz.

For measuring the cylinder pressure, a pressure transducer was fitted to the engine for control and monitoring (Fig. 5.7). The pressure transducer was of the same type as in the Volvo D12C engine set-up.

Data Acquisition and Control Cards

The same data acquisition and control cards as in the Volvo D12C set-up was used.

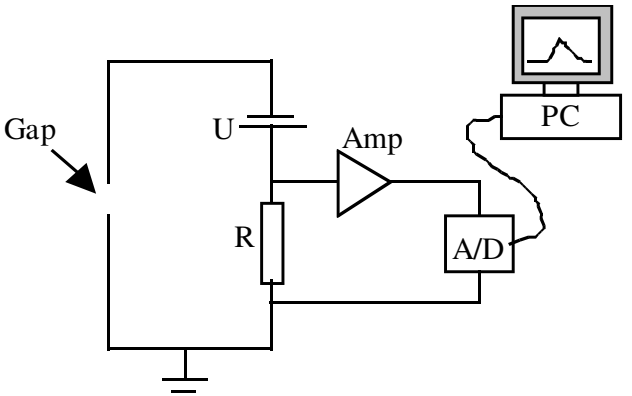

Figure 5.8 Schematics of the ion current measuring system.

Control System

The same control system as in the Volvo D12C set-up was used. The only differences were the modification to control only one cylinder and that the heater was controlled by a separate computer.

5.4 Graphical User Interface

The user interface allowed manual control of injection and control valve lift timing as well closed-loop control. Closed-loop control could be performed with different controllers, but only one controller could be loaded at each time. If a PID controller is active then the PID-parameters could be set by the user interface. The user was continuously updated with pressure curves and heat release curves for the six cylinders. Also the current values of α_{50}, injected fuel energy, $IMEP_{net}$, peak pressure, maximum pressure increase, fuel ratio and IVC timing as well as various temperatures were presented. Figure 5.9 shows a screen snapshot during an open-loop control experiment.

5.5 Fuel property and fuel injection system

The fuels used for the 12 l heavy duty engine were ethanol (C_2H_5OH) and n-heptane (C_7H_16). Ethanol has been shown be an excellent fuel for HCCI [Christensen *et al.*, 1997]. It has high resistance to autoignition, together with a high heat of vaporization. The high autoignition resistance

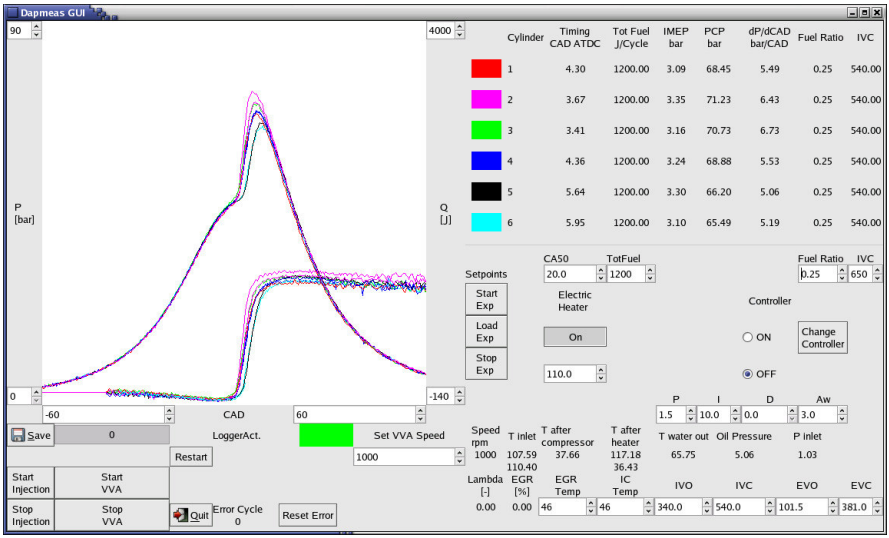

Figure 5.9 A screen snapshot of the GUI during an experiment.

property makes it suitable for control of HCCI combustion at higher loads. N-heptane, is quite the opposite of ethanol. It is very reactive and auto-ignites easily. N-heptane is used as a norm when testing octane ratings and by definition it has the octane number of 0.

As open-loop experiments and control studies were performed, soot could have been a problem. An advantage of using these two fuels are that there were no problem with soot formation.

At the beginning of this project, there were no good solution for direct injected HCCI. Therefore was the engine fitted with a dual fuel port injection system. The port injection system made it possible to individually control fuel and fuel ratio to each of the cylinders. The port fuel system was a custom made system, since the engine was originally a direct injection diesel engine.

5.6 Discussion

A desired feature in the experimental set-up was the ability to design the controllers in Simulink, as this is a powerful tool for prototyping and designing controllers. There are several commercial solutions providing system where the controller are designed in Simulink, for example dSPACE and xPC Target [dSPACE, 2004; xPC Target, 2004]. The reason why none

of these solutions were used in the experimental set-up was that none of the systems supported data acquisition card with sampling of at least 6 channels simultaneous and event-based sampling and possibility to save the measured data[2]. Therefore an in-house solution based on Simulink and Real-Time Workshop for C-code generation of the controllers were implemented. The platform used was Linux and it was found that ordinary Linux distributions were sufficient to fulfill the time-demands for cycle-to-cycle control, and real-time Linux versions, for example KURT, did not need to be used. The use of standard PC made it possible to have a flexible platform for development of customized control systems, as for example a wide range of data acquisition cards were accessible. Previously, Windows 95 and Windows XP was used as operating system in all experiments at the Division of Combustion Engine. The Windows based system had several sample delays in the system and system crashes took place.

During a valve lift the valve lift signal saturated in our configuration and only the beginning and ending of the lift could be measured. As the VVA system used was an electro-hydraulic one with a camshaft to lift the valves, the amplitude of the valve lift will be lower if the timing of IVO or EVO are retarded.

In the experiential set-up the dual-fuel system was more precise in the actuation that the VVA system. In comparison, the fuel injectors were more precise in the injected amount of the injected amount of fuel than the VVA-system was in achieving a specific IVC crank angle. This was due to the mechanic construction of the used VVA system.

The number of sensors used in the experimental set-up are beyond what later will be used in production, but for laboratory purpose these sensors are useful.

5.7 Summary and Concluding Remarks

This chapter has discussed the experimental set-ups used. The set-ups have been designed in order to provide feedbacks for control and to monitor the engine system. The proposed control structure using controllers designed in Simulink and the possibility to change the controller used on-line gives an flexible solution suitable for laboratory research.

[2]This was the situation in the year 2002.

6

Candidate Feedback Sensors

For feedback control of HCCI suitable feedback of the combustion phasing is necessary. As described in Sec. 5.3 the set-up had sensors for both measuring cylinder pressure and cylinder ion current. An ion current sensor is less expensive and more environmentally robust, therefore it is interesting to compare the combustion phasing information on a HCCI engine from the two different sensors. From the pressure measurements there are several methods to obtain a combustion phasing information. As the feedback are used on a cycle-to-cycle basis, the method should preferable have low complexity in order to fulfill the real-time demands. In the second part of this chapter a comparison of various methods are presented.

6.1 Cylinder Pressure vs Cylinder Ion Current

Currently, cylinder pressure transducers are expensive and have short life span. It is therefore interesting to find a cheaper sensor with long durability. In this section, ion current measurements and pressure measurements at HCCI operating points are studied and compared. The experiments have been performed on the experimental set-up described in Sec. 5.3. All the experiments were performed in open-loop at steady-state. Petter Strandh and Magnus Christensen performed the experiments. The contribution of the author, consisted in the analysis of the experiment. In the comparison between α based on cylinder pressure and on ion current measurements, an experimental set-up with dual fuels and a single-cylinder engine was used, see Sec. 5.3. Pressure-based α calculated via heat-release is denoted α_{50} and α based on ion current is denoted α_{50}^{ion}. We will show that it is possible to observe a measurement from the ion cur-

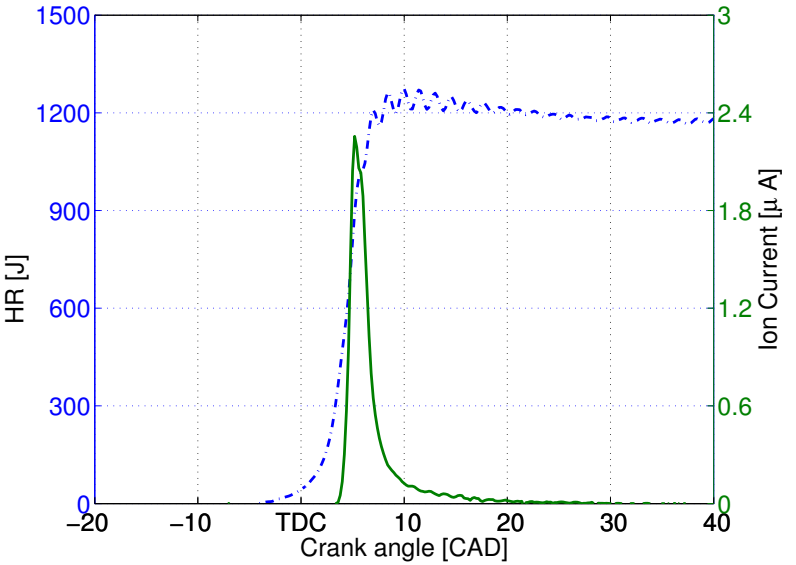

Figure 6.1 Ion current (*solid*) and heat release (*dashed-dotted*) for a single cycle.

rent measurements which coincides well with α_{50} measurements. The integrated ion current signal can be interpreted as a Mass Fraction Burned (MFB) signal. It gives no absolute pressure information, but gives information of the on-going combustion.

Figure 6.1 shows a single cycle of ion current and heat release. Note that the ion current rise time and heat release coincide. Another characteristic is that there is heat release before the appearance of any ion current. This suggests that ion current measurements are local, not global as cylinder pressure measurements. Hence, an open question is whether this still can be used for control. Experiments with and without EGR were performed, in order to study the effect of EGR on the ion current signal.

Combustion Phasing Information in Ion Current Data

The most distinct feature of the ion current trace at HCCI operation is the leading edge, as can be seen in Fig. 6.2. For consecutive cycles at constant operating point the amplitude can differ by a magnitude of 2-3. How then to obtain a measurement similar to α_{50}? The idea here is to use the rising flank to detect the combustion phasing and the midpoint of the flank is designated α_{50}^{ion}. Figure 6.3 shows ion current and cylinder pressure for one engine cycle. Note that the ion current rising flank corresponds to the cylinder pressure increase due to the combustion.

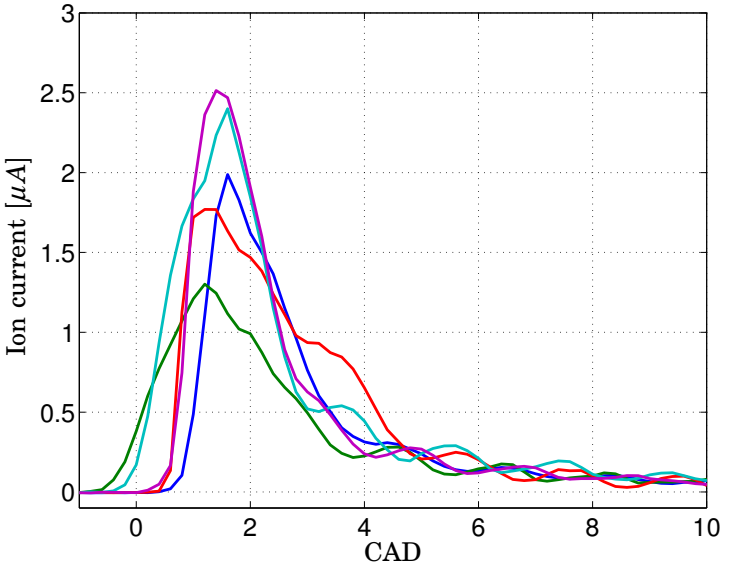

Figure 6.2 Ion current from five consecutive cycles. Notice that the cycles has a spread in amplitude. The spread in phasing is correlated to α_{50}.

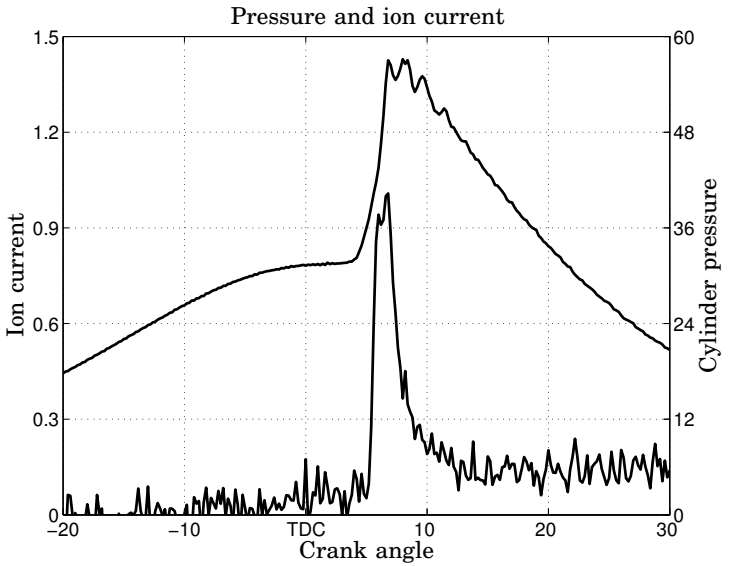

Figure 6.3 Ion current (*solid*) and cylinder pressure (*dashed*).

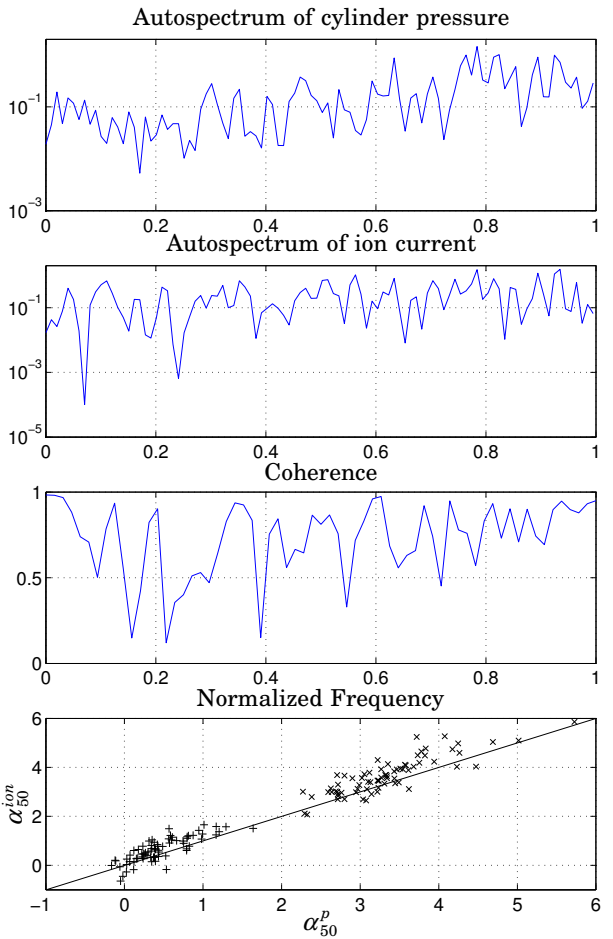

Figure 6.4 Autospectrum of α_{50}^{p} (*upper*) and α_{50}^{ion} (*middle*). Coherence spectrum between α_{50}^{ion} and α_{50}^{p} (*middle*). Correlation between α_{50}^{ion} and α_{50}^{p}. Two cases, 'x' and '+' (*lower*).

Comparison between Cylinder Pressure and Ion Current

Figure 6.4 shows the correlation between α_{50}^{ion} and α_{50} for two cases, noted as '+' and 'x'. It is well centered along the line representing identity. Both cases have a correlation coefficient of 0.87. The experiments were carried out in open loop at constant operating point. The variance of α_{50}^{ion} was 0.30 for case '+' and 0.64 for case 'x'. This can be compared with the variance of α_{50} which was 0.22 for case '+' and 0.47 for case 'x'.

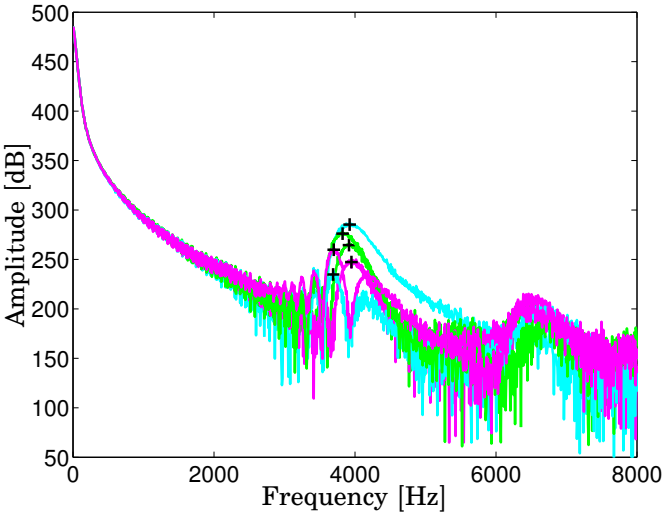

Figure 6.5 Power spectrum of 6 consecutive pressure measurements. The '+' marks are located at the maximal peak of the resonance.

Frequency Analysis The data used in the following frequency analysis was from a case where the engine was operated at 1000 rpm and α_{50} around 0.4 CAD. The sampling rate was 30 kHz at 1000 rpm and the pressure transducer has a natural frequency of 45 kHz.

The autospectrum of α_{50}^{ion} and α_{50} is shown in Fig. 6.4. The coherence spectrum between α_{50}^{ion} and α_{50} is fairly close to one for several frequencies, suggesting that a linear relationship between α_{50}^{ion} and α_{50} might exist (Fig. 6.4). In some cases the pressure traces in HCCI exhibit pressure oscillations [Griffiths and Whitaker, 2002]. At higher load the phenomenon occurs very frequently, but even at low loads it can appear. Very often the pressure traces which exhibit the phenomenon also have a faster pressure increase than pressure traces at the same operating point which does not exhibit the phenomenon. This fact could be used in order to predict the phenomenon, which could be called *HCCI knock* [Yelvington and Green, 2003; Oakley *et al.*, 2001]. Since this phenomenon is important to capture, it is interesting to compare the phenomenon in cylinder pressure measurements with ion current measurements. Figure 6.5 shows the auto spectrum for six consecutive pressure traces, which all exhibits oscillations. It is seen that frequencies around 3.7–4.2 kHz are amplified, and the '+' marks are at the maximum peak. Figure 6.5 could then be compared with Fig. 6.6, which shows the power spectrum for the corre-

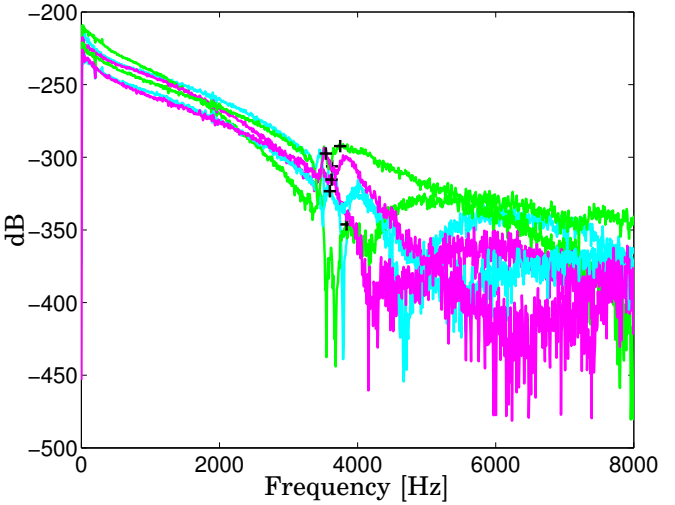

Figure 6.6 Power spectrum of 6 consecutive ion current measurements. The '+' marks are located at the maximal peak of the resonance.

sponding ion current traces. It is seen that frequencies around 3.5–4.1 kHz are amplified, and the '+' marks is at the maximum peak. Both the ion current and the cylinder pressure have amplitudes increasing in the same frequency interval. Hence, one interpretation is that the ion current sensor and the pressure transducer measure the same underlying combustion dynamics. The origin of the oscillations is not yet fully understood. An explanation can be that the air/fuel mixture is not spatially homogeneous. The thermal distribution in the chamber is neither homogeneous, as the wall temperature and the mixture temperature differs, this results in partly inhomogeneous ignition. An explanation for the oscillating frequency content could be that it is a circumferential oscillation mode. Figure 6.7 shows the two first circumferential modes and one radial mode.

$$f_{m,n} = \frac{C\ \rho_{m,n}}{\pi\ B} \tag{6.1}$$

Equation 6.1 is the acoustic pressure wave formula presented by C.S. Draper [Draper, 1938], where $f_{m,n}$ is the oscillation frequency, C is the velocity of sound in the cylinder, $\rho_{m,n}$ is the vibrational mode factor and B is the cylinder bore. The most frequent mode is [1,0]. When the engine speed was lowered, the response peak decreased. The same observation was made when the phasing was changed to later at constant load.

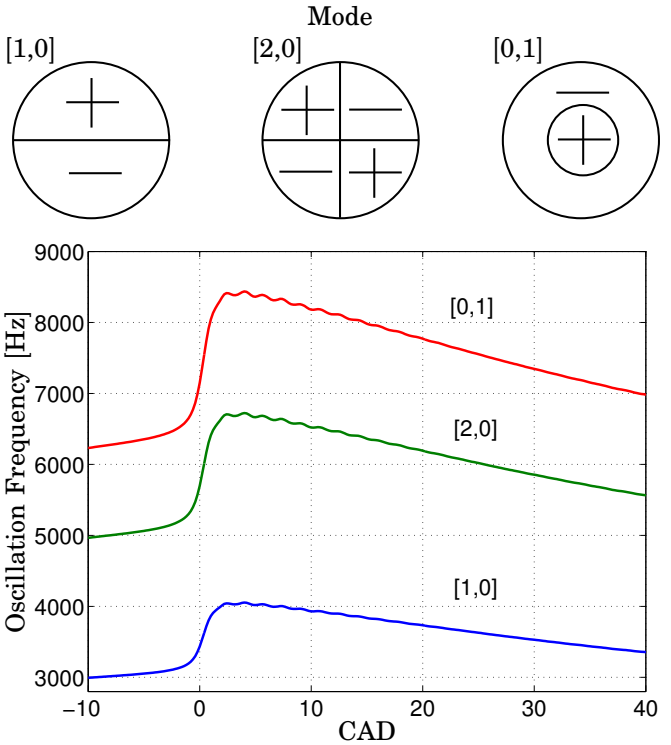

Figure 6.7 Oscillation frequency modes [1,0], [2,0] and [0,1].

There is one difference between the cylinder pressure and the ion current in that the pressure has a second resonance peak, around 6.6 kHz which is not present in the ion current measurements. An explanation for this could be that the second oscillation is due to mechanic oscillations which the pressure transducer will measure, but the ion current will not measure. Another explanation could be that it is due to a second circumferential mode and since the ion current sensor is located in the center of the combustion chamber it will not pick up this frequency. By bandpass filter properties, the pressure and the ion current, the amplitude of the ripple could be studied and it was found that the correlation between the changes in the amplitude of the ripple of the pressure measurements and the ion current measurements was 0.64, this correlation indicating dependencies in amplitude changes of the pressure and the ion current signal.

6.2 Candidates for combustion phasing feedback

What signal is best suitable for closed-loop control of an HCCI engine? The signal should be accurate, robust and estimated during the combustion cycle, in order to be used for cycle-to-cycle control. As briefly mentioned in Sec. 2.4 there are several alternatives. In this section several candidates of combustion phasing, α, for feedback control of HCCI engine. The studied candidates are

- 50% of heat release, α_{50}
- 50% of net heat release with fixed κ, α_{50}^{net}
- Maximum heat release rate, α_{max}^{dQ}
- Maximum pressure, α_{max}^{p}
- Maximum pressure increase by combustion, $\alpha_{max}^{p,c}$
- 50% of maximum pressure increase by combustion and compensation of the volume changes, $\alpha_{50}^{p,c,v}$
- Rassweiler&Withrow method for 50% mass fraction burned, α_{50}^{MFB}

A common notation for the different α candidates is $\alpha_{\texttt{criterion}}^{\texttt{method}}$ where superscript defines which signal is used, and subscript defines the criteria for finding the crank angle. The only discrepancy is α_{50}, which lacks stated method in superscript notation. All candidates are based on the property that cylinder pressure is measured. There exists more candidates, for example α_{max}^{dp}, but the chosen candidates catch most of the properties of cylinder pressure based α estimations.

As the combustion is global, the heat release slope is steep and heat release is close to symmetric, the crank angle of 50% burned (α_{50}) representing a robust measure of the phasing of combustion. This also implies that other choices of measures like for instance α_{20} or α_{80} will not have as high robustness against noise as α_{50}, since an error in percentage released energy will correspond to a larger error in crank angle.

In the following study, α_{50} from heat release analysis as in Sec. 2.5 is considered to be the best measure of the combustion phasing, α, and all the other alternatives are evaluated in terms of how well they correspond to α_{50}. The accuracy of α_{50} depends on how well the model parameters are tuned and on pressure measurement noise. Hence, tuning was carefully performed.

α_{50} based on Q_{hr}

The heat release is calculated as described in Sec. 2.5, α_{50} then being estimated by finding the crank angle where half of the energy has been

released. This is when the bulk of combustion takes place, and the slope of the Q_{hr}-curve is steep. This property makes it robust to noise and errors in the physical constants and is a candidate for the determination of α.

α_{50}^{net} based on Q_{hr}^{net}

α_{50}^{net} can be found at the crank angle where Q_{hr}^{net} reaches half its maximum value. Heat release analysis has the drawback that it cannot calculate α_{50} until the expansion stroke is finished and it uses several sub-calculations, for example calculation of the heat transfer. Instead of using heat release, net heat release can be used. If κ is well chosen, the maximum value of Q_{hr}^{net} is reached before the end of the expansion cycle. The calculation complexity is decreased as well, Q_{hr}^{net} being given by

$$\frac{dQ_{hr}^{net}}{d\theta} = \frac{\kappa}{\kappa - 1} p \frac{dV}{d\theta} + \frac{1}{\kappa - 1} V \frac{dp}{d\theta} \tag{6.2}$$

where a constant κ is used. If we compare this with the complete heat release Eq. (2.11), we notice that the difference is that κ is constant and Q_{ht} and Q_{cr} is not taken into account. The quantity Q_{hr}^{net} gives a good approximation of α_{50} since the slope of the Q_{hr}^{net} and Q_{hr}-curves are very steep and coincides. Also Q_{hr}^{net} is calculated by integration. In order to perform a fast α determination, without using the complete cylinder pressure trace, for online cycle-to-cycle feedback control the κ value in the Q_{hr}^{net} calculation was set to a lower value than the expected physical κ. The lower κ assures an early and robust detection of α, since the Q_{hr}^{net} has an early global maximum, caused by the negative slope in the Q_{hr}^{net} curve.

α_{max}^{dQ} based on maximum Q_{hr} rate

The crank angle of the maximum heat release rate, dQ_{hr}^{max}, can also be used as an estimation of α, but it has the drawback of being more noise sensitive. The benefit is that it provides a fast estimate as it only requires pressure measurements until the maximal slope has been reached.

α_{max}^{p} based on maximum pressure

The crank angle of the maximum pressure, p^{max}, during the cycle—also called location of peak pressure (LPP)— can be used as an estimation of α, based on the assumption that the crank angle where the pressure has its maximum is in the vicinity of the middle of the combustion since the combustion rate if fast. This is a rough estimate, but it has the benefit of not needing any calculations or calibrations. Using the crank angle of p^{max} as an estimation of α fulfills our requirements on fast calculation. However, this approach only works when there is a global maximum pressure

due to combustion. In cases of combustion before TDC or late combustion where the peak pressure is at TDC, α^p_{max} therefore fails to give an estimate of α. Since the HCCI combustion is governed by the state of the engine, it is vital to have a robust feedback signal. α^p_{max} gives the same α for a cycle which misfired and for one cycle which had very late combustion. A misfired cycle resulting in lower engine temperature and in unburned exhaust gases. But a very late combustion will only decrease the engine temperature slightly and result in none or only a small amount of unburned exhaust gases. The difference between these two cases, have large impact on the next cycle. Therefore, α^p_{max} is not a accurate or robust measurement of α. Another drawback is that α^p_{max} is closely tied to the combustion volume and it would, if used as feedback of α, pull the estimate towards TDC. This results in a poor estimate in the vicinity of TDC where knocking combustion is likely to occur.

$\alpha^{p,c}_{max}$ based on maximum pressure increase due to combustion

One method of achieving a more robust estimate is to subtract the motored pressure from the measured pressure. Then, the new pressure curve represents the increased pressure due to combustion, p^c. This would give a global maximum even for late combustions and for combustion before TDC. Based on the assumption that the maximal pressure for this new pressure curve is in the vicinity of the middle of the combustion for high combustion rates, α could then be found.

$\alpha^{p,c,v}_{50}$ based on pressure increase due to combustion

As α^p_{max} and $\alpha^{p,c}_{max}$ fail to give a good indication of α, the following approach is suggested: Find the crank angle where pressure increase due to combustion has reached half its maximum level when compensating for the volume change, $\alpha^{p,c,v}_{50}$. $\alpha^{p,c}_{50}$ is when not compensating for the volume change. The volume compensation is achieved by multiplying the pressure trace due to combustion with the volume change. This results in an estimation of α with similar properties as α_{50}. The slope of the pressure curve is at $\alpha^{p,c,v}_{50}$ steep. The benefits with this method are several. Since only pressure trace is used, it is not necessary to have absolute pressure, instead relative pressure is sufficient. The cylinder pressure transducers only measure relative pressure and for heat release calculation the offset must be calculated. Also there is no need in calibration of parameters. In the heat release calculations, several parameters are needed to be tuned, such as the parameters in the heat transfer equations. It can be calculated before the engine cycle is finished and can be used for cycle-to-cycle control. Finally, it also has low complexity.

$\alpha^{p,c,v}_{50}$ is one measurement of the combustion phasing, whereas also other levels could be interesting. It could be that the pressure increase

should reach a certain level, absolute or percentage of the maximum. these level could also be changed for different operating conditions. Since an HCCI engine has cycle-to-cycle variations, models of the pressure increase could be used to design model predictive control of this pressure level, in order to assure that the pressure increase starts at the right CAD.

α_{50}^{MFB} based on MFB estimation

The Rassweiler and Withrow method is a well established method for estimating the mass fraction burned, MFB [Rassweiler and Withrow, 1938]. The method decomposes the actual change in cylinder pressure, from one pressure sample to the next, into the change in pressure which would result if no combustion were taking place (polytropic process) and an additional change which is the result of combustion. It is then assumed that the increase in MFB is proportional to the change in pressure from combustion. Thus, for pressure sample i,

$$(\Delta p_c)_i = p_i - p_{i-1}\left(\frac{V_{i-1}}{V_i}\right)^{\kappa}$$

where Δp_c is the increase in cylinder pressure due to combustion and κ (constant) is the polytropic exponent, MFB can now be computed as

$$\frac{m_{b(i)}}{m_{b(total)}} = \frac{\sum_{j=0}^{i}\Delta(p_c)_j}{\sum_{j=0}^{N}\Delta(p_c)_j}$$

where it is assumed that sample 0 is between inlet valve closing and the start of combustion, and that sample N is after combustion has finished. The method has limitations, heat transfer effects are included only to the extent that the polytropic exponent κ differs appropriately from γ. In the limit when the crank angle step $\Delta\theta \to 0$, the difference equation for Δp_c becomes a differential equation. This differential equation can be derived starting from the differential form of a polytropic process

$$d(p_v V^{\kappa}) = 0$$

which can be rewritten as

$$V^{\kappa} dp_v + \kappa p_v V^{\kappa-1} dV = 0$$

Thus, the polytropic pressure differential can be written as

$$dp_v = -\kappa \frac{p}{V} dV$$

The pressure differential caused by combustion can now be expressed as the difference between the actual pressure differential and the polytropic pressure differential

$$dp_c = dp - \left(-\kappa \frac{p}{V} dV\right) = dp + \kappa \frac{p}{V} dV.$$

The expression for dp_c can be compared to dQ from a net heat release calculation which is

$$\begin{aligned} dQ_{hr}^{net} &= \frac{1}{\gamma - 1} V dp + \frac{\gamma}{\gamma - 1} p dV = \frac{c_v}{R} V dp + \frac{c_p}{R} p dV \\ &= \frac{c_v}{R} V \left(dp + \frac{c_p}{c_v} \frac{p}{V} dV\right) = \frac{c_v}{R} V \left(dp + \gamma \frac{p}{V} dV\right) = \frac{c_v}{R} V dp_c \end{aligned} \tag{6.3}$$

If κ is assumed to be equal to γ. Thus,

$$dp_c = \frac{R}{c_v V} dQ_{hr}^{net} \tag{6.4}$$

which is a somewhat distorted version of the net heat release. The faster the combustion and the closer to TDC ($\frac{dV}{d\theta}$ small), the smaller the distortion, since the volume then becomes closer to constant over the calculation interval. It does not have the benefit of being fast either since it needs measurements for the whole cycle. Thus, it can be improved by using the value of $m_{b(total)}$ from the last cycle in the calculation. Then, α_{50}^{MFB} can be estimated the median is reached. This approximation is valid only if the operating point changes little from cycle to cycle.

6.3 Comparison of combustion phasing candidates

In the comparison of the different candidates of α, four different cases of combustion have been used (Fig. 6.8).

- Case 1 has a global pressure maximum due to combustion (normal case).
- Case 2 has a local pressure maximum due to combustion.
- Case 3 has increased pressure due to combustion but lacks local maximum.
- Case 4 has combustion before TDC.

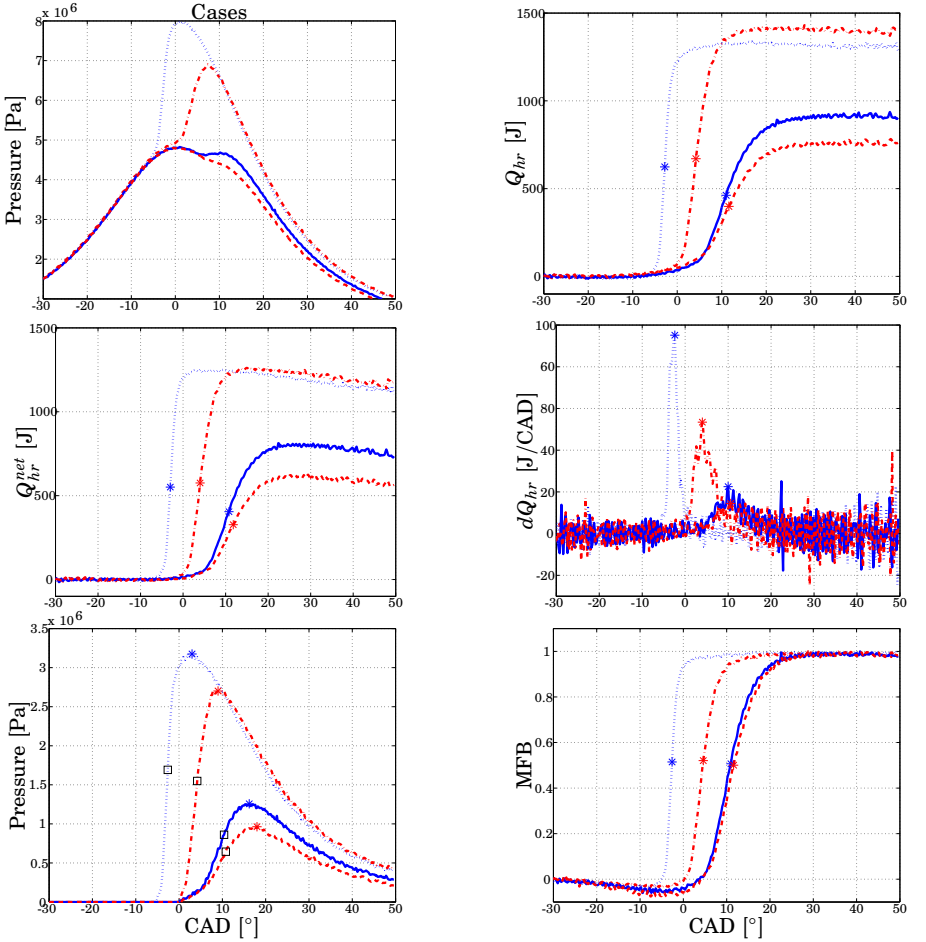

α	α_{50}	α_{50}^{net}	α_{max}^{dQ}	α_{max}^{p}	$\alpha_{max}^{p,c}$	$\alpha_{50}^{p,c,v}$	α_{50}^{MFB}
Case 1	4.2°	4.0°	4.0°	7.4°	9.0°	4.2°	4.6°
Case 2	11.0°	10.8°	10.0°	0.2°	16.2°	10.4°	11.0°
Case 3	11.6°	11.8°	10.6°	0.2°	18.0°	10.8°	11.6°
Case 4	-2.8°	-3.0°	-2.4°	1.0°	3.0°	-2.6°	-2.6°

Figure 6.8 Cylinder pressure traces for different combustion cases(*Upper left*). Case 1: Global maximum due to combustion (*dash-dotted*). Case 2: Local maximum due to combustion (*solid*). Case 3: No local maximum due to combustion (*dashed*). Case 4: Combustion before TDC (*dotted*). The other figures show Q_{hr}, Q_{hr}^{net}, dQ_{hr}, p^c, MFB for the 4 cases. The '*' marks the CAD for the estimated α-values. The square marks the $\alpha_{50}^{p,c,v}$-value. The table shows the α for the different cases and candidates.

Table 6.1 Correlation and standard deviation (std) information for the four studied cases expressed in crank angle degree. The residual, e, is the error between α_{50} and the other α candidates.

α candidates	α_{50}	α_{50}^{net}	α_{max}^{dQ}	$\alpha_{max}^{p,c}$	α_{max}^{p}	$\alpha_{50}^{p,c,v}$	α_{50}^{MFB}
Corr. to α_{50}	1.000	0.998	0.713	0.801	0.835	0.997	0.943
Std of α (1)	0.396°	0.395°	0.503°	0.641°	0.449°	0.376°	0.382°
Std of e (1)	0.000°	0.109°	0.411°	0.505°	0.577°	0.121°	0.118°
Std of α (2&3)	0.829°	0.809°	8.114°	1.054°	3.594°	0.825°	0.813°
Std of e (2&3)	0.000°	0.232°	7.892°	0.751°	4.163°	0.262°	0.273°
Std of α (4)	0.226°	0.214°	0.370°	0.516°	0.366°	0.237°	0.226°
Std of e (4)	0.000°	0.094°	0.330°	0.627°	0.351°	0.098°	0.089°

In Fig. 6.8, Q_{hr}, Q_{hr}^{net}, dQ_{hr}, p^c, MFB and their estimates of α are shown for the four different cases. In case 1, α_{max}^{p} and $\alpha_{max}^{p,c,v}$ gives late estimation of α and α_{max}^{p} but fails completely to estimate of α in cases 2 and 3. What also can be noted is that $\alpha_{50}^{p,c,v}$ gives similar indication of α as α_{50}, but tends to give an earlier indication in the late combustion cases. In Fig. 6.9, the different candidates of α are shown for several cycles. In order to better visualize the trends, the figure shows both low-pass filtered α and non-filtered α. From the non-filtered α it can be observed that they all have similar high frequency properties. From the low-pass filtered α it can observed that α_{50}, α_{50}^{net}, $\alpha_{50}^{p,c,v}$ and α_{50}^{MFB} give very similar α-value. But α_{max}^{p} and α_{max}^{pv} give late α-values, not near the actual combustion phasing. α_{max}^{dQ} tends to give too early α-values. Also $\alpha_{50}^{p,c}$ has this problem, but $\alpha_{50}^{p,c,v}$ where the volume changes are taken into account give an estimate that is close to α_{50}. It can be noticed that the difference between α_{50} and $\alpha_{50}^{p,c,v}$ becomes larger when the combustion phasing moves toward late combustion.

As previously mentioned α_{50} is assumed to be the best possible estimate of α. Therefore, it is interesting to study coherence between α_{50} and the other candidates (Fig. 6.10). In Table 6.1 the correlation between α_{50} and the other α candidates are presented. α_{50}^{net}, α_{MFB} and $\alpha_{50}^{p,c,v}$ gives highest coherence spectrum, close to one. The table also presents the variance of α and the residuals, e, where the residuals are the difference between α_{50} the other α candidates. We note that α_{max}^{dQ} and α_{max}^{p} have high variance in Case 4. In the case of late combustion α_{max}^{dQ} is noise sensitive since only partial combustion occurs, which makes the variance of the α estimate large.

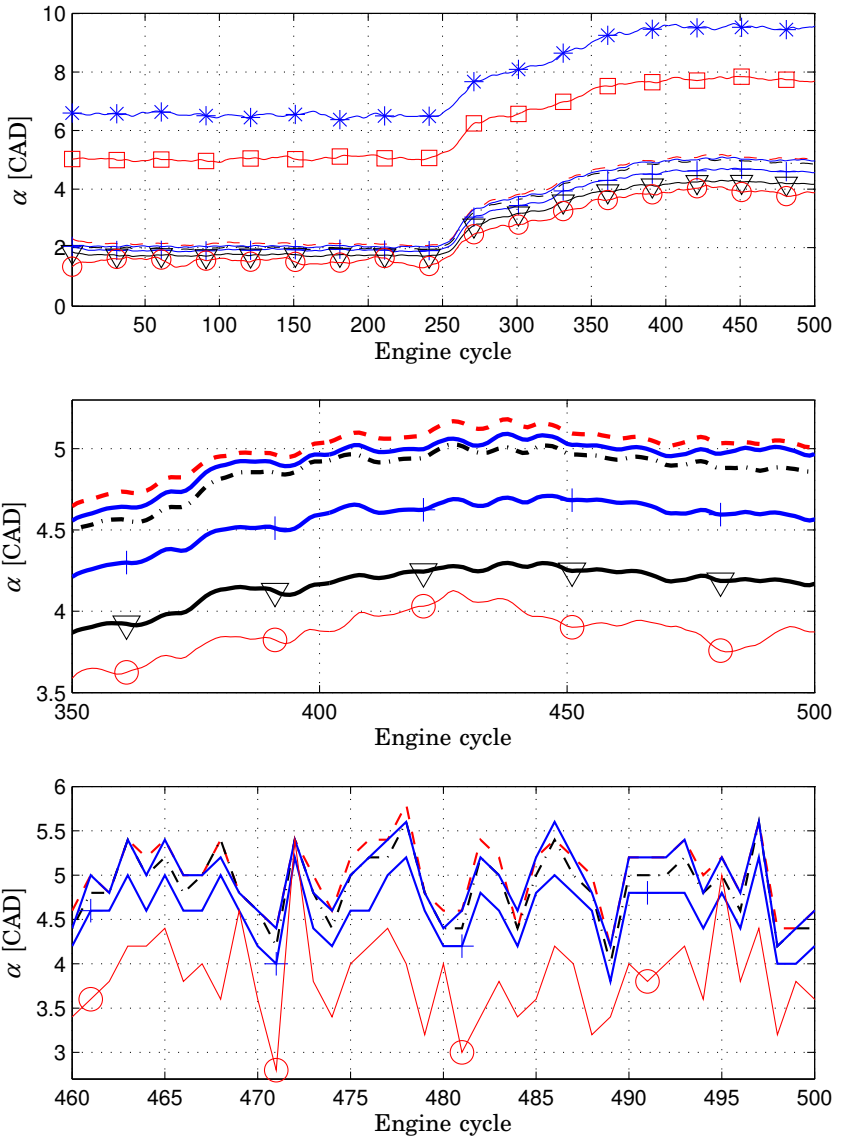

Figure 6.9 Various α-candidates: $\alpha^{p,c}_{max}$ (*solid with '*' marks*), α^{p}_{max} (*solid with '□' marks*), α_{50}(*dashed*), α^{MFB}_{50} (*solid*), α^{net}_{50} (*dash-dotted*), $\alpha^{p,c,v}_{50}$ (*solid with '+' marks*), $\alpha^{p,c}_{50}$ (*solid with '▽' marks*) and α^{dQ}_{max} (*solid with 'o' marks*). The upper figure shows the low passed filtered result when α_{50} reference value is changed from 2 to 5 CAD. The middle figure shows a blow-up view of the low pass filtered α_{50}, α^{MFB}_{50}, α^{net}_{50}, $\alpha^{p,c,v}_{50}$, $\alpha^{p,c}_{50}$ and α^{dQ}_{max}. The lower figure shows the non-filtered α_{50}, α^{MFB}_{50}, α^{net}_{50}, $\alpha^{p,c,v}_{50}$, $\alpha^{p,c}_{50}$.

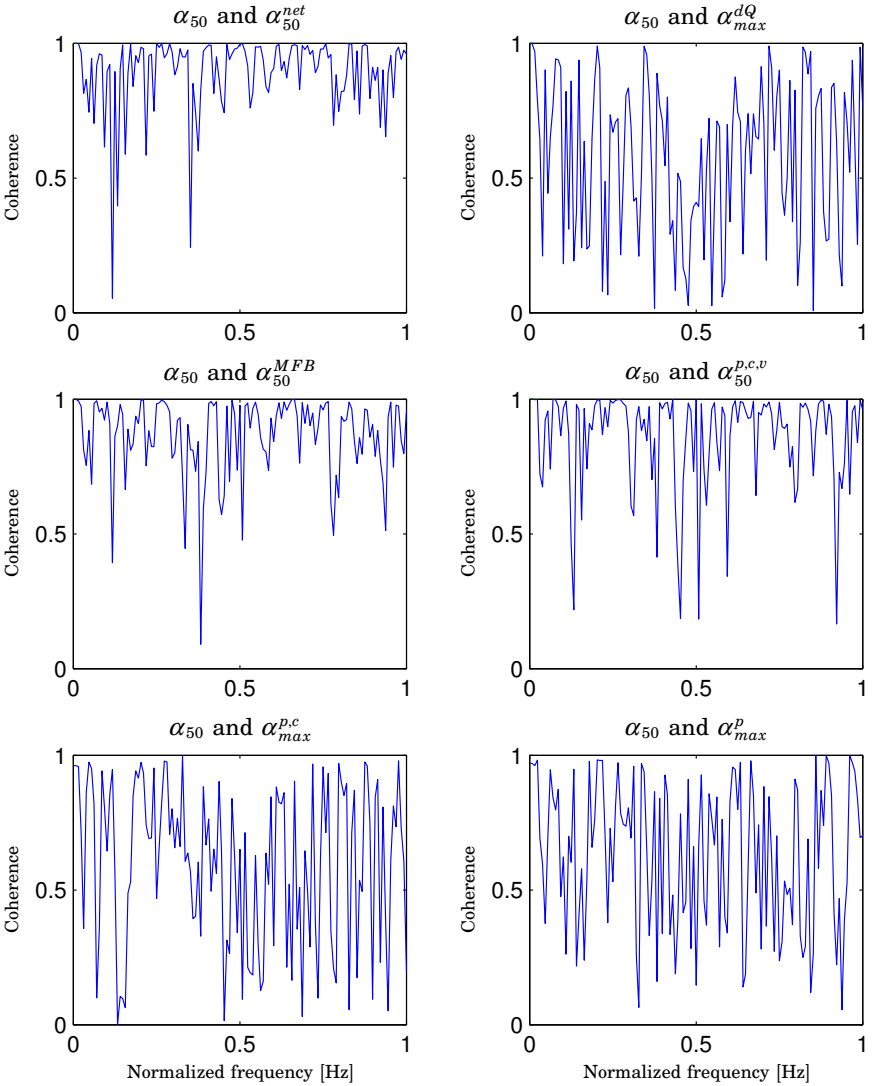

Figure 6.10 Coherence estimates between α_{50} and the other candidates.

In comparison to α_{50}, α_{50}^{net}, α_{MFB} and $\alpha_{50}^{p,c,v}$ give accurate results for all studied cases, α_{50}^{net} having the highest correlation score and smallest standard deviation. Note that α_{max}^{dQ} and α_{max}^{p} fail to estimate α in case of late combustion.

Even if it was already pointed out that α_{max}^{p} also called LPP—is not

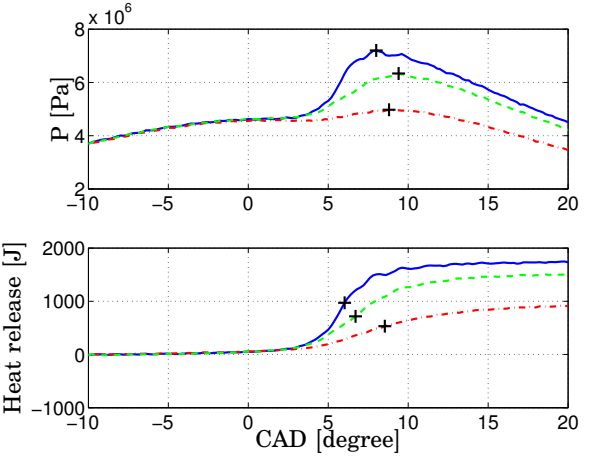

Figure 6.11 Pressure traces and heat release curves at different load conditions: 1700 J (4 Bar IMEP) (*solid*), 1500 J (3.4 Bar IMEP) (*dashed*) and 1000 J (1.8 Bar IMEP) (*dash-dotted*). In the upper figure, '+' marks the location of α^p_{max} and in the lower figure, '+' marks the location of α^{net}_{50}.

a robust measurement of the combustion phasing, a more detailed study shows the problem. In Figs. 6.11 and 6.12, the cylinder pressure curves and the corresponding heat release are shown for three different load cases; 1000 J, 1500 J and 1700 J. It can be observed that α^p_{max} and α^{net}_{50} give different indication of α. It can also be observed that the combustion duration differ, but it is strongly dependent on the λ value. Since α^p_{max} gives an indication when almost all fuel have been burned, the combustion duration have significant effect on α. In the experiments the engine speed, inlet temperature and fuel ratio were kept constant, only the total amount of injected fuel was varied. It was found that the distributions between the two measurements were similar, but there are statistical offsets (Fig. 6.13). The bias between α^p_{max} and α^{net}_{50} are: for the 1000 J load case less than a half CAD; for the 1500 J load case approximately 2 CAD; for the 1700 J load case approximately 2.5 CAD. It can also be noted that the α^p_{max} is not significantly affected by the load change. The 1000 J load case also includes three cycles where the combustion occurred so late that the maximum pressure was at top dead center, which also can be seen in Fig. 6.13. Due to all these properties that α^p_{max} has, it seems to be far from the best feedback alternative in order to control HCCI. But thereby it can not be concluded that it can not successfully be used. In production, cost-effective sensors are essential and α^p_{max} might provide sufficiently

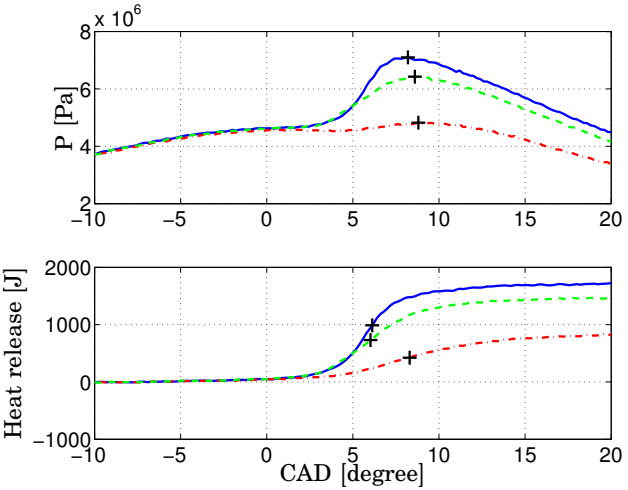

Figure 6.12 Pressure traces and heat release curves at different load conditions: 1700 J (4 Bar IMEP) (*solid*), 1500 J (3.4 Bar IMEP) (*dashed*) and 1000 J (1.8 Bar IMEP) (*dash-dotted*). In the upper figure, '+' marks the location of α^p_{max} and in the lower figure, '+' marks the location of α^{net}_{50}.

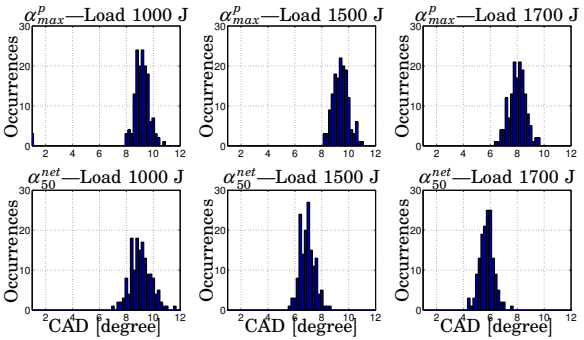

Figure 6.13 Histogram of α^p_{max} and α^{net}_{50} at three different loads.

accurate signal in the whole operating range to successfully be used in feedback control of HCCI.

Study of different pressure levels

As was mentioned in Section 6.2, feedback based on pressure increase could be interesting. The feedback could be the crank angle where the pressure increase had reached a certain level, absolute or percentage of the maximum. It is not obvious that the feedback based on α_{50} or a similar signal, which try to indicate the crank angle where 50% of the energy has

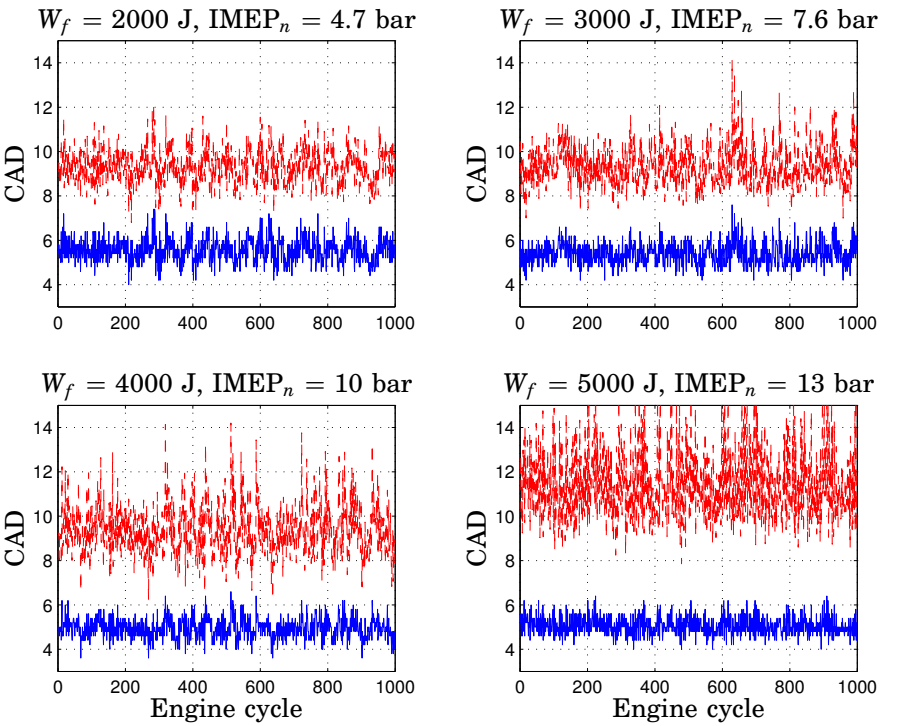

Figure 6.14 The combustion phasing for α_{50} (*dashed*) and α_{05}^{p} (*solid*)

been released or 50% of the fuel has burned, would give the best result from a control point of view. As the combustion rate depends on the operating condition, a feedback signal which also would catch the difference in the combustion duration is desirable, for example, use feedback based on the threshold value of the pressure, which could vary depending on the operating condition. This argument is of course also applicable to various α-energy levels. Figure 6.14 shows α_{50}^{net} and $\alpha_{05}^{p,c,v}$ for four different load cases. The index on α stands for the pressure threshold level expressed in bar. It can be noted that $\alpha_{05}^{p,c,v}$ is a poor choice in determination of α, as it is not significantly affected by changes in the operating condition. It can also be observed that the cycle-to-cycle variations in α_{50}^{net} become larger when increasing the load. Note that even if $\alpha_{05}^{p,c,v}$ was almost unaffected by the change in the operating conditions, it should not be interpreted that the combustion duration was constant. How different threshold levels affect the α estimations and comparison with α_{50}^{net} and α_{50}^{p} are shown in Figs. 6.15 and 6.16. The combustion rate is dependent on the amount

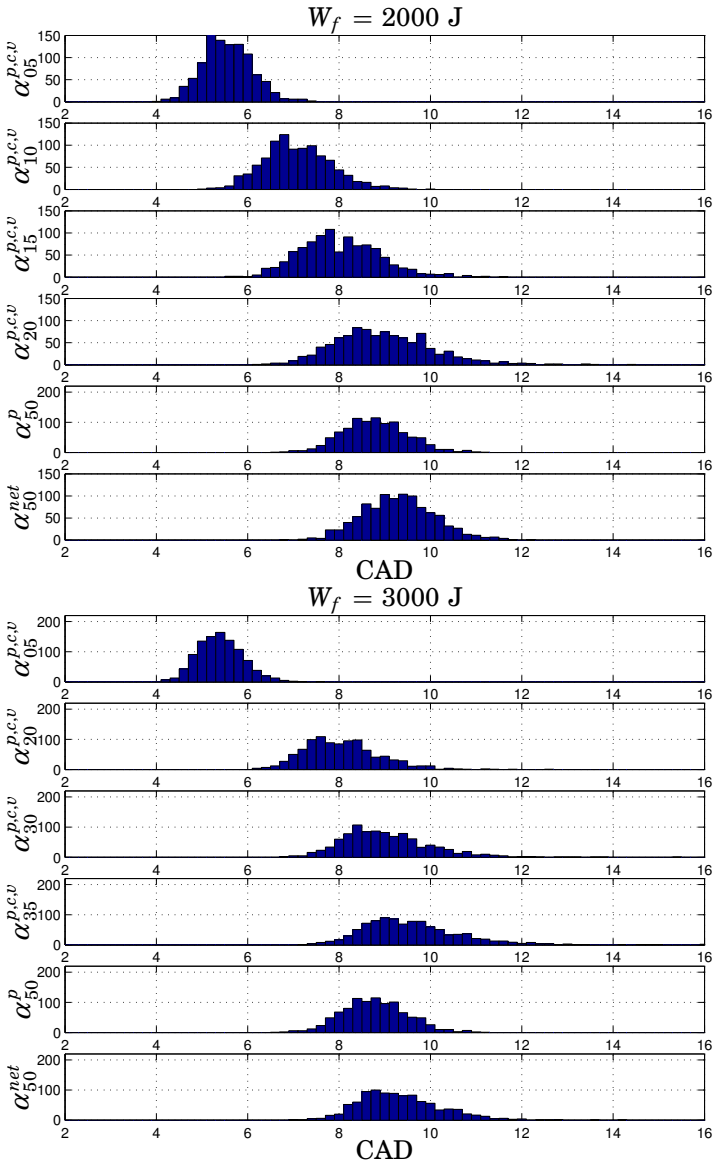

Figure 6.15 Histogram of various $\alpha_{level}^{p,c,v}$, α_{50}^{p} and α_{50}^{net} at load 2000J (*upper*) and at load 3000J (*lower*).

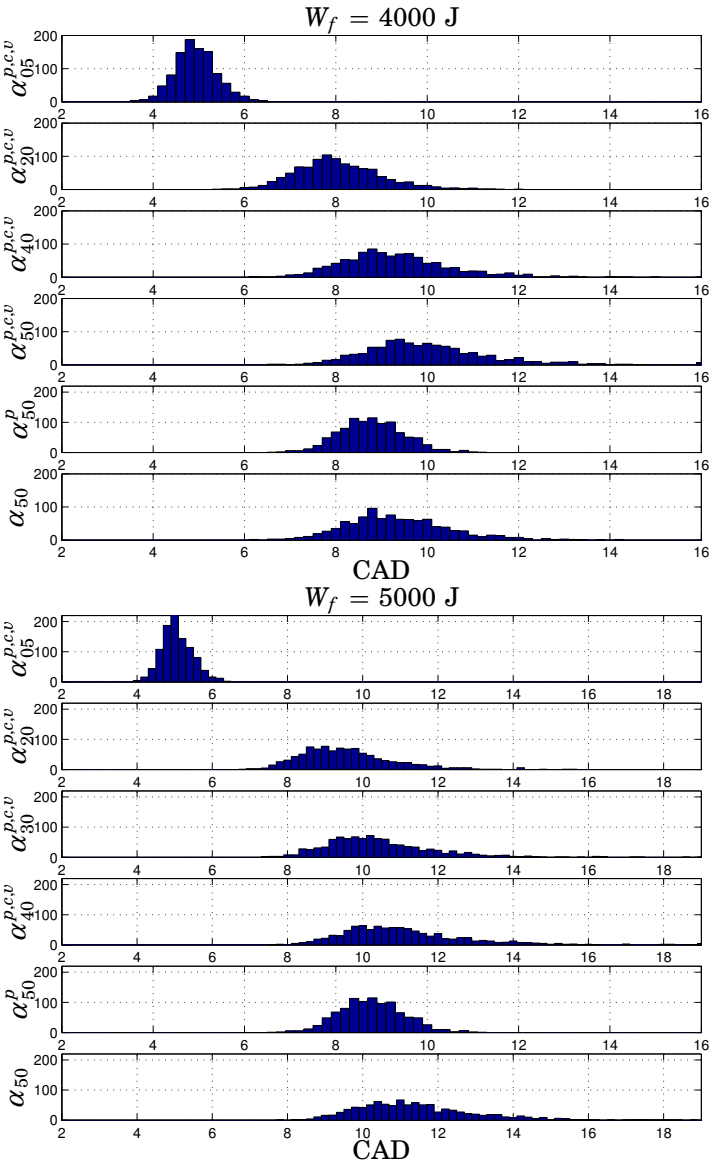

Figure 6.16 Histogram of various $\alpha_{level}^{p,c,v}$, α_{50}^{p} and α_{50}^{net} at load 4000J (*upper*) and at load 5000J (*lower*).

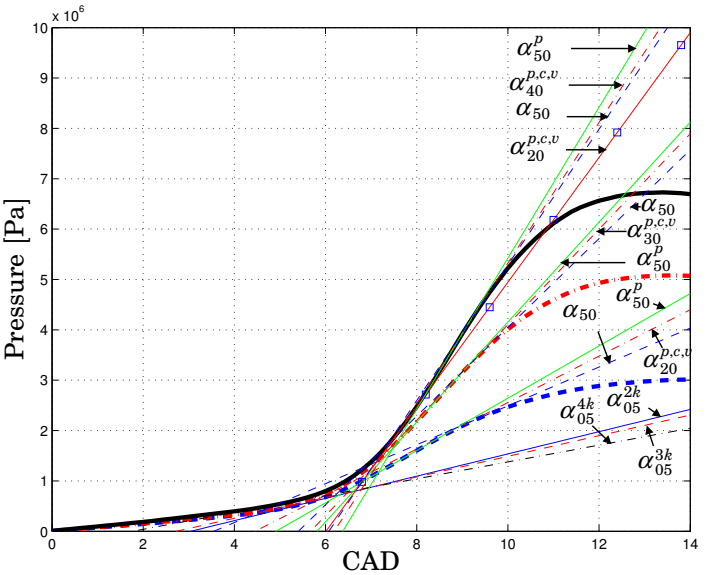

Figure 6.17 Combustion rates at various loads, when the inlet pressure and inlet temperature are constant. The thick lines correspond to the pressure due to combustion, when the load is 2000J (*dashed*), 3000J (*dash-dotted*) and 5000J (*solid*). The thick lines are mean value curves of 500 cycles. The thin lines are tangents taken at the point stated in the figure. The indices 2k, 3k and 4k correspond to the three load cases.

of fuel. The combustion rate at various loads, when the inlet pressure is constant, can be seen in Fig. 6.17. Note that as the load increases, the combustion rate increases.

Effects of low resolution and low engine sampling rate

As resolution of the pressure transducers and sampling rates in production systems is not as high as in our experimental set-up, it is interesting to study how well the best candidates for α perform when the resolution of the cylinder pressure transducer is low and the sample rate is low. In Fig. 6.18, the result of α_{50}, α_{50}^{net} and α_{50}^{MFB} where the cylinder pressure has 6 bits resolution and a full engine cycle consists of 240 samples for Case 1, resulting in a sampling interval of 3 CAD. This is to be compared with the normal 14 bits resolution and 3600 samples for a full engine cycle. In order to increase the accuracy of the estimation of α linear interpolation of the cylinder pressure trace was used. In the experiments, the α_{50} was changed from 4 to 6 CAD. The correlation and standard deviation of α for

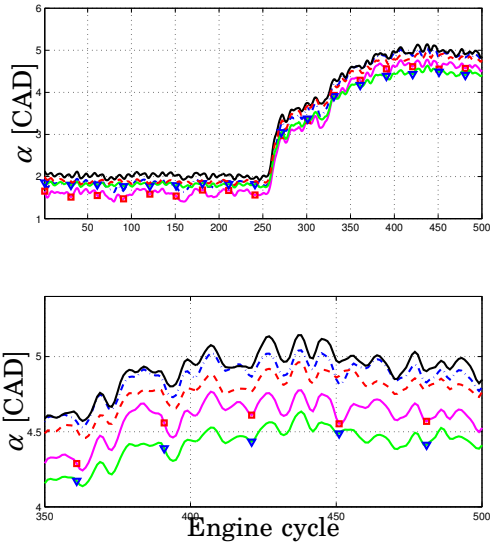

Figure 6.18 Different α-candidates when using low resolution and low sampling rate: α_{50} (*dash-dotted*), α_{50}^{net} (*solid with '□' marks*), $\alpha_{50}^{p,c,v}$ (*solid with '▽' marks*, α_{50}^{MFB} (*dashed*). These could be compared with α_{50} when using the resolution and sampling rate that normally was used in the experimental setup (*solid*). The signals are filtered in order to better visual the differences. The lower figure is a closer view of the engine cycles 350 to 450.

Table 6.2 α candidates when the pressure trace has low resolution and sampled with low sampling rate. Correlation between α_{50} with high resolution and high sampling rate. Standard deviation (std) information for the various α estimate, expressed in CAD. The residual is the error between α_{50} with high resolution and high sampling rate and the other candidates.

α candidates	α_{50}	α_{50}^{net}	$\alpha_{50}^{p,c,v}$	α_{50}^{MFB}
Correlation	0.9921	0.8818	0.9967	0.9879
Std of α (Case 1)	1.563°	1.611°	1.589°	1.562°
Std of residual (Case 1)	0.189°	0.186°	0.173°	0.157°

in this low resolution and low sampling rate case are presented in Table 6.2. Even this low resolution and low samples rate case, α based on α_{50}, α_{50}^{net}, $\alpha_{50}^{p,v,c}$ and α_{50}^{MFB} are fairly accurate. The standard deviation has increased in comparison to our normal experimental set-up conditions, but it still suggests that α based on low resolution sensors and low sampling rate can be used for feedback control.

Discussion

In Sec. 6.1 it was observed that when the engine speed was lowered, the response peak decreased. The same observation was also made when later phasing was chosen at constant load. The observation, that the resonance peak becomes less significant when later phasing at constant load could be due to that the effective volume is larger. The larger volume resulting in that the pressure rise will not become as large as in cases of early phasing.

The clearcut relationship between cylinder pressure and ion current measurement suggests that one measurement may be reconstructed from the other for instance by means of a Kalman filter or some other full-order observer.

Apparently, cylinder pressure measurements provide a more robust α estimation than ion current measurements and in this experimental set-up, the upper limit of λ-value (relative air/fuel ratio) seems to be 2.7 for a reliable ion current signal. At higher λ-values, the noise level corrupts the measurements. The rich limit for HCCI operation without EGR is λ=2. Questions not yet fully addressed are what is the limit of operating conditions, and whether the ion current measurements could replace pressure sensors in a production-like environment. It was found that the placement of the ion current sensor has influence on the ion current signal and a more detailed study was performed in [Vressner *et al.*, 2004].

An ion current signal is local, therefore was measurements with a modified spark plug without a side electrode performed in order to study if a more global measurement could be achieved [Strandh *et al.*, 2003] Both the 'standard' and the 'modified' spark plug cases were found to give reliable combustion information. However, the ion current signal was found to be higher in the 'modified' spark plug case. It seems likely that the modified spark plug provides a somewhat less local measurement due to less shielding by the side electrode.

Estimations of α based on maximum pressure α_{max}^{p} and $\alpha_{max}^{p,c,v}$ give a later combustion phasing, which can be explained by the fact that even if the combustion duration is short, it still has a duration of few to several CAD and the maximum pressure is reached near the end of the combustion. The fact that the combustion is not symmetric could be because that the combustion having a tail due to after-oxidation which might also influence the maximum pressure phasing. Another drawback is that the maximum pressure estimate is sensitive to noise and fails to indicate when the combustion occurs, particularly in the most important cases of late combustion or early. The estimates α_{50}, α_{50}^{net}, $\alpha_{50}^{p,c,v}$ and α_{50}^{MFB} give similar results, whereas α_{max}^{dQ} gives different results. The reason that α_{max}^{dQ}

differs is that the combustion is not symmetric, which leads to an earlier indication than α_{50} and it is more sensitive to noise at late combustion. The small difference between α_{50}^{MFB} and α_{50}^{net} could be explained by slower combustion with later phasing. Hence, the volume change during the calculation of MFB will result in a distortion relative to α_{50}, see Eq. (6.4). Both α_{50}^{MFB} and α_{50}^{net} does not take heat transfer and crevice effects into account, but since they only have a marginal effect on the maximum of heat release the error in α becomes very small. $\alpha^{p,c,v}$ show similar accuracy as α_{50} but it tend to indicate too early α values. Even so $\alpha^{p,c,v}$ has several attractive benefits over α_{50}, α_{50}^{net} and α_{50}^{MFB}. It is directly based on cylinder pressure measurements and there is no need to calculate the pressure offset in the measurements. There is no need for calibration or modeling of heat release parameters. It has similar robustness and computational complexity as the other candidates. It is therefore an interesting alternative for feedback control and it will be analyzed in Chapter 8.

The control performance is often limited by the presence of sensors and the control designer is often given a plant or process with existing hardware and software. The plant might have sensors or not. The control designer then has limited possibility to add extra sensors or other changes of hardware and the problem consists of design of a controller to the given system. In this thesis there were few limitations of what sensors to be used, since the objective with the experimental set-up was already from the beginning giving a good platform for control studies of HCCI control.

6.4 Summary and Concluding Remarks

An alternative sensor to cylinder pressure transducer for measuring of the progression and completeness of the combustion reactions in HCCI was presented. The alternative is ion current measurements which provide information about HCCI combustion, using the electronic conductive properties of the reaction zone. Combustion phasing information as well as pressure oscillations can be observed from the measurements. It is a possible candidate for feedback control. The operating range of λ values in this experimental set-up was $\lambda \in [2, 2.7]$.

A comparison of various candidates for combustion phasing feedback variables in real-time has been presented. Several of the candidates had similar accuracy in comparison with α_{50}, calculated using full heat release model. Among candidates tested, it was α_{50}^{net}, α^{MFB} and $\alpha_{50}^{p,c,v}$ which were found to be the best suited candidates as the estimation of the combustion phasing was robust to both late and early combustion and the estimation calculation had low complexity, suitable for usage in real-time control of combustion phasing.

7

Identification of HCCI Engine Dynamics

In order to understand HCCI engine dynamics and to design controllers, system identification is a key tool. Moreover, the combustion phasing control design requires appropriate models and system output variables for feedback design. As the engine set-up had two different actuators for the cycle-to-cycle control of the combustion phasing, dual-fuel and VVA, system dynamic models for each of them will be estimated in the first part of this chapter. In the second part of this chapter, dynamic models of the cylinder pressure trace and the ion current trace, and combustion phasing based on ion current trace will be estimated.

7.1 Model Variables

An HCCI engine is a complex multiple-input, multiple-output, MIMO, system with interacting inputs and output. The most important problem to solve is the control of the combustion phasing, as this stabilizes the combustion, effects the performance in load changes and affects the exhaust emissions. Fast response in load changes is necessary for car and truck end-users, but perhaps less important if the engine is to be used as a power generator. As the combustion phasing is the most critical and difficult to control, the engine models can be simplified to a multiple-input, single-output, MISO, system, where the combustion phasing α is the output. There are many variables which affect α and only some of them are directly controllable, for example the inlet temperature is controllable while the wall temperature is a result of previous combustions. Since the control objective is the purpose of the modeling, it is natural to use all the available control signals, specified in Sec. 5.2 for our experimental set-up, and model their influence on the combustion phasing. Also other

signals could be interesting to use in the identification, such as exhaust temperature and oil temperature. Currently, the cylinder wall temperature is difficult to measure and our experimental set-up lacks a cylinder wall temperature sensor. Instead, the exhaust temperature and the oil temperature could be used to obtain information about the wall temperature. The available inputs in our experimental set-up were described in Sec. 5.1.

The main objective of the identification was to obtain models suitable for control design, in this case combustion phasing control. Hence, the models should be able to describe the behavior of the combustion phasing. For this objective there are two approaches: to estimate models where combustion phasing is the output or to estimate models where the pressure trace is the output, and then calculate the combustion phasing from the trace using some of the methods suggested in Sec. 6.2. The second method is an indirect method for obtaining the combustion phasing. The advantage with this method is that more than α can be estimated, for example the temperature. This makes the model suitable for simulations.

Among the good candidates for α presented in section 6.2, α_{50} based on pressure trace was chosen as the time where the combustion occurred.

Methods and Model Structures

Several methods for estimating dynamic models and model representations exist, each having their benefits and drawbacks [Johansson, 1993]. The methods and linear model structures used in this thesis were

Difference Equation Models

ARMAX The ARMAX models (AutoRegressive Moving Average with eXogeneous input) have the following structure

$$A(z^{-1})y(k) = z^{-d}B(z^{-1})u(k) + C(z^{-1})e(k) \tag{7.1}$$

where d is a time delay and A, B, C are polynomials.

PEM The PEM models (Prediction Error Method) have the following model structure

$$A(z^{-1})y(k) = z^{-d}\frac{B(z^{-1})}{F(z^{-1})}u(k) + \frac{C(z^{-1})}{D(z^{-1})}e(k) \tag{7.2}$$

where d is a time delay and A, B, C, D, F are polynomials. The model is written as a difference equation. It is the prediction error estimate of a general linear model, where also a different denominator for the input and noise can be chosen.

State-Space Models

The estimated models are on state-space form

$$x(k+1) = Ax(k) + Bu(k) \tag{7.3}$$
$$y(k) = Cx(k) + Du(k) \tag{7.4}$$

Subspace-based Identification There are several subspace-based methods for identification of state-space models. Among the most well known are the the multi-variable output-error state-space model algorithm, MOESP [Verhaegen, 1994], and the canonical variable algorithm, CVA [Larimore, 1990].

Realization based Impulse Response Analysis A realization based approach is to identify a state-space realization of this linear system by using realization based algorithms [Ho and Kalman, 1966], [Juang and Pappa, 1985].

Realization based Step Response Analysis The following step response analysis (proposed by Rolf Johansson) is a further extension of the impulse response algorithm. The method is based on the use of Markov parameters $\{H_k\}$, the coefficient matrices of the step response data $y_k{}_{k=1}^{N}$. The method works by, for suitable r, s such that $k+r+s \leq N$ where N is the number of data points, arranging the Markov parameters in a Hankel matrix structure

$$H_{r,s}^{(k)} = \begin{pmatrix} y_{k+1} & y_{k+2} & \cdots & y_{k+s} \\ y_{k+2} & y_{k+3} & \cdots & y_{k+s+1} \\ \vdots & \vdots & \vdots & \ddots \\ y_{k+r} & y_{k+r+1} & \vdots & y_{k+r+s-1} \end{pmatrix} \tag{7.5}$$

and then computing the singular value decomposition (SVD) of

$$H_{r,s}^{(0)} - H_{r,s}^{(1)} = U\Sigma V^T \tag{7.6}$$

The impulse response algorithm proposed in [Ho and Kalman, 1966] is used to determine a balanced realization with one input, p outputs, and a system of order n modified to be

$$x_{k+1} = A_n x_n + B_n u_k \tag{7.7}$$
$$y_k = C_n x_k + D u_k \tag{7.8}$$

where

$$A_n = \Sigma_n^{-1/2} U_n^T (H_{r,s}^{(1)} - H_{r,s}^{(2)}) V_n \Sigma_n^{-1/2} \tag{7.9}$$

$$B_n = \Sigma_n^{-1/2} V_n^T E_u \tag{7.10}$$

$$C_n = E_y^T U_n \Sigma_n^{-1/2} \tag{7.11}$$

$$D = 0 \tag{7.12}$$

$$E_y^T = [I_{p\times p} \;\; 0_{p\times(r-1)p}] \tag{7.13}$$

$$E_u^T = [1 \;\; 0_{1\times(s-1)}] \tag{7.14}$$

$$\Sigma_n = \text{diag}\{\sigma_1, \sigma_2, ..., \sigma_n\} \tag{7.15}$$

$$U_n = \text{matrix of first } n \text{ columns of } U \tag{7.16}$$

$$V_n = \text{matrix of first } n \text{ columns of } V \tag{7.17}$$

Two different implementations of the MOESP algorithm were used, the N4SID-script in the System Identification (SI) Toolbox version 5.0 for MATLAB and the SMI Toolbox for MATLAB [Haverkamp and Verhaegen, 1997]. One observation regarding the cylinder pressure or the cylinder ion current is that it has features of an impulse response of a linear system. The idea to interpret the pressure trace as a result of an impulse was suggested in [Tunestål, 2001], but not exploited. What is most interesting to model in the traces is the ignition delay and the pressure increase due to combustion, since from this α can be estimated. The duration of the combustion is significant and a new approach is to interpret the trace as a result of a step response. Even if there would be simultaneous ignition, the duration of combustion is several crank angle degrees as the kinetics are time dependent.

In the model selection procedure and the validation of the models standard methods from system identification has been used. In the first selection of model order, the singular values of the Hankel matrix, the value of Akaike Final Prediction Error (FPE), the loss function (V), Variance-Accounted-For (VAF)

$$VAF = 100 \times (1 - \frac{\texttt{var}(y - \widehat{y})}{\texttt{var}(y)})$$

and the percentage of the output variation that is explained by the model (FIT)

$$FIT = 100 \times (1 - \frac{||\widehat{y} - y||}{||y - \bar{y}||})$$

were used. The loss function is equal to the determinant of the estimated covariance matrix of the noise source. In the validation stage, residual

analysis, autocorrelation and cross validation were performed for all the estimated models. Data trends were eliminated before the identification procedure started if not otherwise stated.

7.2 Experiments with Dual Fuel

One of the goals of HCCI engine design, is that an HCCI engine should have similar operation range as a Diesel engine. Hence, models describing the dynamic behavior of the whole operation range are needed. The objective was to find models where the cycle-to-cycle control signal of the HCCI engine dynamics was the fuel ratio between two fuels, R_f. Experiments in a wide range of operating conditions were performed in order to study the effect of R_f, injected fuel energy W_f, inlet temperature T_{in}, inlet pressure P_{in}, and engine speed n, on α. Also, to some extent the effect of EGR and the change of VGT on α have been studied. Since the engine is not stable and since too fast combustion at high load could damage the pressure transducers or the engine, only low-load experiment were carried out in open loop. Higher load experiments were performed in closed loop.

In the open loop experiments, R_f, W_f, T_{in} and n were excited. The R_f, W_f, T_{in} were excited by a pseudo-random binary sequence (PRBS) signal and n was excited manually. In the close loop experiments also a PRBS signal was added on the reference value of the α. During the closed loop experiment, the controller was tuned in a conservative setting. Each of the experiments consisted of 2500 or more engine cycles, which seemed to be sufficient for the identification methods. All the experiments were run several times in order to supply data for both identification and validation. When the experiments started, the engine temperature was at the operating point.

Naturally Aspirated Experiments

In these experiment the VGT was tuned to low boost pressure.

Experiment 1 This experiment was performed in open-loop at low load and the VGT was tuned to low boost pressure. The pressure P_{in} varied between $1.05 - 1.3$ bar. R_f varied between $0.43 - 0.63$ (RON $76 - 86$), W_f varied between $1000 - 1500$ J/cycle (FuelMEP $5 - 7.5$ bar), T_{inlet} varied between $89 - 101^{\circ}C$ and n varied between $750 - 1500$ rpm. A W_f around 1000 J/cycle corresponds to running the engine at idle speed, without transmitting power, and W_f around 1500 J/cycle corresponds to running the engine on a load just above idle. IMEP_n varied between $1.5 - 3.5$ bar.

Experiment 2 This experiment was performed in closed-loop and the VGT was tuned to low boost pressure. The pressure P_{in} varied between $1.1-1.35$ bar. W_f varied between $2000-2300$ J/cycle (FuelMep $10-11.5$ bar). In this experiment air/fuel ratio, λ, was close to 2.6, which is near the limit of possible operation point for HCCI. The reference value for α was kept constant at 11 CAD. A PRBS signal was added on the reference signal with an amplitude of 2 CAD. On the resulting control signal, R_f, a PRBS signal was added with an amplitude of 0.4. The T_{in} varied between $68-77^{\circ}C$ and n varied between $n = 750-1500$ rpm. IMEP_n varied between $5-6$ bar.

Boost Experiments

In these experiments the VGT was tuned to boost pressure.

Experiment 3 This experiment was performed in open-loop and the VGT was tuned to boost pressure. The pressure P_{in} was at 1.3 bar. R_f varied between $0.5-0.9$, W_f was constant at 2000 J/cycle (FuelMEP 10 bar), T_{inlet} was constant at $70^{\circ}C$ and n was constant at 1000 rpm. IMEP_n was around 4.5 bar.

Experiment 4 This experiment was performed in open-loop and the VGT was tuned to boost pressure. The pressure P_{in} varied between $1.25-1.55$ bar. R_f varied between $0.5-0.9$, W_f varied between $1600-2000$ J/cycle (FuelMEP $8-10$ bar), T_{inlet} varied between $70-80^{\circ}C$ and n varied between $900-1200$ rpm. IMEP_n varied between $3-4.5$ bar.

Experiment 5 This experiment was performed in closed-loop and the VGT was tuned to generate boost pressure. The pressure P_{in} was 1.5 bar. W_f varied between $2000-2200$ J/cycle (FuelMEP $10-11$ bar). The reference value for α was kept constant at 9 CAD. A PRBS signal was added on the references signal with an amplitude of 0.6 CAD. On the resulting control signal, R_f, a PRBS signal was added with an amplitude of 0.1. The T_{in} varied between $63-65^{\circ}C$ and n varied between $n = 1200-1400$ rpm. The resulting IMEP_n varied between $4-4.7$ bar.

Experiment 6 This experiment was performed in closed-loop and the VGT was tuned to generate boost pressure. The pressure P_{in} was 1.8 bar. W_f varied between $3000-3200$ J/cycle (FuelMEP $15-16$ bar). The reference value for α was kept constant at 9 CAD. A PRBS signal was added on the reference signal with an amplitude of 0.6 CAD. On the resulting control signal, R_f, a PRBS signal was added with an amplitude of 0.1. The T_{in} varied between $57-59^{\circ}C$ and n varied between $n = 1200-1400$ rpm. The resulting IMEP_n was between $7-7.5$ bar.

Experiment 7 This experiment was performed in closed-loop and the VGT was tuned to generate boost pressure. The pressure P_{in} was 2.1 bar. W_f varied between $4000-4200$ J/cycle (FuelMEP $20-21$ bar). The reference value for α was kept constant at 9 CAD. A PRBS signal was added on the reference signal with an amplitude of 0.6 CAD. On the resulting control signal, R_f, a PRBS signal was added with an amplitude of 0.1. The T_{in} varied between $44-46^{\circ}C$ and n varied between $n = 1200-1400$ rpm. The resulting IMEP_n was between $9.5-10$ bar.

Experiment 8 This experiment was performed in closed-loop and the VGT was tuned to generate boost pressure. The pressure P_{in} was 2.4 bar. W_f varied between $5000-5200$ J/cycle (FuelMEP $25-26$ bar). The reference value for α was kept constant at 9 CAD. A PRBS signal was added on the reference signal with an amplitude of 0.6 CAD. On the resulting control signal, R_f, a PRBS signal was added with an amplitude of 0.1. The T_{in} varied between $40-42^{\circ}C$ and n varied between $n = 1200-1400$ rpm. The resulting IMEP_n varied between 11-13 bar.

Experiment 9 This experiment was performed in closed-loop and the VGT was tuned to generate boost pressure. The pressure P_{in} varied between $1.4-2.4$ bar. W_f varied between $2000-5000$ J/cycle (FuelMEP $10-25$ bar). The reference value for α varied between $9-11$ CAD. A PRBS signal was added on the reference signal with an amplitude of 0.6 CAD. On the resulting control signal, R_f, a PRBS signal was added with an amplitude of 0.1. The T_{in} varied between $40-43^{\circ}C$ and n varied between $n = 1200-1400$ rpm. The resulting IMEP_n varied between 4-12 bar.

7.3 Combustion Phasing Modeling with Dual Fuel

Naturally Aspirated Experiment

Experiment 1 In Table 7.1 the FPE, V, VAF, and FIT scores are shown for the estimated models of second and third order for cylinder one. The SMI Toolbox does not calculate the FPE or V, instead only the singular values of the Hankel matrix were used in the preliminary model order selection. M1 is the model using the MOESP algorithm in the N4SID script, $MOESP_{N4SID}$ and M2 is the model using the SMI Toolbox, $MOESP_{SMI}$. The PEM model has the lowest FPE and V values, but the difference to the other methods is not large. $MOESP_{N4SID}$ and CVA_{N4SID} gave almost identical results. $MOESP_{SMI}$ gave the highest VAF and FIT scores,

Cylinder 1								
Order	2				3			
Alg.	M1	M2	CVA	PEM	M1	M2	CVA	PEM
FPE	0.203	-	0.203	0.190	0.206	-	0.206	0.190
V	0.200	-	0.200	0.188	0.202	-	0.202	0.188
VAF	80.15	84.17	80.15	66.10	81.13	84.35	81.18	66.05
FIT	55.45	60.21	55.52	42.32	56.56	60.27	56.62	42.32

Table 7.1 Comparison of the estimated models of second and third order for experiment 1.

and PEM the lowest scores. There was no significant achievement in the scores by increasing from a second-order to a third-order model and this was also found true when increasing the model up to a tenth-order model. The measured output and simulated output from the estimated second-order model for the six cylinders is shown in Fig. 7.1. The model was estimated by using the SMI Toolbox. In Fig. 7.4, the pole map of the estimated second-order models for the six cylinders is shown. It can be observed that the cylinders have different dynamics. This is also expected since the cylinders exhibit different conditions, for example the first and the sixth cylinder have only one neighbor resulting in a lower wall temperature. The inlet temperature also differs, as cylinder one has the shortest travel time from the heater and cylinder six the longest. A temperature sensor mounted on each of the intakes of the cylinders could be used to even better capture the differences between the cylinders. Additionally, the cylinders are not exactly identical as some minor manufacturing differences in the dimensions may exist. Even if the dynamics of the models for the cylinders varied it can be observed from Fig. 7.1 that the identification accuracy was similar. In the validation of the estimated models residual analysis, cross validation, and one-step-ahead prediction was used.

The residuals of the second-order model estimated by $MOESP_{SMI}$ and the output were kept almost between ± 1 CAD. The correlation function of the output was kept close to the 99% confidence region around zero (Fig. 7.3), the residual distribution being close to normal (Fig. 7.2). Fig. 7.5 shows the result from one-step-ahead model output and measured output for the second order model estimated by $MOESP_{SMI}$, with VAF score of 91.14 and FIT score of 70.23. The other methods, $MOESP_{N4SID}$, CVA_{N4SID} and PEM gave similar results. The residual from cross validation of the second-order model estimated by $MOESP_{SMI}$ provided a

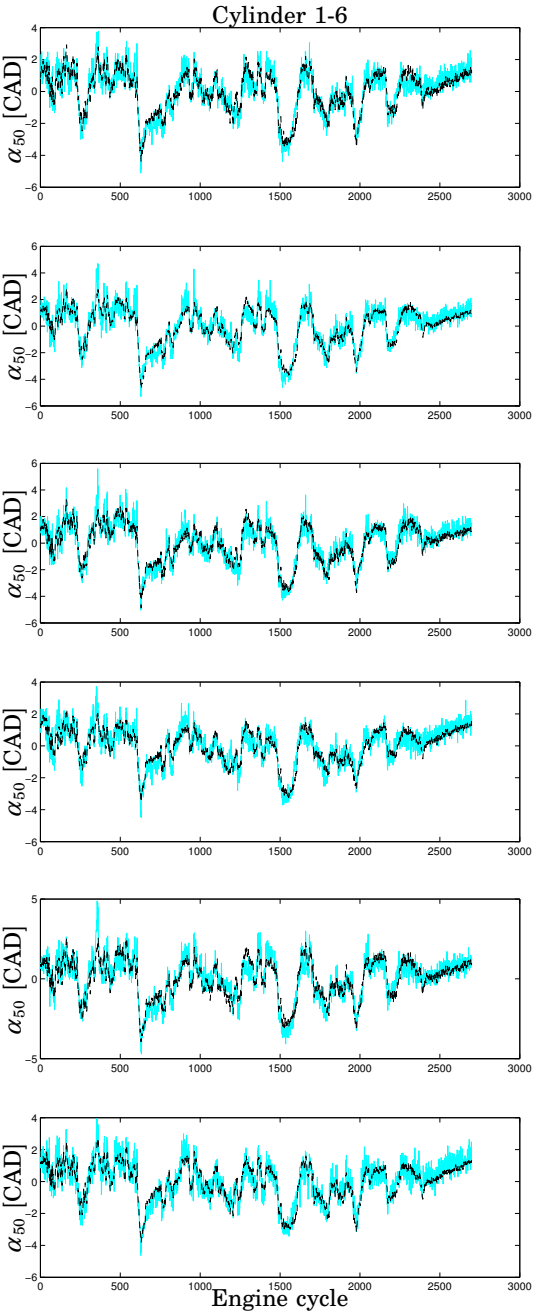

Figure 7.1 Experiment 1: Measured output (*grey*) and simulated output from the estimated second-order model (*black*) for the six cylinders.

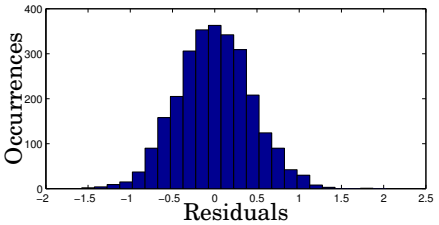

Figure 7.2 Histogram of the residuals of the estimated second-order model.

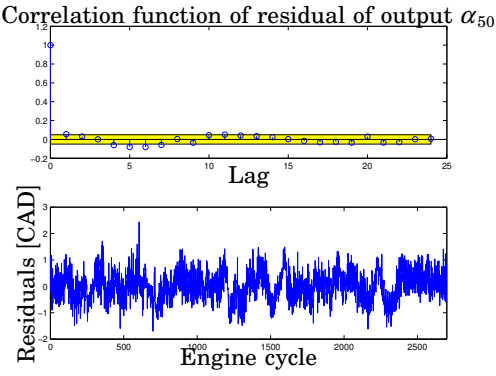

Figure 7.3 Residual analysis of the estimated second-order model.

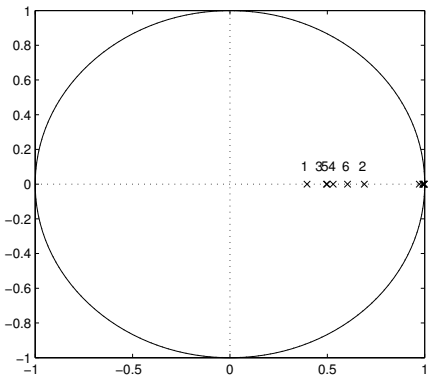

Figure 7.4 Experiment 1: Pole-map of the model for the six cylinders. The numbers represent the corresponding cylinder.

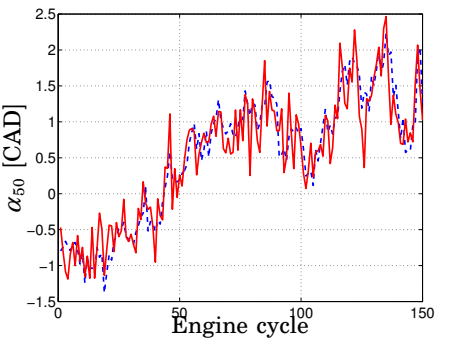

Figure 7.5 Experiment 1: One-step-ahead prediction model output of the estimated second-order model by $MOESP_{SMI}$ (*dashed*) and measured output (*solid*).

VAF score of 82.64 and a FIT score of 58.54. Fig 7.6 shows the simulation result of the cross validation. The other methods, $MOESP_{N4SID}$ and CVA_{N4SID} were close to these values. PEM was significant worse, the difference being around 10%, in both the VAF and the FIT scores.

Experiment 2

In Table 7.2 FPE, V, VAF, and FIT values are shown of the estimated models of second and third order for cylinder one. Of the estimated mod-

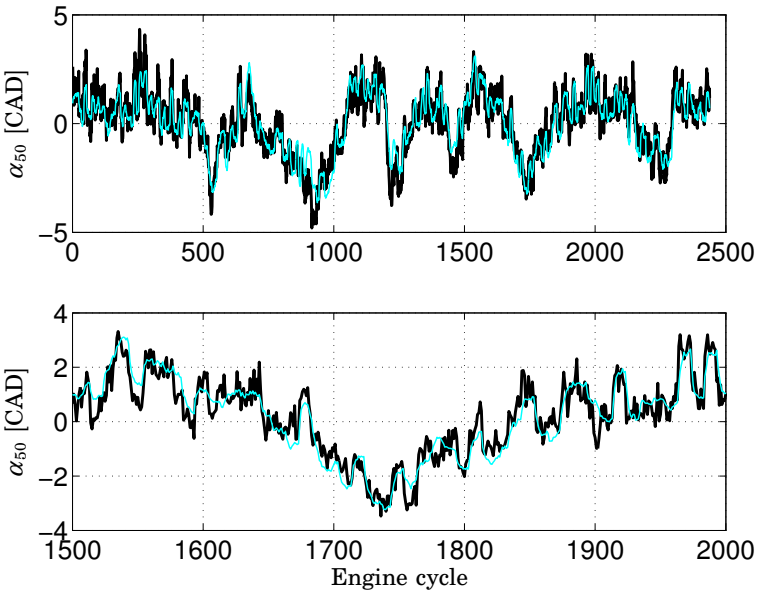

Figure 7.6 Experiment 1: Cross validation of the estimated second-order $MOESP_{SMI}$ model of cylinder one. Measured α_{50} (*black*) and modeled α_{50} (*grey*). The lower figure shows a closer view of the engine cycle 1500 to 2000.

els, PEM models had the lowest FPE and V values. $MOESP_{N4SID}$ and CVA_{N4SID} gave similar results, but has significantly lower VAF and FIT scores than $MOESP_{SMI}$. PEM even failed to give positive values. As for Experiment 1, there was no significant improvements in the scores by increasing the model order above second order. In Fig. 7.7 the result from the estimated second order for cylinder one is shown. The residuals of the second-order model estimated by $MOESP_{SMI}$ were less than ± 2 CAD. The correlation function of the output was kept inside the 99% confidence region around zero. Also in this case, the residuals were found to be nearly normally distributed. Fig. 7.8 shows the result sequence from one-step-ahead model output for the second-order model estimated by $MOESP_{SMI}$ and the measured output. The residuals from the cross validation of the second-order model estimated by $MOESP_{SMI}$ provided a VAF score of 55.6 and a FIT score of 34.3.

Experiment 3 In experiment 3 only the fuel ratio was excited. In this case a second-order model gave good a fit. The simulation result of the

Cylinder 1								
Order	2				3			
Alg.	M1	M2	CVA	PEM	M1	M2	CVA	PEM
FPE	0.43	-	0.43	0.39	0.41	-	0.41	0.39
V	0.41	-	0.41	0.38	0.40	-	0.40	0.37
VAF	60.9	61.2	60.6	43.1	61.3	62.5	61.4	46.5
FIT	41.5	41.7	41.4	35.7	42.6	43.2	42.8	37.3

Table 7.2 Comparison of estimated models of second and third order for experiment 2.

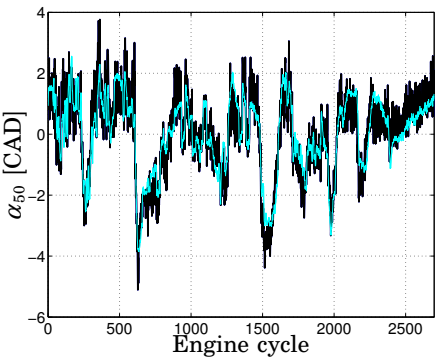

Figure 7.7 Experiment 2: Measured output (*black*) and simulated output from second-order $MOESP_{SMI}$ model (*grey*) for cylinder 1.

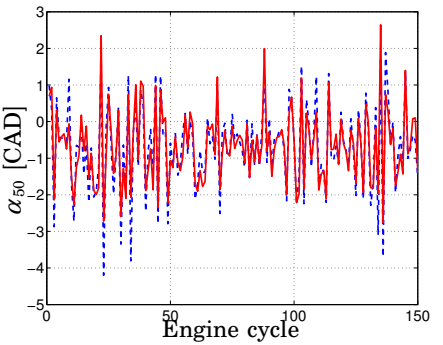

Figure 7.8 Experiment 2: One-step-ahead prediction model output of the estimated second order model by $MOESP_{SMI}$ (*dashed*) and measured output (*solid*).

model is shown in Fig. 7.9. The model had VAF scores of 88.2% and FIT scores of 65.0%. Figure 7.10 shows the residuals and the residual distribution. It can be observed that the residual distribution was similar to a normal distribution with zero mean value.

Experiment 4 As the main objective was to control the combustion phasing, the system was simplified to a MISO system. It was also desired to control the load and avoiding too high pressure gradient per crank angle $dp/d\theta$, therefore MIMO models were needed. The MIMO model had R_f, W_f, T_{in} and n as inputs and α_{50}, IMEP$_n$ and $dp/d\theta$ as outputs. In Fig 7.11, the result from a sixth-order MIMO model is shown. It can be observed

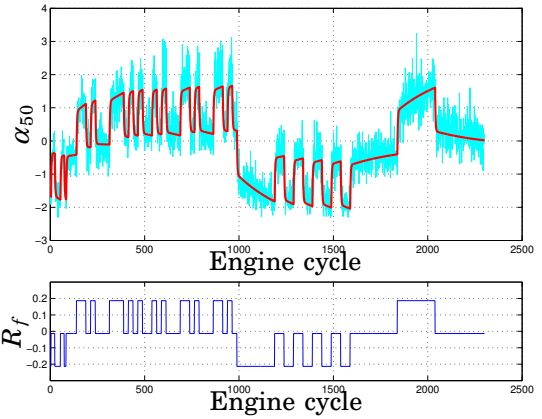

Figure 7.9 Upper figure shows measured output *(gray)* and model output from a second-order model *(black)*. Lower figure shows the input PRBS signal.

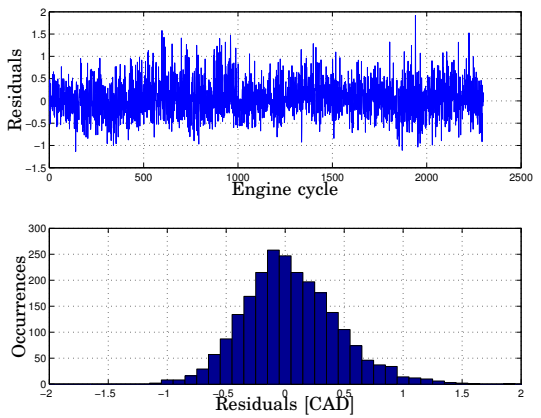

Figure 7.10 Residuals from the second-order model and the residual distribution.

that the model succeeds in capturing the significant dynamics. The model had VAF scores of [86.5% 93.8% 79.2%] and FIT scores of [63.3% 75.1% 54.7%]. Figure 7.12 shows the residuals and the residual distribution. It can be observed that the residual distribution was similar to the normal distribution with zero mean value. Figure 7.13 shows cross-validation of the estimated sixth-order model. For the cross-validation case, the model had VAF scores of [79.8% 87.3% 78.5%] and FIT scores of [55.1% 72.2% 52.4%].

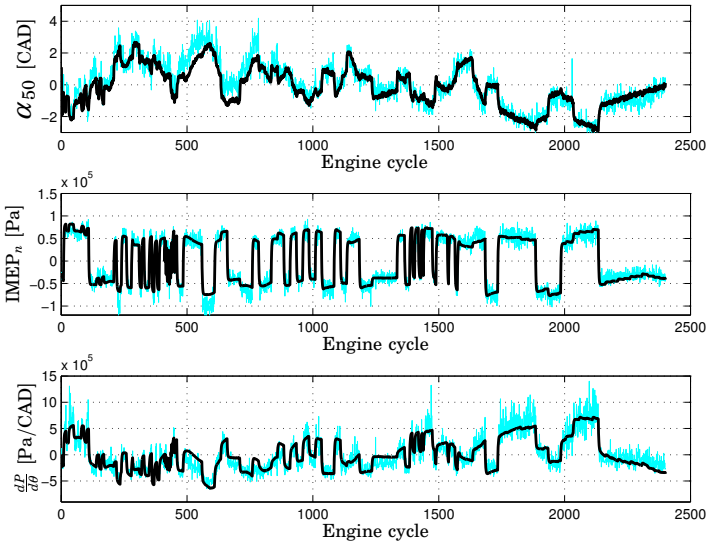

Figure 7.11 Model outputs (*thick line black*) from the sixth-order MIMO model and measured outputs (*thin grey line*).

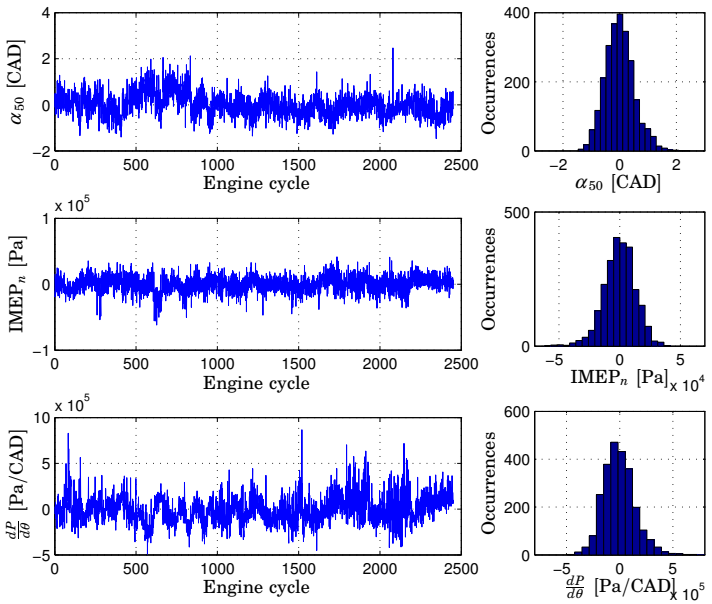

Figure 7.12 Residuals from the sixth-order MIMO model and the residual distribution

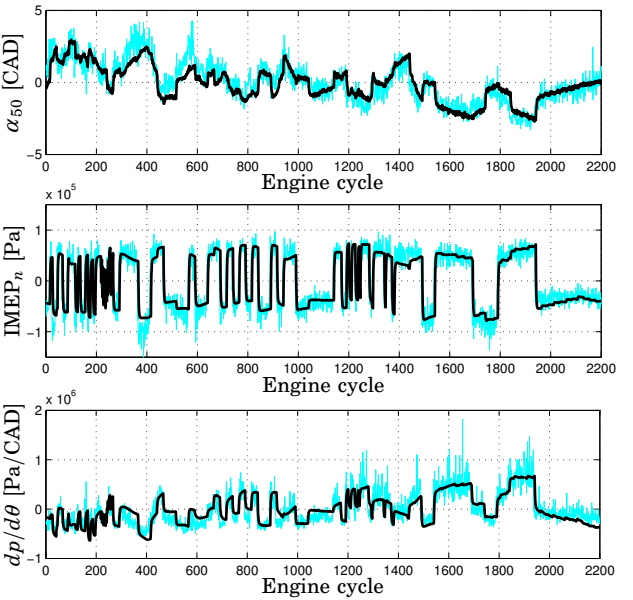

Figure 7.13 Cross-validation of the sixth-order MIMO model. Model outputs (*thick black line*) and measured outputs (*thin grey line*).

Cylinder 1					
Order	1	2	3	4	5
FIT	32.9	35.8	35.7	35.7	35.8
VAF	55.4	59.7	59.1	59.3	60.1

Table 7.3 Comparison of estimated models for experiment 5.

Boost Experiment

As it was found that the various subspace algorithms gave similar performance, only results using the $MOESP_{N4SID}$ algorithm are presented.

Experiment 5 In Table 7.3, VAF and FIT values are shown of the estimated models of second- to fifth-order for cylinder one. As for the naturally aspirated experiments, there were no significant improvements in the scores by increasing above second order. In Fig. 7.14 the result from the estimated second-order model for cylinder one is shown. The singular values of the Hankel matrix are shown in Fig. 7.15 and indicating that higher-order models will probably not increase the model accuracy and that the noise level is significant. Cross validation gives good results,

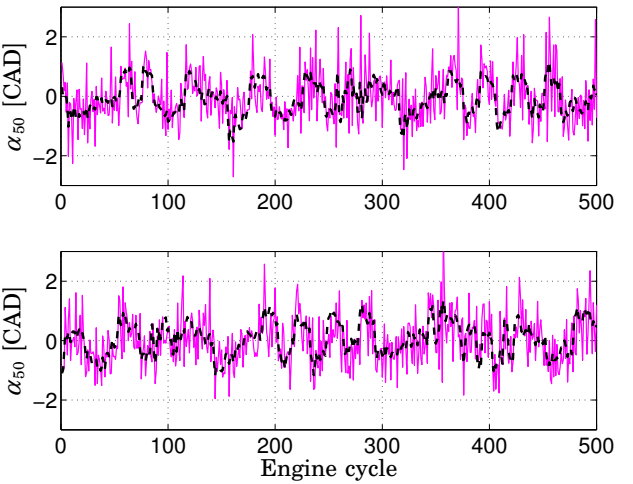

Figure 7.14 Experiment 5: Upper figure shows measured output (*solid*) and simulated output from second-order $MOESP_{SMI}$ model (*dashed*) for Cylinder 1. Lower figure shows cross validation of the second-order $MOESP_{SMI}$ model. Measured output (*solid*) and model output (*dashed*).

Cylinder 1					
Order	1	2	3	4	5
FIT	29.5	31.8	31.9	32.3	32.5
VAF	50.2	53.1	51.3	51.9	52.2

Table 7.4 Comparison of estimated models of experiment 6.

almost the same VAF and FIT scores as for the identification data set, the VAF score being 52.4 and the FIT score being 30.7.

Experiment 6 In Table 7.4, VAF and FIT values are shown of the estimated models of second to fifth order for cylinder one. As for the naturally aspirated experiments, there were no significant improvements in the scores by increasing above second order. In Fig. 7.16 the result from the estimated second order for cylinder one is shown. The singular values of the Hankel matrix are shown in Fig. 7.15 indicates that higher-order models will probably not increase the model accuracy and that the noise level is significant. It can also be noted that it suggests a third-order model. Cross validation gives good results, with almost the same VAF and FIT scores as for the identification data set, the VAF score being 47.7 and the FIT score being 27.5.

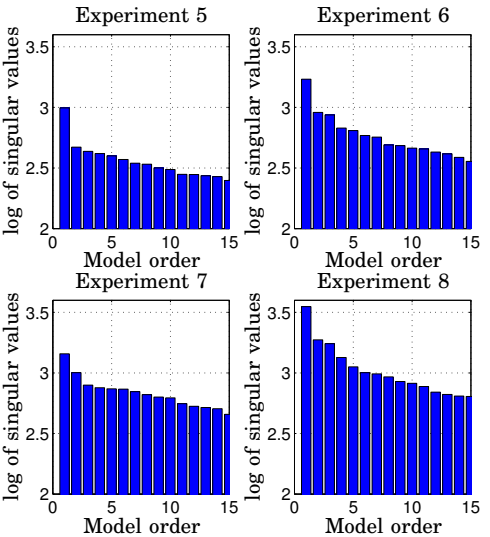

Figure 7.15 Singular values of the Hankel matrix used in the model order choice for experiment 5–8.

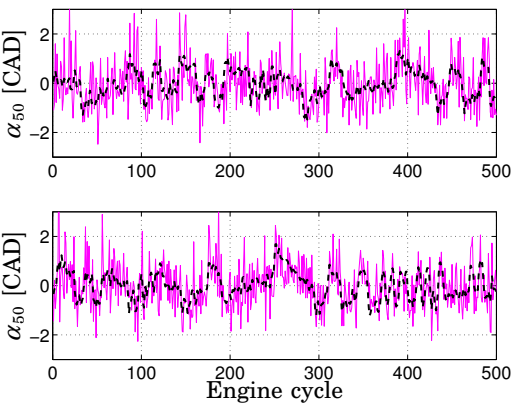

Figure 7.16 Experiment 6: Upper figure shows measured output (*solid*) and simulated output from second-order $MOESP_{SMI}$ model (*dashed*) for cylinder 1. Lower figure shows cross validation of the second-order $MOESP_{SMI}$ model. Measured output (*solid*) and model output (*dashed*).

Experiment 7 In Table 7.5, VAF and FIT values are shown of the estimated models of second to fifth order for cylinder one. As for the naturally aspirated experiments, there were no significant improvements in the scores of model orders higher than two. In Fig. 7.17 the result from

Cylinder 1				
Order	2	3	4	5
FIT	30.17	30.38	30.89	31.19
VAF	51.54	50.58	51.16	51.21

Table 7.5 Comparison of estimated models for experiment 7.

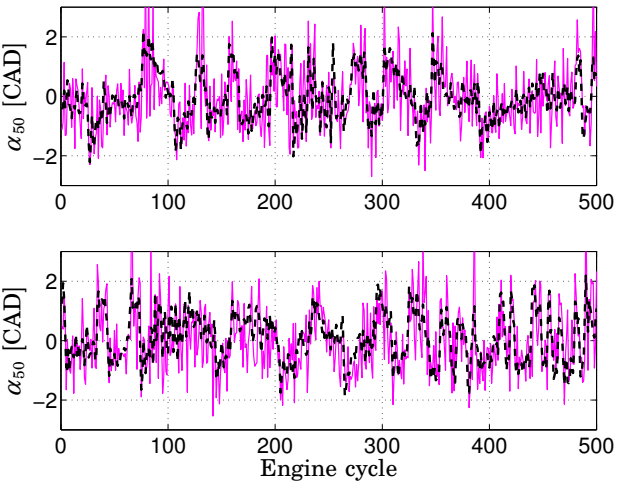

Figure 7.17 Experiment 7: Upper figure shows measured output (*solid*) and simulated output from second-order $MOESP_{SMI}$ model (*dashed*) for cylinder 1. Lower figure shows cross validation of the second-order $MOESP_{SMI}$ model. Measured output (*solid*) and model output (*dashed*).

the estimated second order model dynamics for cylinder one is shown. The singular values of the Hankel matrix are shown in Fig. 7.15, indicating as previously that higher-order models will probably not increase the model accuracy and that the noise level is significant. Cross validation gives similar VAF and FIT scores as for the identified data set, the VAF score being 42.73 and the FIT score being 24.49.

Experiment 8 In Table 7.6, VAF and FIT values are shown of the estimated models of model orders $n = 2 - 7$ for cylinder one. As for the naturally aspirated experiments, there were no significant improvements in the scores of model orders higher than two and in Fig. 7.18 the result

Cylinder 1						
Order	2	3	4	5	6	7
FIT	17.52	19.85	19.97	20.27	20.45	20.46
VAF	28.03	31.19	31.38	31.89	32.19	32.40

Table 7.6 Comparison of estimated models for experiment 8.

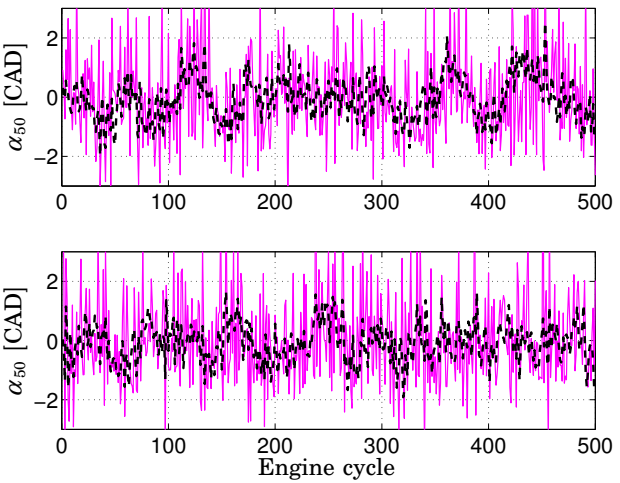

Figure 7.18 Experiment 8: Upper figure shows measured output (*solid*) and simulated output from second-order $MOESP_{SMI}$ model (*dashed*) for cylinder 1. Lower figure shows cross validation of the second-order $MOESP_{SMI}$ model. Measured output (*solid*) and model output (*dashed*).

from the estimated second order for cylinder one is shown. The singular values of the Hankel matrix are shown in Fig. 7.15 indicating as previously that higher-order models will probably not increase the model accuracy and that the noise level is significant. Cross validation gave good results, as the residual distribution being close to normal with zero mean and similar VAF and FIT scores as for the identified data set, the VAF score being 25.8 and the FIT score being 16.1.

Experiment 9 In Table 7.7, VAF and FIT values are shown of the estimated models of model orders $n = 2 - 7$ for cylinder one. As for the naturally aspirated experiments, there were no significant improvements in the scores of model orders higher than three and in Fig. 7.19 the result from the estimated third-order model for cylinder one is shown. Cross

Cylinder 1						
Order	2	3	4	5	6	7
FIT	17.2	22.0	24.5	24.8	25.9	25.5
VAF	31.9	39.1	42.9	44.3	45.6	45.3

Table 7.7 Comparison of estimated models for experiment 9.

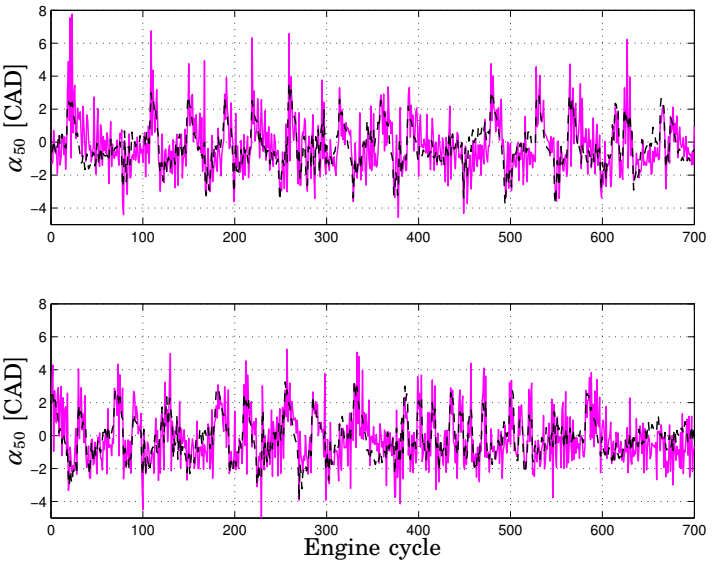

Figure 7.19 Experiment 9: Upper figure shows measured output (*solid*) and simulated output from third-order $MOESP_{SMI}$ model (*dashed*) for cylinder 1. Lower figure shows cross validation of the third-order $MOESP_{SMI}$ model. Measured output (*solid*) and model output (*dashed*).

validation gave good results, as the residual distribution being close to normal with zero mean and similar VAF and FIT scores as for the identified data set, the VAF score being 37.5 and the FIT score being 20.7.

In this experiment the amplitude of the cycle-to-cycle variations were changed. The variance increased when the load increased, and the model fail to well describe the changed cycle-to-cycle variance.

7.4 Experiments with VVA

The objective was to find models of the HCCI engine dynamics when the IVC phasing was used as the cycle-to-cycle control signal. Experiments in a wide range of operating conditions were performed in order to study the effect of IVC phasing, injected fuel energy W_f, inlet temperature T_{in}, inlet pressure P_{in}, and engine speed n, on α.

Experiment 10

This experiment was performed in open-loop at low load and the VGT was tuned to low boost pressure, P_{in} varied between 1.04-1.07 bar. IVC varied between 525-565 CAD, R_f was constant at 0.87 (RON 95), W_f varied between $1000 - 1400$ J/cycle (FuelMEP $5 - 7$ bar), T_{inlet} varied between $102 - 114^{\circ}C$ and n was constant at 1200 rpm. IMEP_n varied between $1.5 - 3.5$ bar.

Experiment 11

This experiment was performed in open-loop at low load and the VGT was tuned to low boost pressure, P_{in} varied between 1.04-1.07 bar. IVC varied between 555-595 CAD, R_f was constant at 0.87 (RON 95), W_f was constant at 1200 J/cycle (FuelMEP 6 bar), T_{inlet} was constant at $110^{\circ}C$ and n was constant at 1100 rpm. IMEP_n was around 3 bar.

7.5 Combustion Phasing Modeling with VVA

Experiment 10

In Fig. 7.20 the results from a fourth-order model are shown, the FIT score being 53.87%. The model was estimated using the N4SID_{MOESP} algorithm in Matlab. This fourth-order models are able to capture most of the dynamics, but it can be observed that it has some problem to capture the low frequency behavior correctly. At some operating conditions the gain of the model is too low, for example at cycle 300-400 in Fig. 7.20 and for other operating conditions the models gain is too high, see for example at cycle 1200-1400 in Fig. 7.20. In the experiment the IVC was varied in a wide range and the results indicate that the relationship between IVC and α_{50} is nonlinear. In order to capture the behavior, several piecewise linear or nonlinear models are needed.

Experiment 11

By changing the IVC crank angle the effective compression ratio is changed, resulting in a cylinder temperature change and a change in α_{50}. Due to

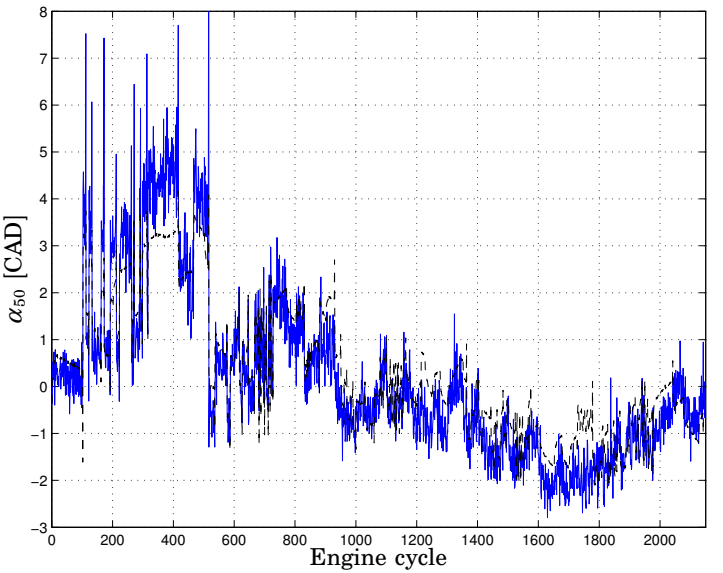

Figure 7.20 Experiment 10: Measured output (*solid*) and simulated output from fourth-order $MOESP_{SMI}$ model (*dashed*) for cylinder 1.

the movement of the piston, a change of θ_{IVC} has a nonlinear effect on α_{50}, Figure 7.21. It can be noted that there are two possibilities to obtain the same α_{50}, either by closing the inlet valve during the expansion before BDC or during the compression after BDC. This experiment included only IVC phasing at or after the BDC.

The static nonlinearity can be estimated as a polynomial of fourth order. A method to linearize the system was to estimate the inverse of the nonlinearity and add this to the system, see Figure 7.22. The system was then approximately linear from $\bar{u}^{'}$ to $\bar{u}$.

Figure 7.23 shows the result of the compensation of the static nonlinearity. As the compensation was successful $\bar{u}$ can be approximated by $\bar{u}^{'}$. The inverse was obtained using a look-up table.

As the nonlinearity could be described by a polynomial of power four, a method to identify the dynamics is to use inputs up to power four. Figure 7.24 shows the inputs and output used in the identification.

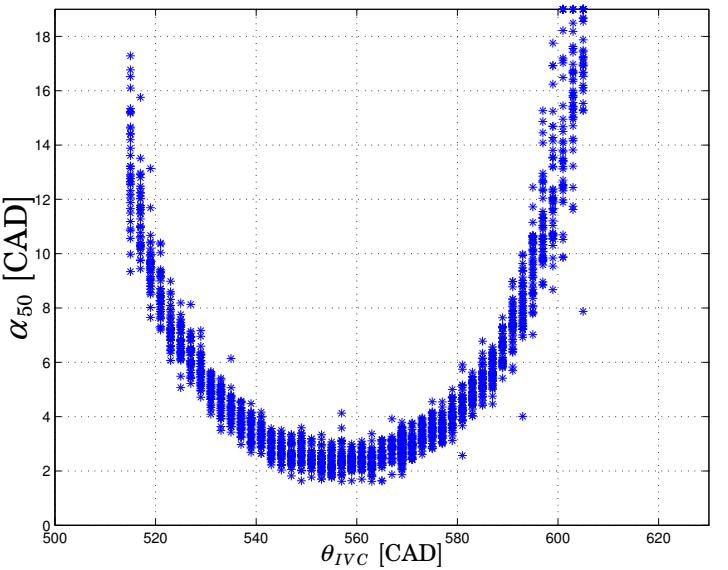

Figure 7.21 The effect of IVC changes on α_{50} at steady-state.

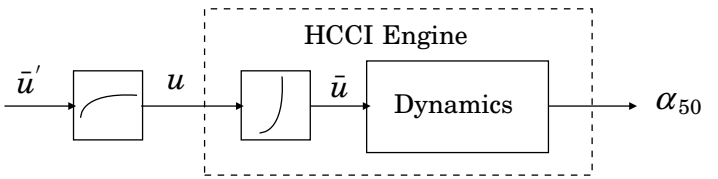

Figure 7.22 Compensating for the nonlinear characteristics of IVC control, where u is θ_{IVC}.

The identified models were obtained in state space representation:

$$\begin{aligned} x(k+1) &= Ax(k) + B \begin{bmatrix} u(k) \\ u^2(k) \\ u^3(k) \\ u^4(k) \end{bmatrix} \\ y(k) &= C(x(k) + Du(k) \end{aligned}$$

The experiment were performed in open-loop and at low load. In order to have persistent excitation, θ_{IVC} was excited by a PRBS signal. In this

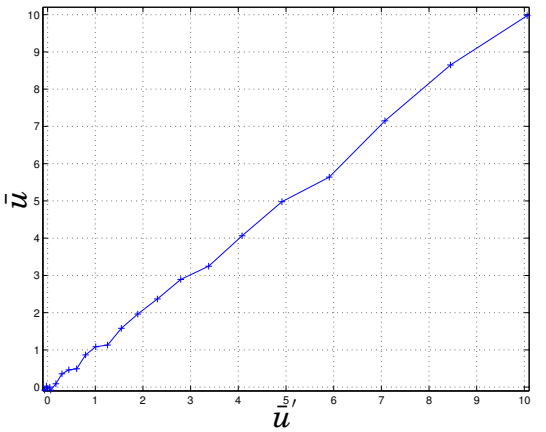

Figure 7.23 Result of the compensation of the static nonlinearity.

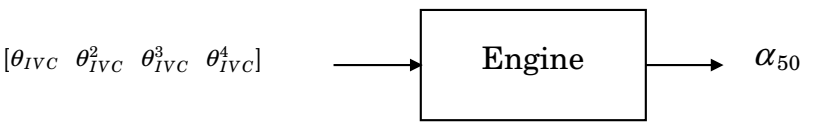

Figure 7.24 Inputs and output used in the identification.

experiment the VGT was tuned to a low-boost pressure. Offsets have been removed from all of the data.

In Figure 7.25 result from a second-order model and the measured α_{50} is shown. It can be observed that second-order model was able to catch most of the engine dynamics. Figure 7.25 also shows the input PRBS signal. Figure 7.26 shows a closer view of the identification result. Figure 7.27 shows the residuals, the difference between measured output and the model output. It can be observed that the residual distribution was similar to the normal distribution with zero mean value. It can also be noted that the residual magnitude increases with later combustion phasing, higher α_{50}-value.

The identified B matrix has dimension $n \times 4$ (n=model order). The identified B matrix had rank one, hence the system could be written as a linear system

$$x(k+1) = Ax(k) + \bar{B}\bar{u}$$

This system is linear and linear control design methods can be used.

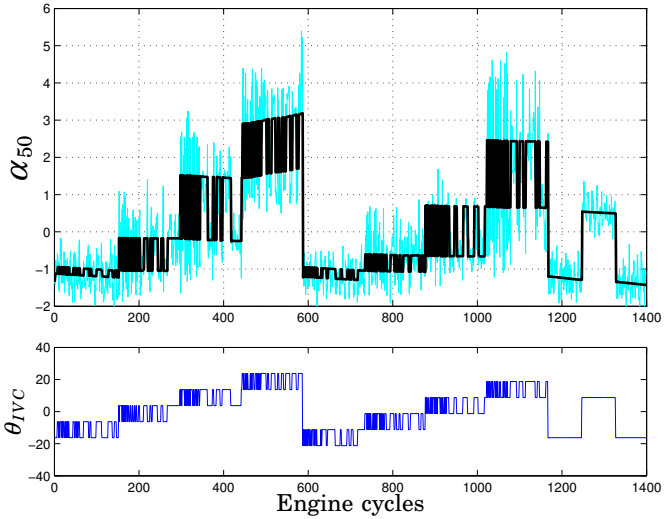

Figure 7.25 Experiment 11: Upper figure shows measured output *(gray)* and model output from a second-order model *(black)*. Lower figure shows the input PRBS signal.

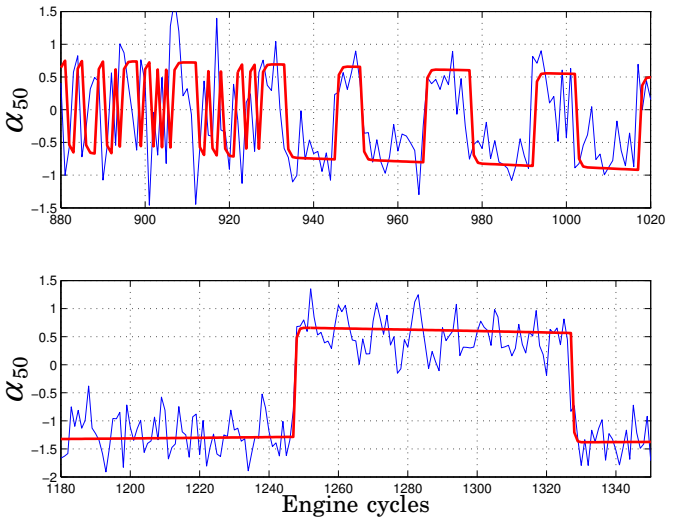

Figure 7.26 Experiment 11: Closer view of the measured output *(thin line)* and the model output from a second-order model *(thick line)* presented in Fig. 7.25.

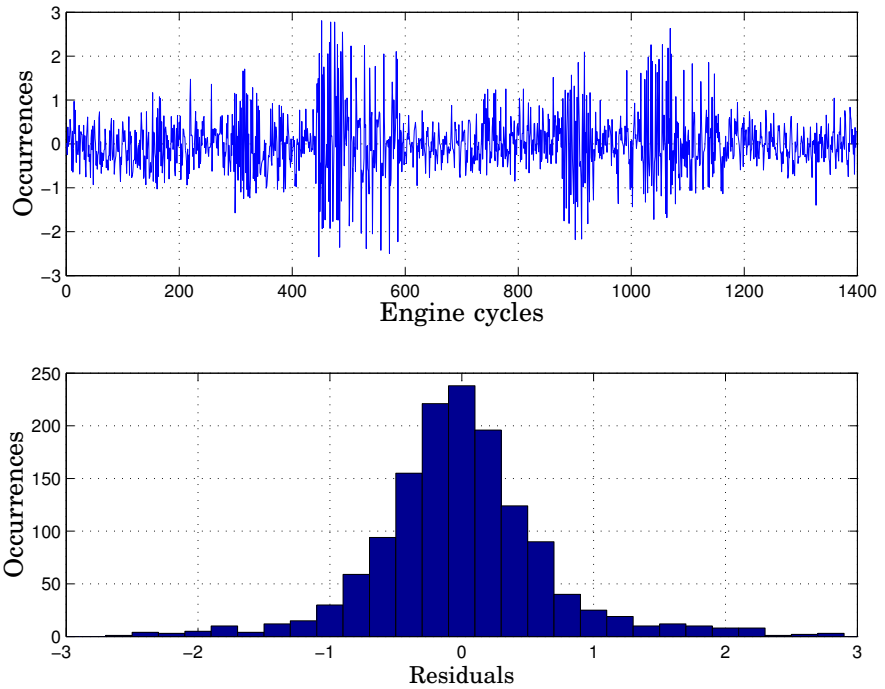

Figure 7.27 Identification residual and its distribution

7.6 Combustion Phasing Effect in Load Changes

Fast changes of the load is a vital property for successful automotive application. A driver wants to have a fast response when pressing the accelerator. Whereas the load is very dependent on the injected fuel energy, the load can be changed almost instantaneously in our experimental set-up, at higher loads there is a one cycle delay because the fuel injectors are not capable of injecting all the fuel before IVC. This problem could be solved by using higher pressure in the injector and hence increasing the injected volume. What actually limits the change of load is the control of the combustion phasing. The combustion phasing needs to be stable, even at fast load changes. In Fig. 7.28, the injected fuel energy was changed from 1000J to 1500J (FuelMEP $5-7.5$ bar) resulting in a change of IMEP from 2.2 to 4.0 bar. The fuel ratio was kept constant at 0.2 and the inlet temperature was kept constant at 87 $^{\circ}C$. It can be observed that α is advanced from approximately 7 to 3.5 CAD. The explanation is that the wall temperature increases and the concentration of fuel increases. The

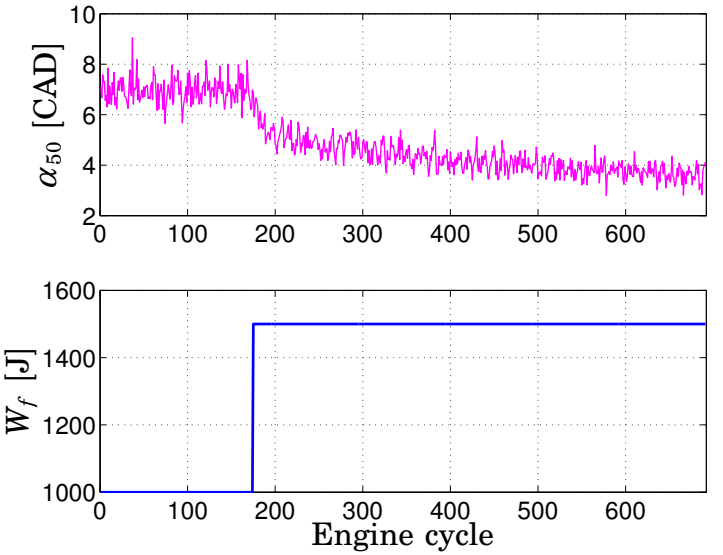

Figure 7.28 Step response in α_{50} of injected fuel energy

wall temperature increases, due to the faster pressure increase and higher maximum level. In Fig. 7.29, the injected fuel energy was also changed from 1000J to 1500J (FuelMEP $5-7.5$ bar) resulting in a change of IMEP from 2.5 to 4.0 bar. The fuel ratio was kept constant at 0.9 and the inlet temperature was kept constant at 100 $^{\circ}C$. Initially, it can be observed that α was retarded from approximately 7 to 8.5 CAD and thereafter slowly advanced to 6 CAD. The explanation for the initial retardation is that the vaporization of the fuel lower the temperature of the mixture. Higher load increases the combustion temperature, resulting in that the cylinder walls become warmer which leads to advanced phasing. Either of these two effects can dominate. After the transient, the phasing can be either earlier or later depending on the mode of operation. In order to be able to control α_{50} at a load change models are needed. An approach is to model the wall temperature effect as a first-order system and the vaporization effect of the fuels as a direct term (Fig. 7.30).

The transfer function from w_f to α_{50} is then given by

$$D - \frac{k}{1+\frac{s}{T}} = \frac{(D-k)+\frac{D}{T}s}{1+\frac{s}{T}} \tag{7.18}$$

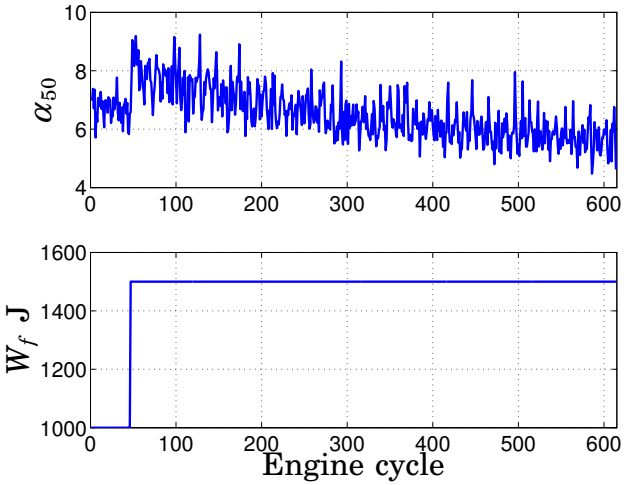

Figure 7.29 Step response in α_{50} of injected fuel energy

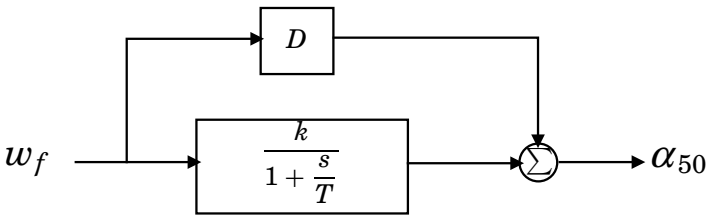

Figure 7.30 Model of load changes effect on α_{50}.

The parameters D, k and T vary and depend on the operating conditions. An approach to obtain the parameters are to fit first-order system models to the experiments and then use linear regression to obtain the parameter dependency of the operating condition. The idea is that the parameters are a function of w_f, Δw_f, R_f and α_{50}. An approach is to use the following parameterization of D, k and T

$$D = a_1 w_f^i + a_2 \Delta w_f + a_3 \alpha_{50}^i R_f^i + a_4 \tag{7.19}$$

$$k = b_1 w_f^i + b_2 \Delta w_f + b_3 R_f^i + b_4 \alpha_{50}^i \tag{7.20}$$

$$T = c_1 w_f^i + c_2 \Delta w_f + c_3 R_f^i + c_4 \alpha_{50}^i + c_5 \alpha_{50}^i R_f^i \tag{7.21}$$

where index i indicates the condition when the change of load occur. In

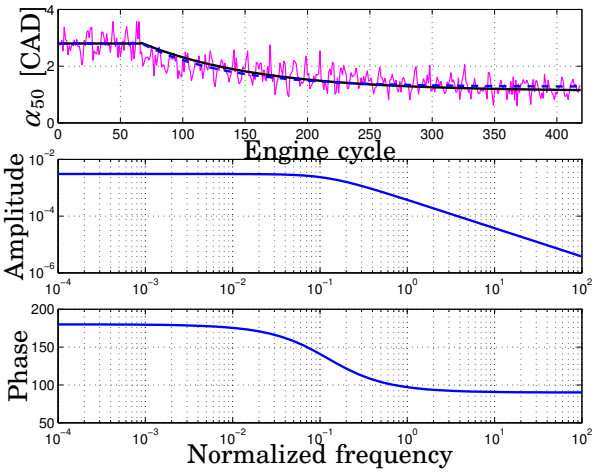

Figure 7.31 Experiment where the injected fuel energy changes from 1000J to 1500J (FuelMEP $5-7.5$ bar) and where the fuel ratio is 0.5. The upper figure shows experimental data (*thin grey*), model output from fitted first-order model (*thick solid*) and model output using the parameters obtained by linear regression (*thick dashed*). The lower figures show the Bode diagram of the model with the parameters obtained by linear regression.

Figs. 7.31, 7.32 and 7.33 the fitted first-order models and the models with D, k and T parameters obtained from linear regression are shown.

It can be noted that the estimated models capture most of the dynamics, and that the dynamic behavior varies significantly depending on the step size and the operating conditions.

In order to be able to design a feedforward controller it is most vital to capture the variations of the D-parameter, as the slow change in α_{50} due to changed wall temperature can be stabilized by a feedback controller. The signals w_f, Δw_f, R_f and α_{50} together give an estimation of the engine state and in Fig. 7.34 the estimation results of D, k and T are shown. It can be noted that in all cases the signals w_f, Δw_f, R_f and α_{50} can be used to give accurate estimations of the parameters. The first-order model and parameter function approach have been validated with cases which were not used in the estimation of the function parameters, a, b and c (Fig. 7.35).

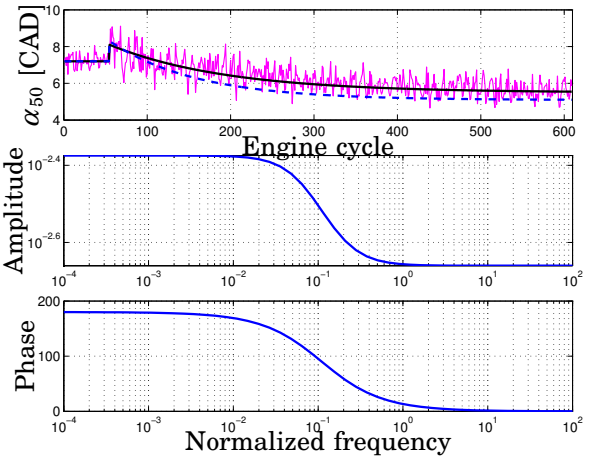

Figure 7.32 Experiment where the injected fuel energy changes from 1000J to 1500J and where the fuel ratio is 0.5. The upper figure shows experimental data (*thin grey*), model output from fitted first-order model (*thick solid*) and model output using the parameters obtained by linear regression (*thick dashed*). The lower figures show the Bode diagram of the model with the parameters obtained by linear regression.

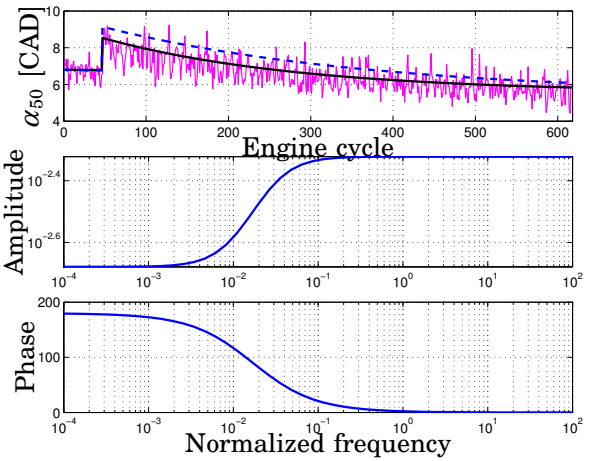

Figure 7.33 Experiment where the injected fuel energy changes from 1000J to 1500J and where the fuel ratio is 0.9. The upper figure shows experimental data (*thin grey*), model output from fitted first-order model (*thick solid*) and model output using the parameters obtained by linear regression (*thick dashed*). The lower figures show the Bode diagram of the model with the parameters obtained by linear regression.

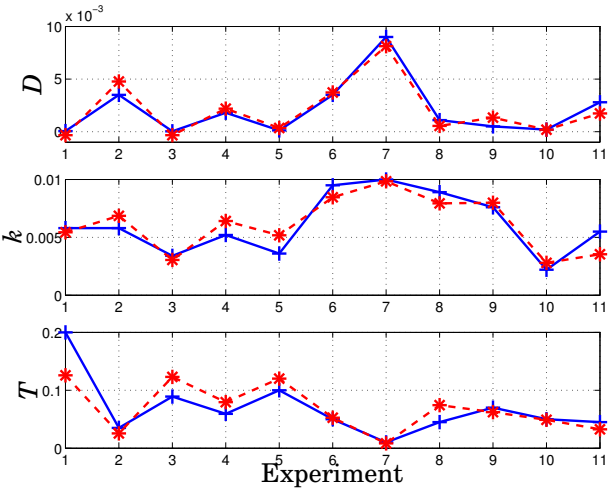

Figure 7.34 Parameter variation of D, k and T. The '+' marks is the parameters from the fitted first-order model and the '*' marks are result from the linear regression.

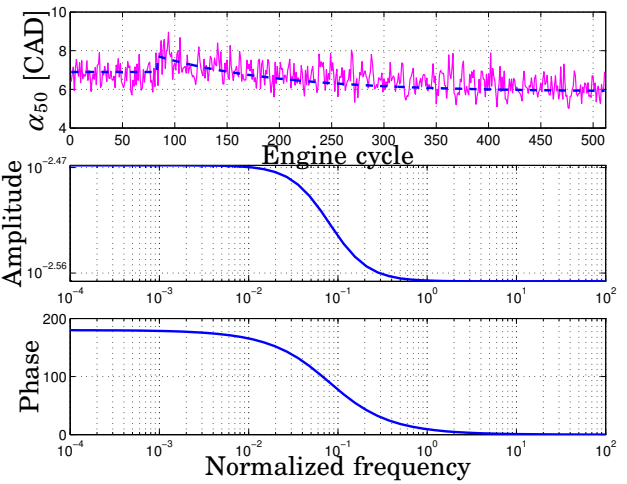

Figure 7.35 Experiment where the injected fuel energy changes from 1500J to 1800J and where the fuel ratio is 0.5. The upper figure shows experimental data (*thin grey*), model output from fitted first-order model (*thick solid*) and model output using the parameters obtained by linear regression (*thick dashed*). The lower figures show the Bode diagram of the model with the parameters obtained by linear regression.

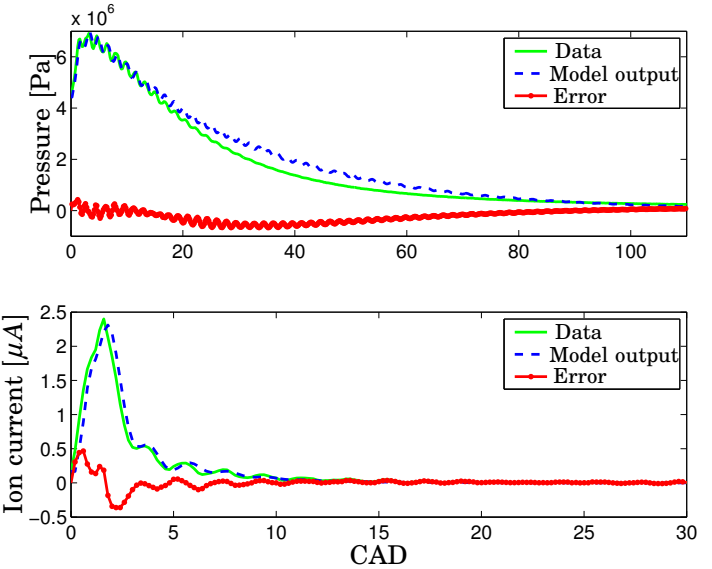

Figure 7.36 Upper figure: Measured pressure (solid) and output a 4th-order state space model (dashed). Lower figure: Measured ion current (solid) and output a 7th order state space model (dashed)

7.7 Pressure Trace and Ion Current Trace

In the previous sections, dynamic models of α_{50} have been estimated, but it is also possibly to estimate dynamic models of the cylinder pressure and ion current trace. One observation regarding the combustion is that it has features of an impulse response of a linear system. Hence, an approach to identify dynamic models of the increased pressure and ion current due to the combustion is to use impulse response analysis. A realization based-approach is to find a state space realization of this linear system that reproduces the given impulse response [Ho and Kalman, 1966]. Figure 7.36 shows a cylinder pressure trace and the impulse response from an identified fourth-order model starting from TDC. Even this low-order model reproduces the pressure trace fairly well. It reproduces the oscillation and the rise time constant, but it has problems in the relaxation time constant. Even so the model parameter should contain relevant thermodynamical and combustion information. In order to obtain models with similar accuracy of the ion current trace the model order needed to be increased. Figure 7.36 shows an ion current trace and the impulse response from an identified 7:th order model starting from

TDC. It is seen that the ion current trace is reproduced quite accurately by the identified model, both the oscillation and the time constants.

One way to parameterize the identified model could be to present them as a continuous-time impulse response describing linear system dynamics

$$y(t) = \int_{-\infty}^{t} h(t-s) \underbrace{u(s)}_{=\delta(s)} ds = h(t). \tag{7.22}$$

The identified 4th-order state-space model for the cycle pressure can the be written as a impulse response:

$$\begin{aligned} h(t) = \; & 8.10 \cdot 10^6 \cdot e^{-0.99t} - 3.81 \cdot 10^6 \cdot e^{-0.85t} \\ & + 2.92 \cdot 10^{10} \cdot e^{-0.73t} \cdot \sin(0.67t) + 4.44 \cdot 10^6 \delta(t) \end{aligned} \tag{7.23}$$

This fourth-order model is one estimation of the pressure, but we have no claim that it is the best possible model. In this parameterization, the rise and fall time constants and oscillation frequency can easily be found.

Whereas the signals representing ion current and pressure signal are intimately related, they are not identical. A Bode diagram representing the transfer function from ion current to pressure is given in Fig. 7.37, and in Fig. 7.38 the simulated model output together with measured output are presented. The transfer functions were identified by estimating ARMAX models [Johansson, 1993]. It can be observed from Fig. 7.38 that the pressure trace can be reconstructed from the ion current signal, even if the signals differ. The Bode diagrams (Fig. 7.37) of the transfer function between ion current and pressure indicate has a resonant peak at 23 k rad/s. In Sec. 6.1 frequency content of cylinder pressure and ion current showed that the both measurements had resonant peak at $3.5-4.2$ kHz. 23 k rad/s expressed in Hz is approximately 3.7 kHz which fits well in the interval of $3.5-4.2$ kHz. Transforming the estimated discrete model to continuous-time and written in transfer function form gives

$$\begin{aligned} G(s) &= \frac{B(s)}{A(s)} \\ A(s) &= s^4 + 1880s^3 + 7.03 \cdot 10^8 s^2 + 5.45 \cdot 10^{11} s + 1.06 \cdot 10^{14} \\ B(s) &= 6630s^4 + 1.36 \cdot 10^9 s^3 + 9.23 \cdot 10^{13} s^2 + 2.07 \cdot 10^{18} s - 1.16 \cdot 10^{21} \end{aligned}$$

Modeling of α_{50}^{ion}

Also models which had α_{50}^{ion} and α_{50}^{net} as output were estimated, which could directly be used in the control synthesis. The input to the process was the fuel ratio, R_f, and $IMEP_{net}$. Removal of offsets and/or trends

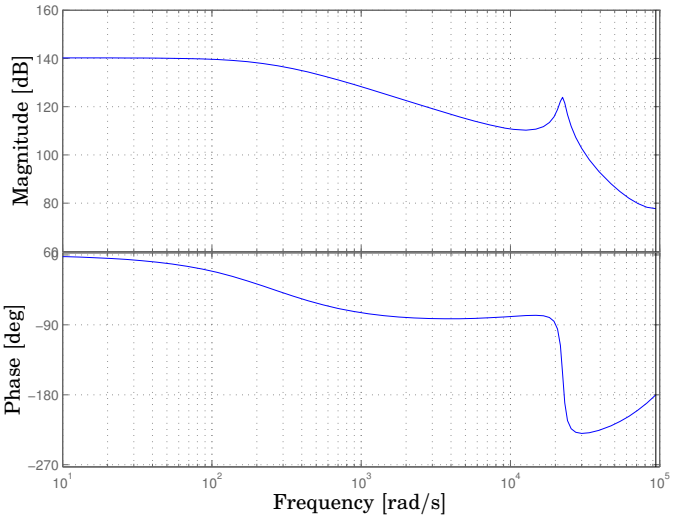

Figure 7.37 Bode diagram of the transfer function between ion current measurement without side electrode and pressure. Ion current is input and pressure is the output of the 6th-order ARMAX model.

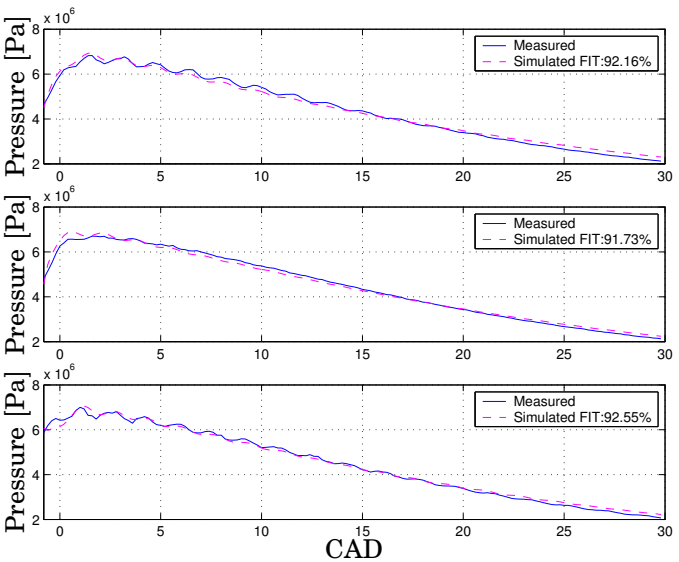

Figure 7.38 The simulated model pressure output (*dashed*) together with measured pressure (*solid*). The upper figure shows result when using the data used in the identification, the middle and lower figures show cross-validation results, the model used being the same as in Fig. 7.37.

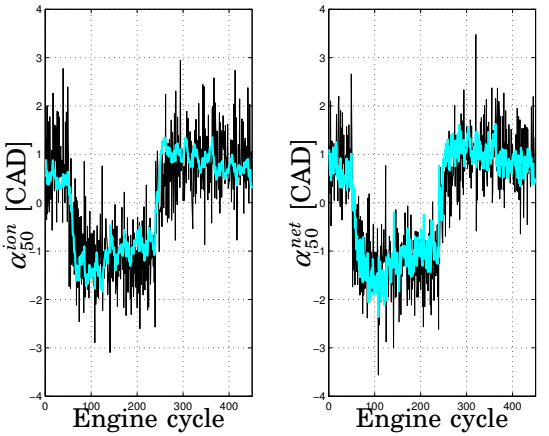

Figure 7.39 Responce in α_{50}^{net} and α_{50}^{ion} to step changes in CA50 reference. Left figure: model output from a second order model(*grey*) and α_{50}^{net} (*black*). Right figure: model output from a second order model (*grey*) and α_{50}^{ion} (*black*)

were performed before the identification procedure started. Linear models were identified by using subspace-based methods [Verhaegen, 1994]. The identification results, where VAF and FIT scores, residual analysis and cross validation were performed indicated that lower order models were sufficient. Figure 7.39 shows the simulation results from two identified models, α_{50}^{net} output model and α_{50}^{ion} output model. Both models were of second order. Figure 7.40 shows the Bode diagram and Fig. 7.41 shows the Nyquist diagram of the second-order models from fuel ratio and $IMEP_{net}$ to α_{50}^{ion} and α_{50}^{net}. Both the Bode and the Nyquist diagram indicate as expected that there are substantial similarities between the models of α_{50}^{ion} and α_{50}^{net}. The differences are essentially the gain, but also the phase differs at higher frequency. The phase graph of the model of α_{50}^{ion} is higher than Bode diagram phase of the model of α_{50}^{net} at higher frequencies.

Step Response Analysis

In Fig. 7.42 results from models estimated using step response analysis are shown. The models are of third order and the results indicate that for the load cases 1000J to 1500J (FuelMEP $5 - 7.5$ bar) a third-order model is sufficient. The most interesting part of the pressure trace to capture is the part from TDC to the maximum pressure and the models capture both the ignition delay and the pressure increase. When the load increases, the modeling of the pressure tail becomes poor, and higher-order models are needed in order to capture the pressure tail. The poles

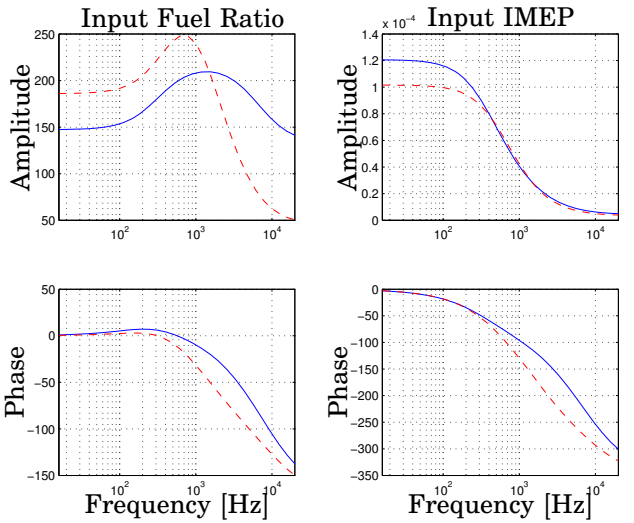

Figure 7.40 Bode diagram (*left*) showing the transfer function from fuel ratio to α_{50}^{ion} (*solid*) and α_{50}^{net} (*dashed*). Bode diagram (*right*) showing the transfer function from IMEP to α_{50}^{ion} (*solid*) and α_{50}^{net} (*dashed*).

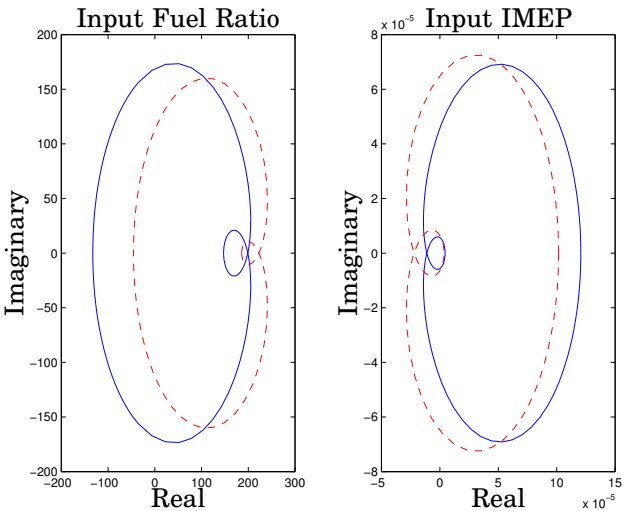

Figure 7.41 Nyquist diagram (*left*) from fuel ratio to α_{50}^{ion} (*solid*) and α_{50}^{net} (*dashed*). Nyquist diagram (*right*) showing from IMEP to α_{50}^{ion} (*solid*) and α_{50}^{net} (*dashed*).

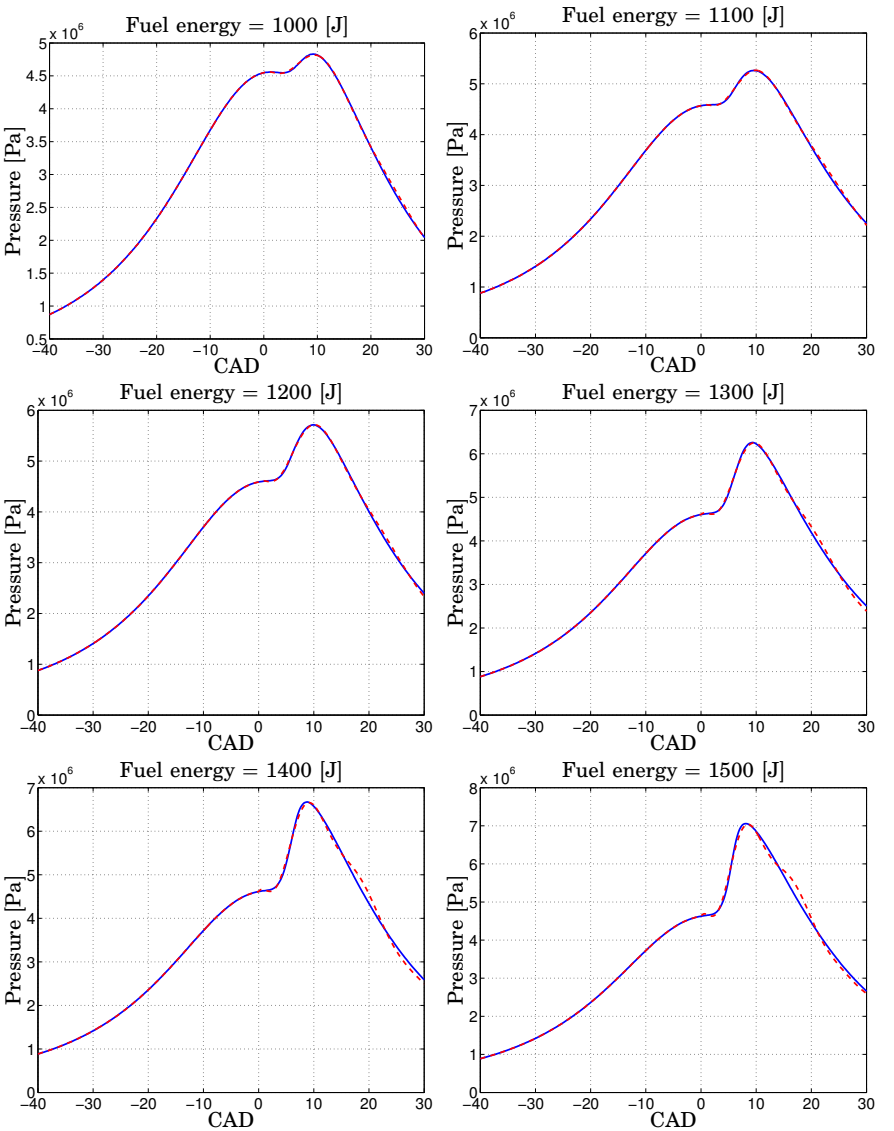

Figure 7.42 Mean pressure traces for different load cases (*solid*) and model output (*dashed*).

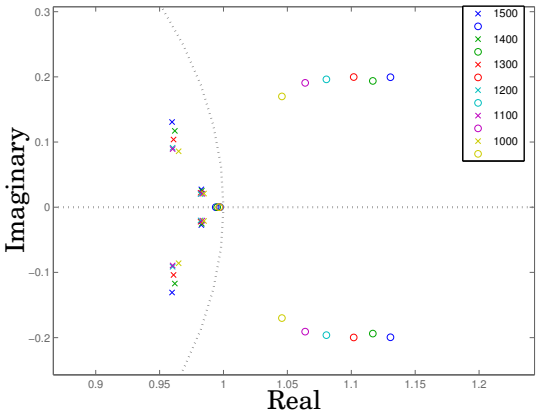

Figure 7.43 Poles and zeros of the estimated third-order model. The number stands for injected fuel energy in Joule.

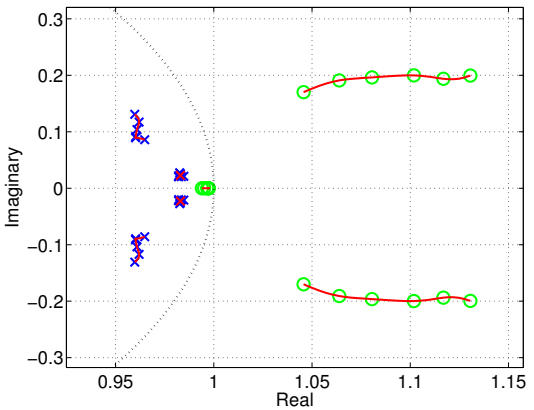

Figure 7.44 Interpolation of transfer function poles and zeros of the estimated third-order model.

and zeros of the estimated models are shown in Fig. 7.43 and it can be noticed that the poles and zeros vary when the load increases. As the variations are almost on a one-dimensional manifold, an approach is to interpolate the pole locations to get a description of the behavior at other loads (Fig. 7.44).

7.8 Discussion

Other variables than α_{50} were found to describe α also well. These variables may also give the same identification result as the ones with α_{50}. All experiments were carried out when the engine initially was at a steady state. What yet remains to be done is to model the transient behavior when the engine starts.

The autoignition depends of the cylinder temperature, but in the experimental set-up used, neither cylinder temperature or cylinder wall temperature were measured. The temperature of the exhaust gas, cooling water, and the engine oil gave a measurement of the slow trend in the cylinder temperature. Identification results, where these three temperatures were added to the already existing inputs and the output was α_{50} showed not better result in comparison with the models without these three temperatures. These measurements are slow and fails to capture the transient behavior. In order to have a better estimation of the cylinder temperature, a cylinder wall temperature sensor may be used. Even if such measurement is local and do not describe the cylinder head temperature, it still may give a better and faster indication of a change in the cylinder temperature. Hence, may such measurement result in better models of α_{50}.

Linear models were estimated, but as an HCCI has nonlinear characteristics, nonlinear models may improve the result. The VAF and FIT scores were used as one among with residual analysis, autocorrelation and cross validation in the evaluation of the models, but only between models based on the same data set. Both VAF and FIT decreases when the cycle-to-cycle variations increases, hence can VAF and FIT not be used as a measure to qualitatively compare models at which have used data from different operation points.

Results from subspace-based methods were presented, but also polynomial structures such as NARMAX models were estimated. The identified NARMAX models also suggested that lower order models were sufficient. This could be explained by the fact that after estimation of the static nonlinearity, the dynamics left are related to temperature, wall and residual gas, which could all be modeled by lower order models.

The reaction kinetics in HCCI combustion are very complex to fully describe, even so the identification results indicate that accurate estimations models with fuel ratio as input and combustion phasing as output can be obtained with lower-order linear models.

7.9 Summary and Concluding Remarks

Dynamic models suitable for control design are needed. In this chapter it is shown that system identification methods can successfully be used as a tool of obtaining dynamic models of HCCI. Among the methods used there was found that the state space models gave better result than the difference equation models in modeling of HCCI. In the case of MIMO modeling the MOESP algorithm in the SMI-toolbox gave significantly better result. The VAF and FIT scores were 40% lower for the two subspace-based algorithm in the System Identification Toolbox.

An HCCI engine is not a linear process, but in the range of the experiments it was found that lower-order linear dynamic models gave good accuracy in modeling of the combustion timing. Identification of models were performed in an IMEP_n load range of [2, 14] bar. Models of the pressure trace and the ion current trace during combustion have been estimated and the models of the two feedback options were similar.

8

Control of HCCI

Today there exists almost no feedback control of the internal combustion engines in production. The two common types, SI and CI, both have direct actuation. The SI engine has some feedback control, since most new engines has knock control and λ control. The motivation for the feedback control is firstly to avoid damaging the engine and secondly to keep the emissions low. Today, most of the control of the combustion is dependent on huge engine maps, where all the engine operating points are covered and used for feedforward control. This strategy is not applicable to control of an HCCI engine, since it is very sensitive to the operating conditions and lacks direct control of the combustion phasing. Additionally, the engine dynamics change and are unstable at some operating points. Therefore, feedback control of the combustion is necessary and pure feedforward cannot solve the problem itself, due to the sensitivity and dynamic properties of the HCCI engine.

It has been demonstrated that an HCCI engine can be unstable [Olsson *et al.*, 2002a], and at some operating point the engine was found to be very sensitive to disturbances. Fig. 8.1 shows an experiment when the pressure gradient reaches the safety limit. At cycle No. 382, the pressure gradient started to grow quickly and at cycle No. 385 the engine was shut down. The engine was operated in open-loop, and the sudden increase of the pressure gradient was probably triggered by excitation. For engine safety reasons, the maximum allowed pressure gradient per CAD was 40 bar/CAD. The experiment shows that feedback control is necessary in order to control the combustion phasing in an HCCI engine.

The combustion phasing estimates α_{50}^{net} and α_{50}^{ion} were used as feedback measurements for the control. The combustion estimate α_{50}^{net} will from here on be referred to as α_{50} in the text.

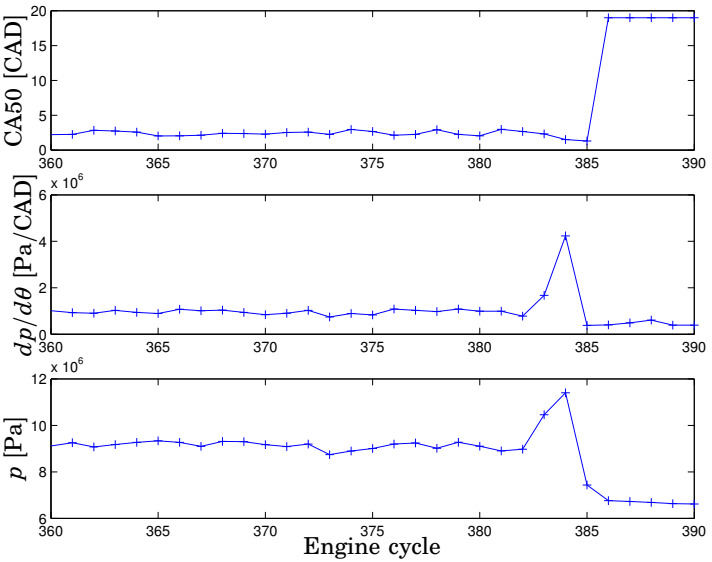

Figure 8.1 Example case of instability. The engine is shut down at engine cycle No. 385.

8.1 Actuation

In this work, two different actuators for closed-loop control of HCCI were investigated, dual fuels and VVA. The control system also included speed control and inlet temperature control. The architecture of the control system is shown in Fig. 8.2.

Dual Fuel

As described in Sec. 5.1, the fuels used were n-heptane and ethanol. Figure 8.3 shows the result when R_f varies between almost zero to almost one. As can be noted, α_{50} can not be changed to later than around 6 CAD at the current operating point. In order to have later phasing the operating point has to be changed, for instance by decreasing the temperature. Cycle-to-cycle control can be achieved for all cases except at high load, as for these cases the fuel injectors are not able to inject all fuel before IVC. The injector continues to inject and the fuel will instead be injected during the next cycle.

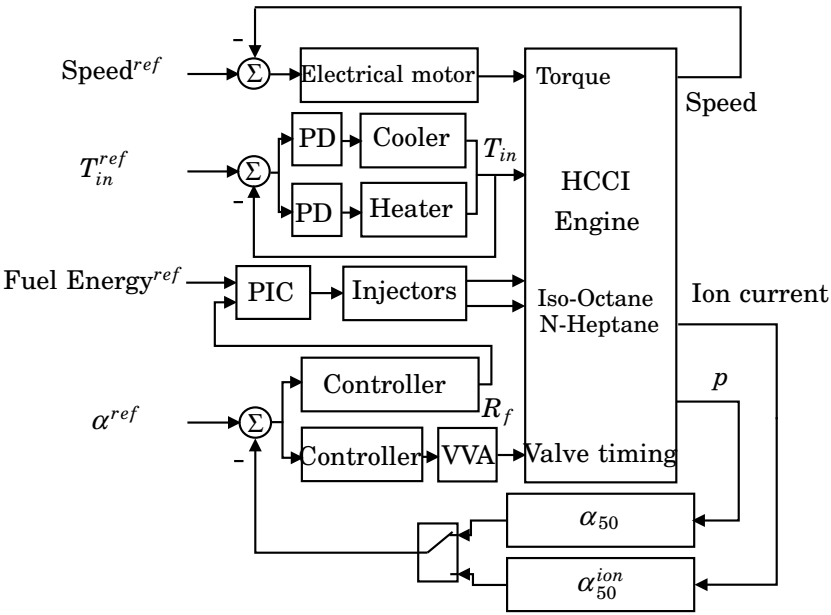

Figure 8.2 The control system.

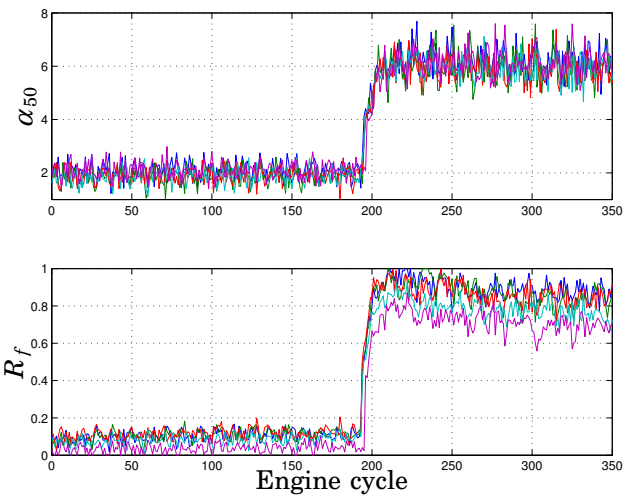

Figure 8.3 Combustion phasing when fuel ratio changes. Experiment conditions: $W_f = 1400$ J (FuelMEP 7 bar), $T_{in} = 95°C$ and $P_{in} = 1.6$ bar.

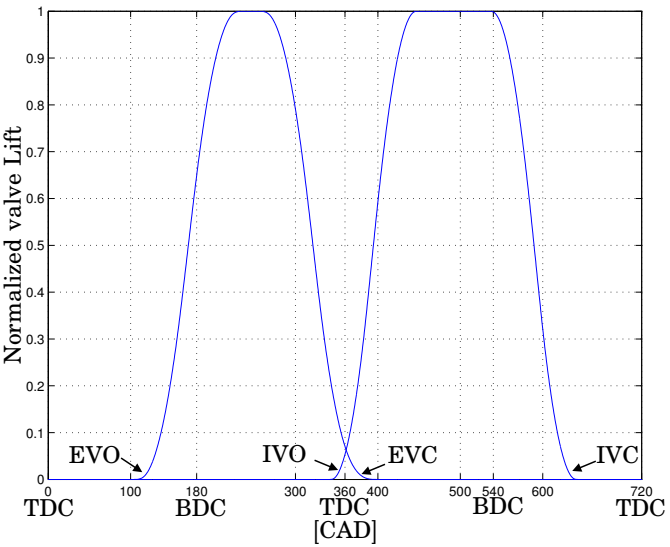

Figure 8.4 Principal view of the valve lifts.

Variable Valve Actuation

By VVA the valve times can be changed and Fig. 8.4 shows a principal view of the valve lift. The combustion TDC is chosen as the zero point and EVO, EVC, IVC, IVO are expressed in CAD after combustion TDC. Change of θ_{IVC} has a limited effect on the combustion phasing. Fig. 8.5 shows experimental results of the combustion phasing variation when θ_{IVC} varies from 515 to 605 CAD after combustion TDC. It can be noted that there are two possibilities to obtain the same α_{50}, either by closing the inlet valve during the expansion before BDC or during the compression after BDC. As the data of Fig. 8.5 suggest that a change in θ_{IVC} is symmetrical, it can be concluded that there is no significant difference between the effect of the two options on the combustion phasing. Even so, there are differences between closing before TDC and closing after TDC. The option of closing during expansion leads to a higher cylinder temperature and the option of closing during the compression will increase the pumping losses, as air has first been sucked in and then been blown out. Since the IVC phasing effect on α_{50} is symmetrical it indicates that these two effects are negligible, and in this thesis results are presented when controlling at BDC or later.

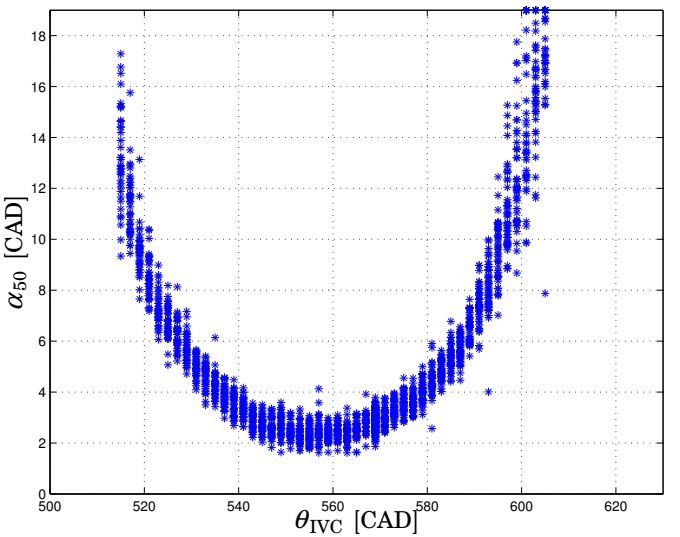

Figure 8.5 Experimental result of the inlet valve lifts effects on the combustion phasing.

8.2 Control Methods

PID Control

Proportional Integral Derivative (PID) control is a well known control algorithm. In continuous time it can be written as

$$u(t) = K(e(t) + \frac{1}{T_i}\int_0^t e(\tau)d\tau - T_d\frac{dy}{dt})$$

where $e = y_r - y$ is the error, T_i is the controller's integral time and T_d is the PID controller derivation time. By standard practice, a pure derivative was not implemented since it would give a very large amplification of measurement noise. Instead the derivation was implemented by approximating the transfer function sT_d as follows

$$sT_d \approx \frac{sT_d}{1 + sT_d/N} \tag{8.1}$$

The transfer function on the right approximates the derivative well at low frequencies, but the gain is limited to N at high frequencies.

LQG Control

Linear Quadratic Gaussian control is a state-space technique for designing optimal dynamic controllers [Anderson and Moore, 1990; Åström and Wittenmark, 1997]. The synthesis problem is formulated as minimization of a criterion, which is a quadratic function of the states and the control signal. The optimal control problem is the problem of finding the admissible control function minimizing the loss function

$$J(u) = E\int_0^\infty x^T(t)Q_1x(t) + 2x^T(t)Q_{12}u(t) + u^T(t)Q_2u(t)dt \qquad (8.2)$$

where x is the vector of system states, u is the control signal and Q_1, Q_{12} and Q_2 are design parameters. As the states were not measurable, they were estimated using Kalman filter. The estimation of the states is optimal in the sense that the variance of the estimation errors are minimized. The subspace-based methods used in Ch. 7 give an estimate of the Kalman filter, which was used in the LQG design. Another approach is to view the covariance of process disturbance and measurement noise as design parameters of the Kalman filter. The LQG controller is a model-based controller and the performance relies on the existence of an accurate model.

Model Predictive Control (MPC)

In the last decades, there has been a significant development in the field of dynamic optimization. In this area, Model Predictive Control (MPC) has been an increasingly attractive topic. It is also a control method which has won widespread use in industry. For the linear case there is theory both for optimization on-line [Maciejowski, 2002] and off-line [Bemporad *et al.*, 2002]. In the linear case there also exist several strong results ensuring robust stability, see [Maciejowski, 2002] for an overview. In many real applications the control signals are restricted due to saturations, which, in turn, limit the performance of the controller. Also, the process outputs or states might need to be limited, for instance due to safety reasons in order to avoid damage of equipment or environment. One of the major motivations for using MPC is that it explicitly takes the constraints into account. Another motivation is that it is well suited for controlling MIMO as well as SISO plants, and can be used to control a great variety of processes, including those with non-minimum phase, long time delays,or open-loop unstable processes. There are many variants of the standard MPC controller, but they all usually share some properties such as [Maciejowski, 2002]:

- Explicit use of a model to predict the future process output.

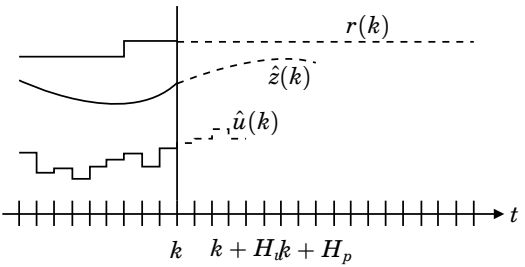

Figure 8.6 The MPC strategy, where $r(k)$ is the reference value, $z(k)$ is the controlled output and $u(k)$ the control signal.

- Calculation of a control sequence by optimizing, usually on-line, a performance index.
- A receding horizon strategy, meaning that at each instant the horizon is moved towards the future and only the current control signal is applied at each step, illustrated in Fig. 8.6.

The MPC strategy used in this thesis can be described as follows: We assume a state-space model of the plant, in the form

$$x(k+1) = Ax(k) + Bu(k) \tag{8.3}$$

$$y(k) = C_y x(k) \tag{8.4}$$

$$z(k) = C_z x(k) \tag{8.5}$$

where $u(k)$ is the input, $y(k)$ is the measured output and $z(k)$ is the controlled output.

- At each sample, the predicted future controlled outputs $\hat{z}(t+k|t)$ over the prediction horizon H_p are calculated. The control signal is assumed to be constant after H_u samples. By making the distinction between H_u and H_p the complexity of the optimization problem can be decreased, if the horizons are chosen as $H_u < H_p$. The number of decision variables in the optimization problem increases with H_u and is independent of H_p.
- The sequence of future control signals is computed by optimizing a performance criterion, penalizing deviations of the controlled variables as well as variations in the control signal. The cost function is quadratic, which in combination with a linear system correspond to

a finite horizon LQ problem:

$$\min_{\Delta u(k|k),\ldots,\Delta u(k+H_u-1|k)} J(\Delta u, x(t)) = \sum_{i=0}^{H_p-1} ||\hat{z}(k+i) - r(k+i|k)||_Q^2 + \sum_{i=0}^{H_u-1} ||\Delta(\hat{u}(k+i|k)||_R^2 \quad (8.6)$$

$$\begin{aligned} \text{subject to } & u_{min} \leq u_{k+i} \leq u_{max} \\ & y_{min} \leq y_{k+i} \leq y_{max} \\ & \Delta u(k+h|k) = 0,\ h = H_u, ..., H_p - 1 \end{aligned}$$

where $\hat{z}(k+i)$ is the predicted controlled outputs at time $k+i$, $\Delta u(k+i|k)$ are the predicted control increments, and $r(k+i|k)$ is the reference value. The matrices $Q \geq 0$ and $R > 0$ are weighting matrices, which are assumed to be constant over the prediction horizon. Notice the difference to the cost function for the LQ control of Eq. (8.2), where u is penalized instead of Δu. This is to avoid the conflict that for a non-zero reference point $r(k)$, the corresponding steady state control signal is usually also non-zero. If there are no constraints, there is no need for on-line solution. Finding the minimum is a convex optimization problem and for this purpose a quadratic programming (QP) solver is used to find the minimum. The output constraints are defined to be soft in order to give feasible solutions.

- Only the current control signal $u(k)$ computed by $\Delta u(k|k)$ is applied to the process. The remaining samples $\Delta u(k+i|k)$ are discarded, and a new optimization problem based on $z(k+1)$ is solved at the next sampling step. Thus $u(k+1)$ is then calculated using the receding horizon concept.

A drawback of MPC is the potentially large on-line computational effort, which has limited its application to relative slow and/or small problems. Today, MPC can be applied in relative fast systems, and we will demonstrate that it can be used for control of HCCI engine dynamics on a cycle-to-cycle basis. The MPC software used in this thesis was the MPC Toolbox 2.0 for Matlab 7. By using Simulink and Real-Time Workshop as described in Sec. 5.2, C-code was generated and used for control of the HCCI engine.

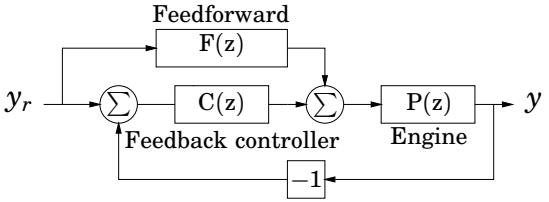

Figure 8.7 The closed-loop control system with feedforward of the reference signal.

Feedforward Control

A general control system should satisfy a number of properties. For example, the system should be able to follow reference signals, reject load disturbances, attenuate measurement noise, reduce the sensitivity to modeling errors, and satisfy constraints on the control signal. For this purpose, the tracking and controller problem were separated by using feedforward of the reference signal (Figure 8.7). The identified model used in the control design was also used in the feedforward design. The closed-loop system including feedforward written in the discrete frequency domain becomes

$$H_{cl}(z) = \frac{P(z)(C(z) + F(z))}{1 + C(z)P(z)}$$

8.3 Sensor Feedback

In Sec. 6.1, it was shown that α_{50}^{ion} and α_{50} had similar feedback properties. As the α_{50}^{ion} has the property of a local measurement, this raises the question if this local measurement is sufficient for closed-loop control of the combustion timing in HCCI? That ion current can be used to control the combustion in SI engines has previously been shown [Eriksson *et al.*, 1997; Andersson and Eriksson, 2000]. In this section results from feedback control based on α_{50}^{ion} and α_{50} of an HCCI engine are presented.

The experiment was performed on the experimental set-up described in Sec. 5.3, and dual fuels were used as the mean to control the combustion phasing. Both cylinder pressure and ion current were measured simultaneously. The PID controllers for the cylinders were manually tuned and the parameters were the same for the two different feedback cases, and no feedforward was present. Figure 8.8 shows the step response where feedback from pressure sensor (α_{50}) was used as well as the corresponding α_{50}^{ion} during the step response. It can be observed that α_{50}^{ion} gives similar indication of α as α_{50}. Figure 8.9 shows the step response where feedback

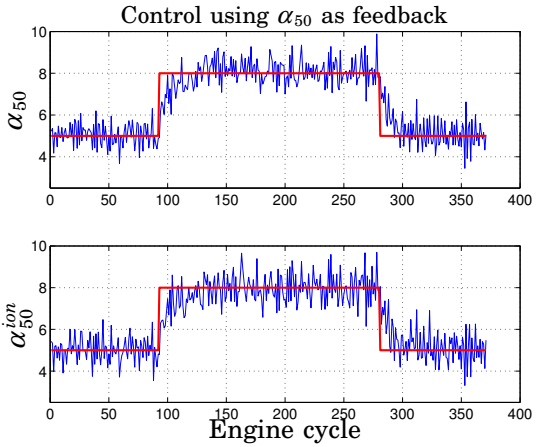

Figure 8.8 Step response of α when using α_{50} as feedback. The thick line is the reference value of α and the figures shows α_{50} (*upper*) and α_{50}^{ion} (*lower*).

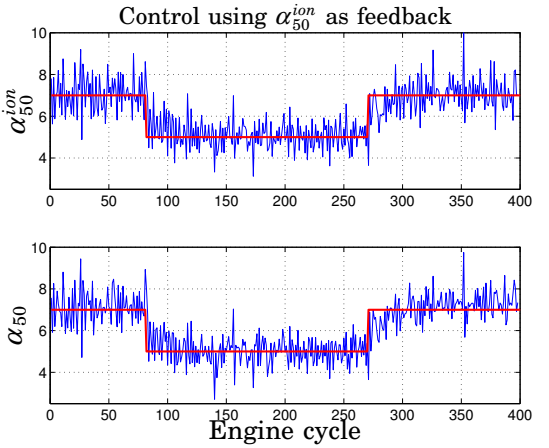

Figure 8.9 Step response of α when using α_{50}^{ion} as feedback. The thick line is the reference value of α and the figures shows α_{50}^{ion} (*upper*) and α_{50} (*lower*).

from the ion current sensor (α_{50}^{ion}) was used as well as the corresponding α_{50} during the step response. From Fig. 8.9, it can be noticed that the α_{50}^{ion} is sufficiently robust and accurate to be used for feedback control, with similar performance as α_{50}. The step responses were both performed at an operating point of 3 bar IMEP_{net}, an inlet temperature of 150°C, and

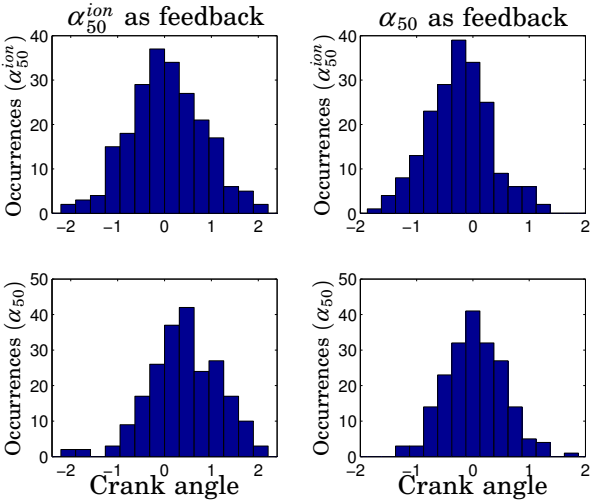

Figure 8.10 The distribution of the residuals when controlling by α_{50}^{ion} (*left*). The residual distribution of α_{50}^{ion} (*upper left*) and α_{50} (*lower left*). The distribution of the residuals when controlling by α_{50} (*right*). The residual distribution of α_{50}^{ion} (*upper right*) and α_{50} (*lower right*).

an engine speed of 1000 rpm and no EGR.

In the experiment, the standard deviation of the α estimation at constant α_{ref} was 0.65 CAD for α_{50}^{ion} and 0.56 CAD for α_{50}. In Fig. 8.10, the distribution of the residuals is shown when controlling using α_{50}^{ion} and α_{50}, respectively. As desired when using α_{50}^{ion} as feedback, we note that the residual distribution for α_{50}^{ion} was similar to a normal distribution with zero mean, while the corresponding residuals for α_{50} had an offset. When using α_{50} as feedback, the residual distribution for α_{50} was similar to a normal distribution with zero mean. The corresponding residuals for α_{50}^{ion} had an offset similar to the case when controlled by α_{50}, the offset between α_{50}^{ion} and α_{50} being 0.2-0.3. The offset compensated for was found to be robust to change in operating conditions over a range of $\lambda \in [2, 2.7]$, as the offset was changed by less than 5%. An explanation for the offset could be that α_{50} is based on heat release calculations using cylinder pressure measurements while α_{50}^{ion} is based directly on ion current. This could be compared with α based on direct pressure measurement and in Sec. 6.2 it was shown that the α based on direct pressure measurement had a small bias.

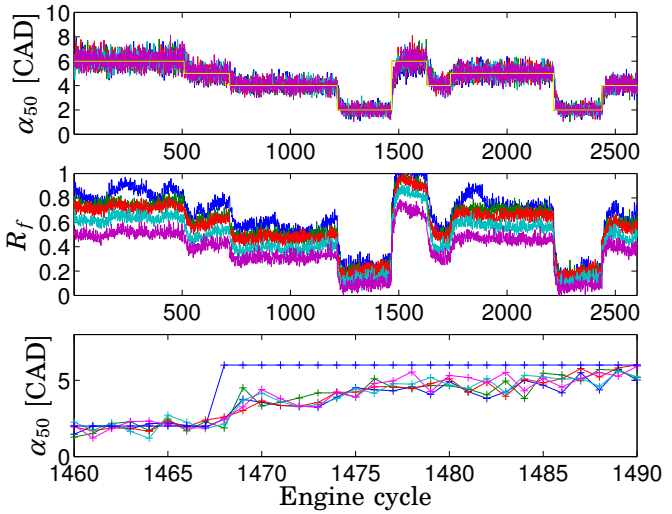

Figure 8.11 PID control without feedforward. Step changes in α_{ref} (*upper*) and resulting fuel ratio when controlled by the LQG controller (*middle*). Closer view of the step at engine cycle No. 1468 (*lower*).

8.4 Dual-Fuel Control

PID Control

The obtained models in Ch. 7 has been used in the PID design as well as manually tuning. Note that fast control of α is necessary since it is a limiting factor for the load control and emission performance. Step responses of α_{ref} were used in order to illustrate the characteristics of the control system, and in Fig. 8.11 the results from several step changes in α_{ref} are shown. It can be noted that a PID controller can control α_{50}, and this has also previously been shown in [Olsson *et al.*, 2001b]. From the figure, it can also be observed that there are differences in the behavior among the six cylinders, but the controllers managed to compensate for the differences. The differences among the cylinders depend on the geometry of the engine set-up. The wall temperature differs among the cylinders, the first and sixth cylinder having only one neighbor. The inlet temperature differs, as the air pipes after the temperature sensor used for control of T_{in} have different length to each cylinder. The air pipe length might also affect the effective air intake. Moreover, from Fig. 8.11 the limitation in

the control signal can be observed. The lower limit could be changed, as $R_f = 0$ corresponds to 50% ethanol and 50% n-heptane. A challenge with controlling an HCCI engine is high load. At high load late combustion is necessary, and then $R_f = 0$ is not a limitation in the control. At this low load operating point, α_{50} can be changed from 2 to 6 CAD at the current inlet temperature. In order to change α_{50} outside this operating point, the inlet temperature and/or inlet pressure must be changed. The PID controller was tuned in order to achieve practical robustness to process variation, which resulted in a fairly slow step response. From the closer view of the step response in Fig. 8.11, it can be noticed that it takes around 25 engine cycles to go from $\alpha = 2$ CAD to $\alpha = 6$ CAD. An HCCI engine is non-linear and to operate the engine at a wide operation range, gain scheduling of the PID parameters was necessary. From Fig. 8.11 it can be noted that there was no time delay in the system. The controller reacts on a cycle-to-cycle basis, for example, at engine cycle number 1468 the step change occurred and the controller changes were in the next cycle. Figure 8.12 shows step changes of α_{ref} and how α_{50} was affected of different disturbances for all the six cylinders. In the beginning, step changes of α_{ref} between 2 and 4 CAD after TDC were performed. Between cycle 200 and 300, the injected energy per cycle into the engine was step changed from 1200 to 1600 J/cycle (FuelMEP $6-8$ bar). Between cycle 350 and 550 the speed was changed from 1100 rpm to 1400 rpm and back again. We note that the system was robust to changes of injected energy, α_{50} kept around 2 CAD after TDC and the disturbance was rejected. The speed changes were rejected and α_{50} was kept around α_{ref}. However, the variance of α_{50} was found to increase during the speed changes.

The model, obtained by system identification, and the controller were used in the design of the feedforward transfer function, and Fig. 8.13 shows the amplitude of the transfer function for the closed-loop system with and without feedforward. The feedforward increased the bandwidth, resulting in a faster response of reference changes. In Fig. 8.14, a closer view of the step response with feedforward for one of the cylinders is shown. It can be noted that the step change from 2 to 4 CAD was carried out in one step. Moreover it can be observed that the controller is also able to compensate for the fuel dynamics, such as wall wetting. The variance in closed-loop and open-loop control was similar, see Table 8.1. In closed-loop control, the cycle-to-cycle variations did not decrease. One reason is that there were no dynamics in the noise, which gave a direct response in α and IMEP. In Fig. 8.15, a histogram of α_{50} during open-loop control and closed-loop control by PID is shown. The empirical distribution of α_{50}, both for the open-loop and closed-loop case, are close to the normal distribution. The reference α_{ref} was set to 6 CAD in the closed-loop operation and as expected the α_{50} distribution was kept around 6 CAD. The same fuel ratio

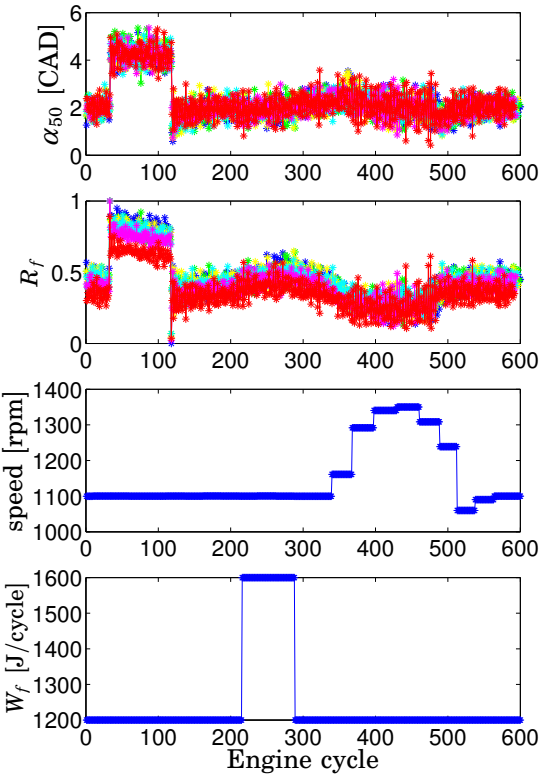

Figure 8.12 PID control: Step changes of α_{ref} (cycle 50-130), injected fuel energy per cycle (cycle 200-300) and speed (cycle 350-550) were performed. The resulting fuel ratio is shown for all the 6 cylinders.

Cylinder	1	2	3	4	5	6
Open-loop	0.2513	0.2259	0.2886	0.2139	0.3146	0.2990
PID	0.3223	0.2866	0.2779	0.2983	0.2751	0.2948
LQG	0.2476	0.2796	0.2583	0.2433	0.2043	0.2248
MPC	0.2886	0.1848	0.2128	0.2986	0.2717	0.2684

Table 8.1 Variance in α_{50} during open-loop and closed-loop control by PID, LQG and MPC.

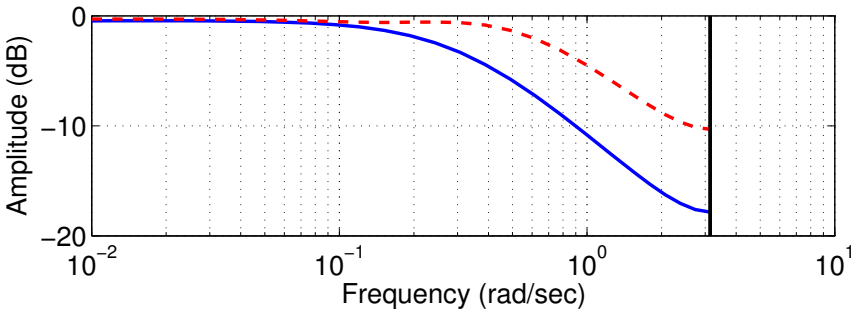

Figure 8.13 Closed-loop control without feedforward (*solid*). Closed-loop control with feedforward (*dashed*).

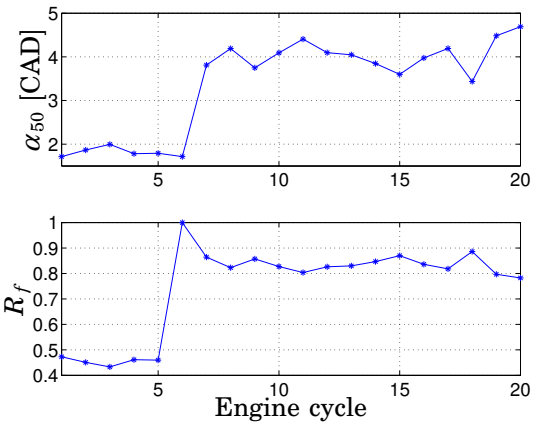

Figure 8.14 PID control: Step change of α_{ref} with resulting fuel ratio.

was applied to all the cylinders in the open-loop case. It can be observed that the variance in open-loop was similar to the variance in closed-loop operation.

LQG Control

Integral action is not inherent in LQG controller design. As integral action was a desired property, an error integral state was included in the process

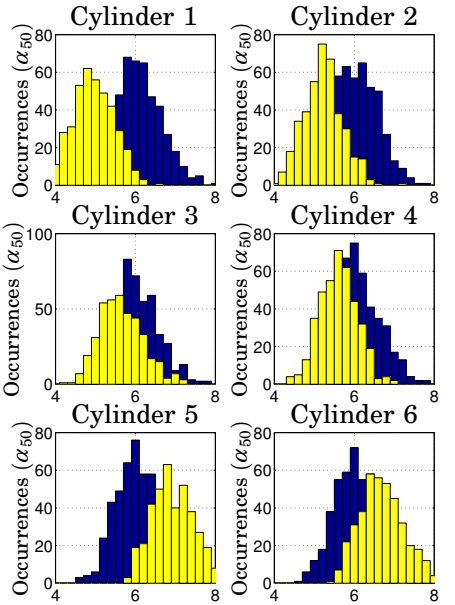

Figure 8.15 Histogram of α_{50} in closed-loop (*dark*) and in open-loop (*light*).

model. The estimated Kalman filter obtained from the identification was used in the control design.

In Figure 8.16 the result from several step changes in α_{ref} is shown. The controller was designed using the identified model in experiment 1 in Sec. 7.3. The experimental conditions were the same as for the PID control experiment showed in Fig. 8.11. Also the LQG controller was tuned in a robust setting. The step response performance is similar to the performance of the PID controller. As it was found in Chapter 7 that lower-order models were sufficient to capture the dynamics of α_{50}, it is no surprise that LQG might not give a significant improvement in comparison to PID.

Figure 8.17 shows the result of step changes of α_{ref} and how α_{50} was affected by different disturbances for all the six cylinders, see also Figure 8.12. A feedforward was designed in order to increase the reference response. Fig. 8.18 shows a closer view of the step response when feedforward was applied for one of the cylinders. The step change from 2 to 4 CAD was performed in one sample. Fig. 8.18 could be compared to Fig. 8.14 as the experimental conditions were the same. The LQG controller was tested outside the area of the excitation data, still the controller was able to stabilize the combustion phasing, see Fig. 8.19. As α_{50} had more

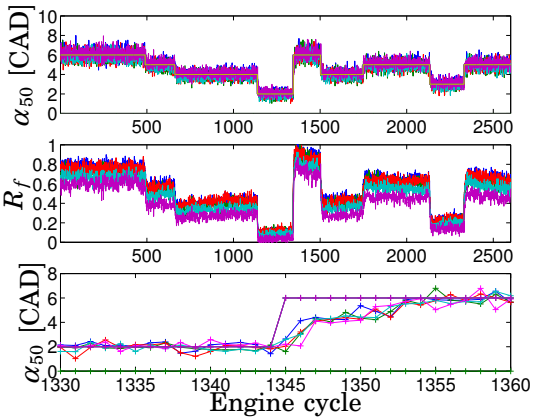

Figure 8.16 LQG control without feedforward. Step changes in α_{ref} (*upper*) and resulting fuel ratio when controlled by the LQG controller (*middle*). Closer view of the step at engine cycle No. 1345 (*lower*).

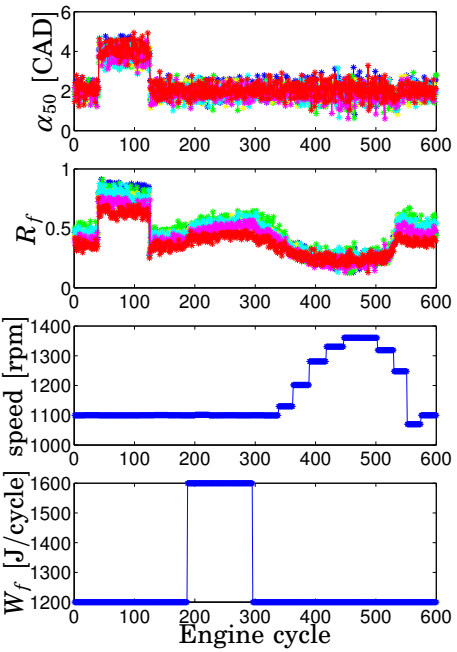

Figure 8.17 LQG control: Step changes of α_{ref} (cycle 50-130), injected fuel energy per cycle (cycle 200-300) and speed (cycle 350-550) were performed. The resulting fuel ratio is shown for all the 6 cylinders.

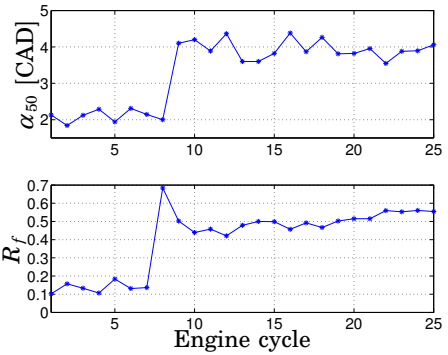

Figure 8.18 Feedforward LQG control: Step change of α_{ref} with resulting fuel ratio.

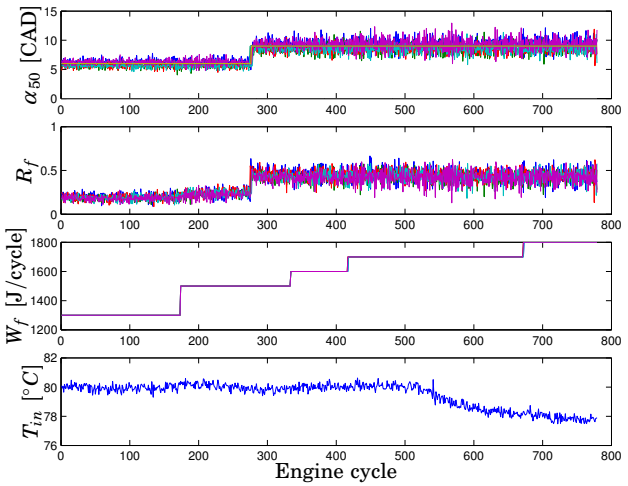

Figure 8.19 Evaluation of the LQG controller. The inputs goes outside the range used in the identification

cycle-to-cycle variations at late combustion, due to increased sensitivity to operating conditions, the noise level increased when the α_{ref} was changed from 6 to 9 CAD after top dead center. Fig. 8.20 shows minimum, mean and maximum of α_{50} and fuel ratio during an experiment where α_{ref} was maintained at 4 CAD and α_{50} was controlled by an LQG controller. It can be observed that the variation range of α_{50} is similar for all of the six cylinders, but the fuel ratio variation range during the experiment differs significantly between the cylinders.

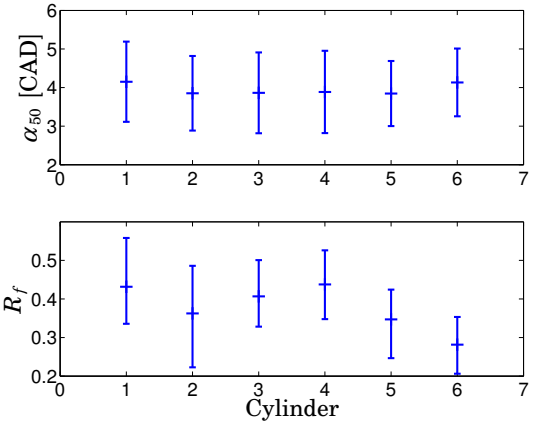

Figure 8.20 α_{50} and fuel ratio for the six cylinders when the α_{ref} was maintained at 4 CAD. The bar for each cylinder shows the minimum, mean and maximum value.

Model Predictive Control

The identified models in Ch. 7, were used in the MPC controllers design. The tuning parameters of the MPC controllers were:

- Constraints: The control constraints were $0 \leq R_f \leq 1$ and $W_f \geq 0$, and the output constraint was $dp/d\theta \leq dp_{\text{limit}}$. The input constraints were hard and the output constraint soft, and a tolerance band was specified to each constraint.
- Weights: Manipulated variable, manipulated variable rate and output variables. The weights also included a slack variable, ρ_ε, used for relaxing the constraints.
- Horizons: The control horizons used were $1 \leq H_u \leq 15$ and the prediction horizons used were $1 \leq H_p \leq 25$.
- State estimation: Input noise, output noise and measurement noise was defined and used in the calculation of the Kalman filter. Another approach used, was to using the estimated Kalman filter obtained by the identification methods used in Ch. 7.

The control of α_{50} may be written as a SISO problem and Fig. 8.21 shows simulation result from step changes in the reference value of α_{50} where a SISO MPC controller was used. From the figure it can be noted that the reference value was followed. At cycle 40 a disturbance in α_{50} was added and suppressed after two samples.

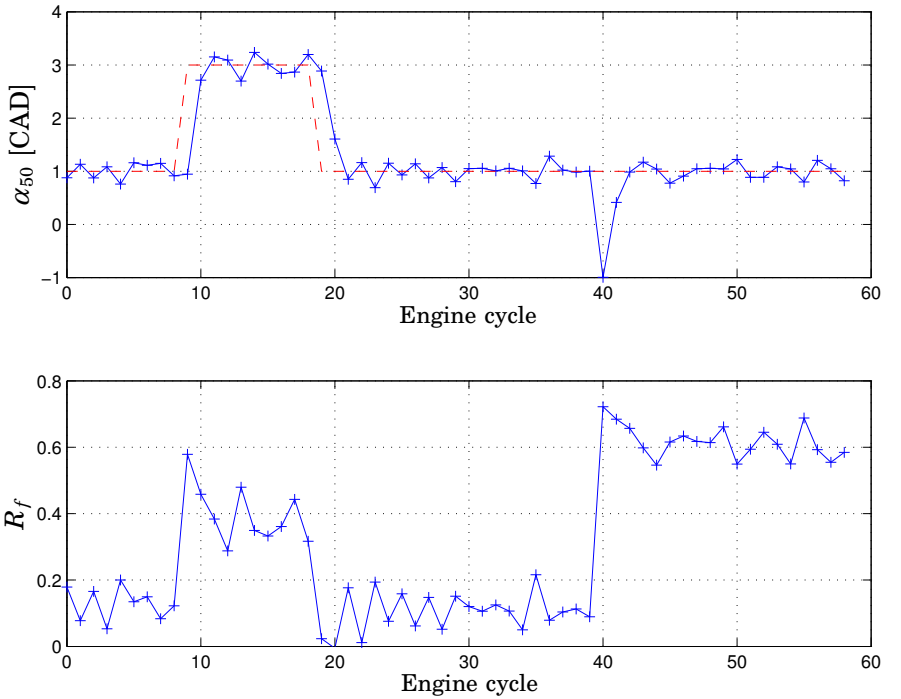

Figure 8.21 Simulation result of step response in α_{50}^{ref} (*dashed*) and resulting α_{50} (*solid*) when measure noise was added. The fuel ratio, R_f was controlled by an MPC controller.

Figs. 8.22 shows experimental step response result from an MPC controller, where the objective was to control α_{50} using dual fuels. During the sequence, T_{in} and R_f were changed, and still the MPC controller kept α_{50} at the reference value.

It can be observed that the step response in the W_f had no noticeable effect on α_{50}, and the new IMEP$_n$ was reached in few samples. The IMEP$_n$ is to a great extent determined by W_f as α has little effect on the IMEP$_n$ [Christensen *et al.*, 2002]. There is dynamics between W_f and IMEP$_n$ which can be observed in Fig. 8.22. Neither IMEP$_n$ nor R_f are changed instantaneously. The dynamics is due to the effect of wall wetting, fuel vaporization and wall temperature. In Sec. 7.6 models of these effects were presented.

A closer view of the step response of α_{50} can be seen in Fig. 8.23. It can be noticed that the step change resulted in that the control signal

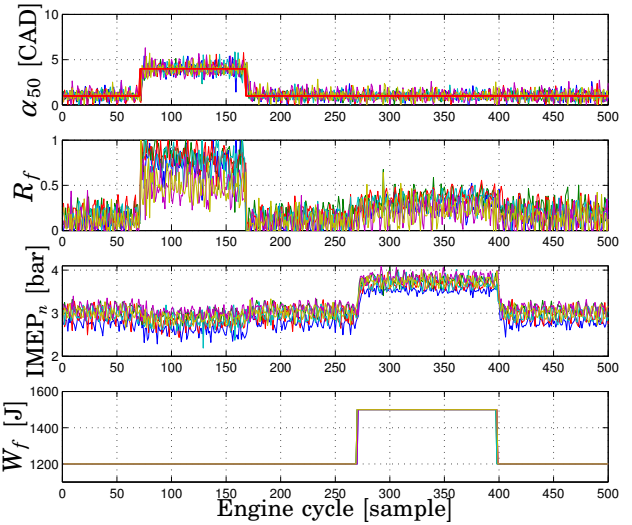

Figure 8.22 MPC control of α_{50} using fuel ratio.

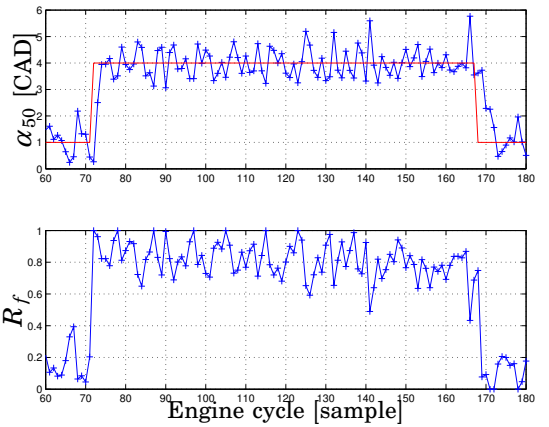

Figure 8.23 A closer view of the step response in Fig. 8.22 for cylinder 3.

was saturated at fuel ratio 1. Fuel ratio equal to one was not sufficient in order to change α_{50} from 1 CAD to 4 CAD in one sample, but in the next cycle α_{50}^{ref} was reached. At cycle 168 a negative step is applied and also in this case the control signal was saturated. Around 4 cycles were needed before the desired α_{50}^{ref} was reached in this case.

A fast and robust control of α is necessary in order to stabilize control

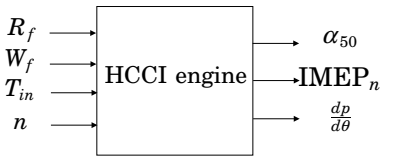

Figure 8.24 The inputs and outputs of the MIMO model used in the MPC design.

an HCCI engine. It is also desired that the load, cylinder peak pressure, and emissions are controlled simultaneous. This is a MIMO control problem where the controller has to be able handle constraints on several variables. We will demonstrate that an MPC controller can be used to control a simplification of this MIMO problem, where the simplification consisted of not directly controlling the emissions. The HC and CO emissions were kept low by aiming at complete combustion. This was achieved by having a early combustion phasing. The NO_x emissions were no problem as the combustion temperature was kept low in the experiments, which can be achieved by not allowing high cylinder pressure. The pressure gradient often reaches dangerous levels for the engine and the sensors, before dangerous levels due to peak pressure are reached. Therefore, the magnitude of cylinder pressure gradient was used as a safety limit instead of cylinder peak pressure. The MIMO control problem can then be formulated as controlling the load, without exceeding limits on the cylinder pressure gradient. The load should be reached by using the minimum amount of fuel and the combustion should be complete. IMEP$_n$ is used as a measurement of the load.

For the MPC design, the identified MIMO model in Sec. 7.3 was used (Fig. 8.24). In order to avoid too high $dp/d\theta$ a maximum constraint was specified. Other constraints were the maximum and minimum constraints of R_f. Control of the load was achieved by using a weight-factor for the load. The objectives to minimize fuel consumption and having complete combustion for the desired load were achieved by weight-factors for α_{50} and W_f, and by setting the reference value for α_{50} to zero. This results in that the earliest possible combustion phasing, while still satisfying the constraint on $dp/d\theta$. The combustion is more complete in early combustion phasing than in late combustion phasing, where the cylinder volume has increased. The increased cylinder volume will decrease the cylinder temperature, and the combustion may stop before all fuel is burned up. The manipulated variables were R_f, W_f, the measured disturbances were T_{in} and n, and the manipulated outputs were α_{50} and IMEP$_n$. The cylinder pressure gradient was not controlled, only measured.

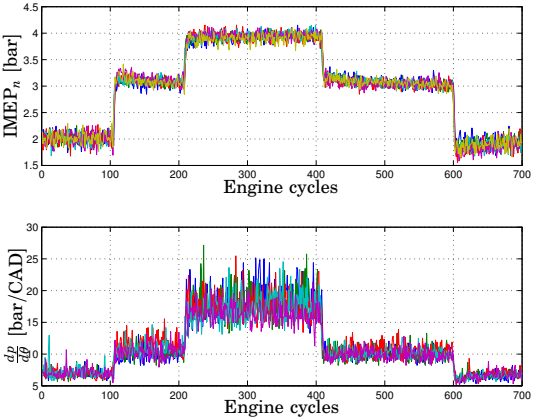

Figure 8.25 Experimental result of a step response in IMEP$_n$, when an MIMO MPC controller was used.

As there are differences between the cylinders, cylinder individual MPC controllers were designed, and in Fig. 8.25 the result of step changes in IMEP$_n$ are shown. In this example, the constraint on $dp/d\theta$ was 20 bar/CAD. It can be observed that the controller are able to control IMEP$_n$. In Fig. 8.26, the results from one cylinder is shown. In the experiment, the reference value of IMEP$_n$ was changed from 2 bar to 4 bar in increments of 0.5 bar, and the constraint on $dp/d\theta$ was 15 bar/CAD. It can be observed that the IMEP$_n$ reference was quickly reached. A closer examination of the IMEP$_n$ reference step, shown that a step response was often reached in 1-2 samples. It can be observed that the constraint on $dp/d\theta$ was exceeded. The constraint on $dp/d\theta$ was set to soft and the cycle-to-cycle variations were significant. Therefore, there is no guarantee that the $dp/d\theta$ constraint is not exceeded. However, $dp/d\theta$ was kept around the limit of 15 bar/CAD, and this was mainly achieved by retarding of α_{50}. When R_f saturate at 1, W_f was used to fulfilling the $dp/d\theta$ constraint. As the result the IMEP$_n$ reference of 4.5 bar was not achieved, as this was not possible when simultaneous satisfying the $dp/d\theta$ constraint. In order to show some practical robustness to various disturbances, results where the engine speed and the θ_{IVC} were changed are shown in Figs. 8.27 and 8.28. From Fig. 8.27 it can be concluded that the MPC controller is able to reject disturbances induced by the engine speed changes in the experiment. In the experiment W_f was increased from 1600 J/cycle to 1800 J/cycle in order to maintain the desired IMEP$_n$ of 4 bar. This was due to the pumping losses which increased with increasing engine speed. The

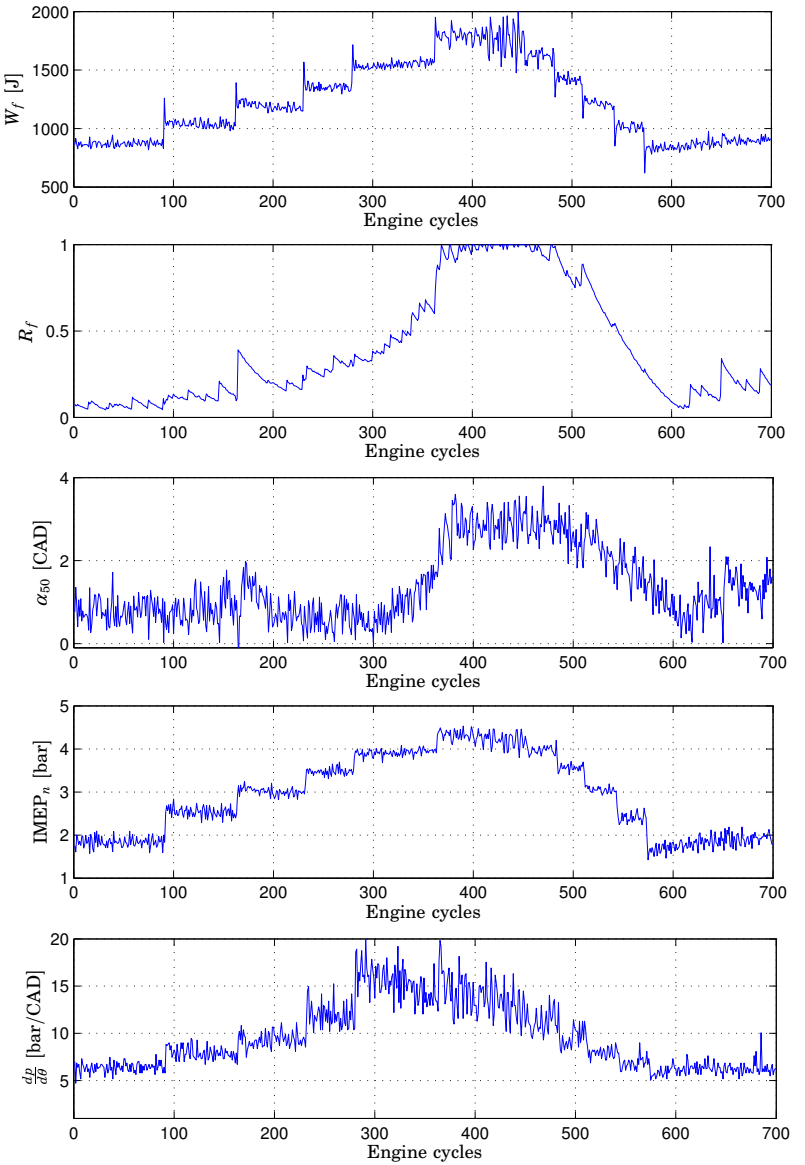

Figure 8.26 Experimental result of a step response in IMEP$_n$ for cylinder 3, when a MIMO MPC controller was used.

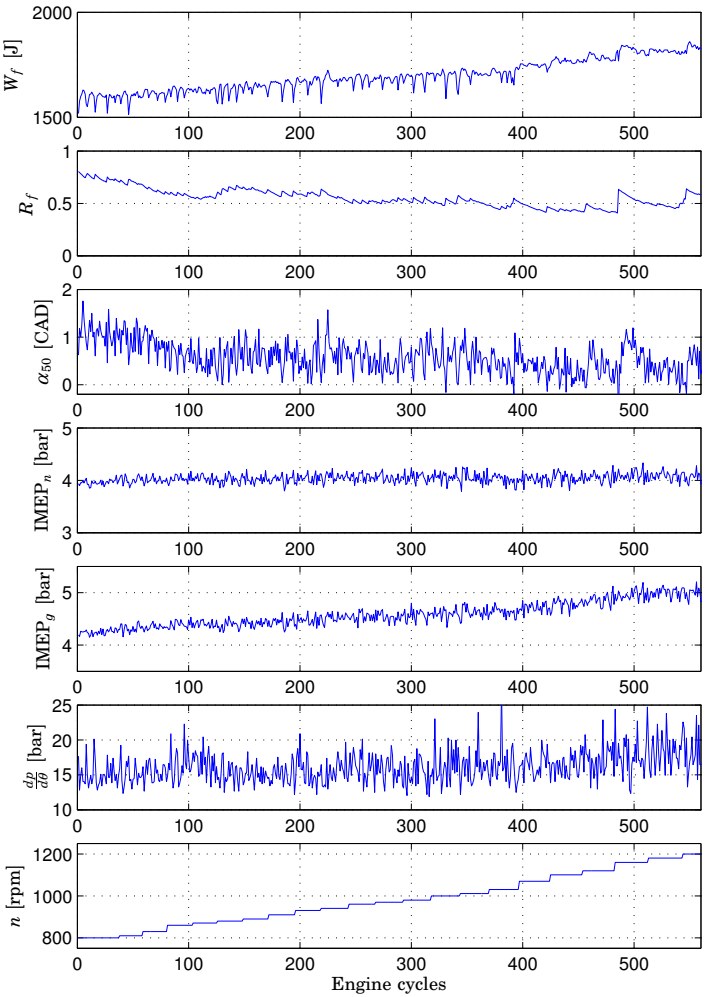

Figure 8.27 Experimental result of a speed ramp response for cylinder 3, when an MIMO MPC controller was used.

pumping losses are significant for a turbo charged HCCI engine at high load, since a HCCI engine has low exhaust temperature [Olsson *et al.*, 2001a].

Recall that the engine speed was included in the model. θ_{IVC} was on the other hand not included in the model, and the experiment shown in Fig. 8.28 demonstrate practical robustness to changes in the θ_{IVC}. The

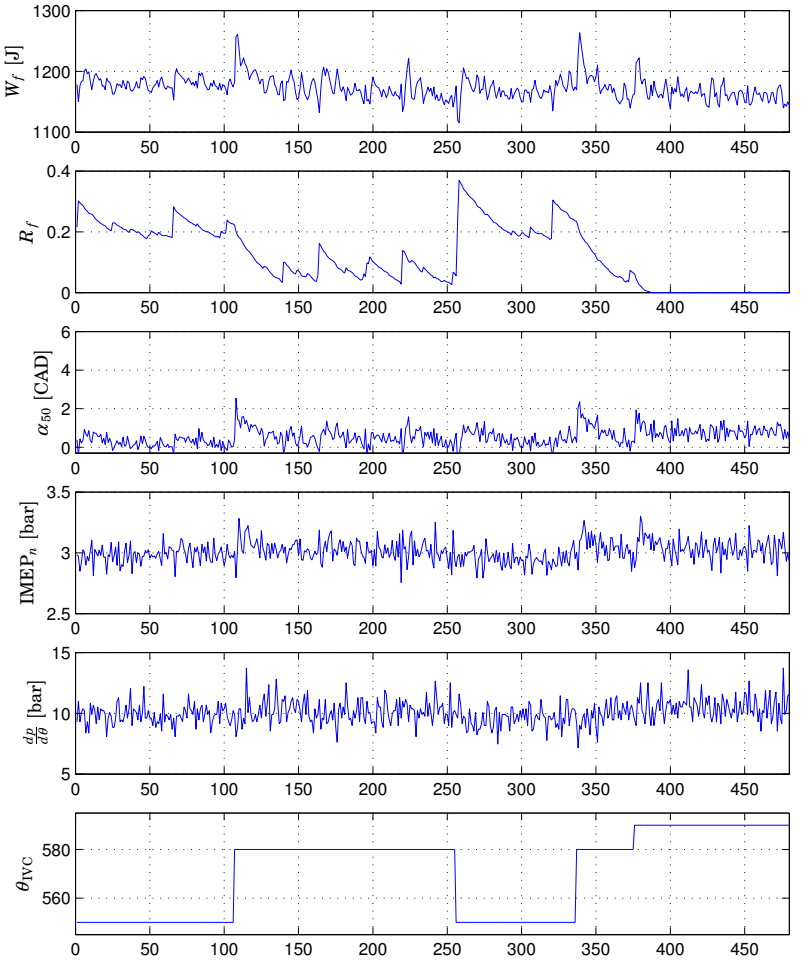

Figure 8.28 Experimental result of θ_{IVC} step responses for cylinder 3, when an MIMO MPC controller was used.

IMEP$_n$ was kept at the reference value of 3 bar.

During the experiments, no problem with computational delay due to solving the optimization problem in the MPC controller was experienced. A feature in the developed control system was that if a control signal was not calculated before the start of injection, a icon was lit in the GUI. The icon was not lit more often when an MPC controller with $H_u \leq 15$ was used than for a PID controller. In practice the icon was never lit during the experiments in the case of $H_u \leq 15$.

Feedforward

In Sec. 8.4 and 8.4, feedforward control of α_{50} was successfully demonstrated. From the end-user point of view the load is more interesting to control. Whereas the control structure with feedforward and closed-loop feedback control could also be used for the load control. The two fuels used have different vaporization properties, which need to be compensated for. In Fig. 8.29, the result in α_{50} of a step response of the injected fuel energy W_f is shown. The fuel ratio during the experiment was 0.5. It can be observed that the α_{50} decreased from 3 to 1.5 CAD and then went back when the fuel energy was decreased. As can be seen in Fig. 8.30, however, the effect in α_{50} could be a non-minimum phase behavior, the combustion phasing being first retarded and then advanced. In this experiment, the fuel ratio was 0.9 and the non-minimum phase behavior was caused by two different phenomena. One effect is the vaporization of the fuel. The heat of vaporization for ethanol is 840 kJ/kg and it is 351.1 kJ/kg for n-heptane at 1 atm and 25°C for liquid fuels. The heat of vaporization for ethanol is high enough to reduce the charge temperature, leading to retarded combustion phasing in this case. The other effect is the increased wall temperature, due to increased injected fuel energy. This effect is slower than the vaporization effect, since it mostly affects the charge temperature by increasing the wall temperature. Both these effects can be compensated for, and feedforward using first order model could be sufficient.

8.5 Variable Valve Actuation Control

Combustion timing control using VVA as actuator were performed using PID, LQG and MPC control. All three controller types were tested at similar operating conditions. Step responses were used in the evaluation of the control performance. The octane number of the fuel mixture was 95 and the two fuels were n-heptane and ethanol. Two experiments were carried out on the three controller types. In the first experiment (Case 1), the reference value for α_{50} was changed between 2 and 5 CAD, the injected fuel was changed between 1500J and 2000J, which corresponds to an IMEP_n change between 3.4 and 4.6 bar. In the second experiment (Case 2), the injected fuel was changed between 2400J and 2600J, which corresponds to an IMEP_n change between 5.6 and 6.4 bar. All cylinders were individually controlled on a cycle-to-cycle basis. Hence, there was no delay in the control loop.

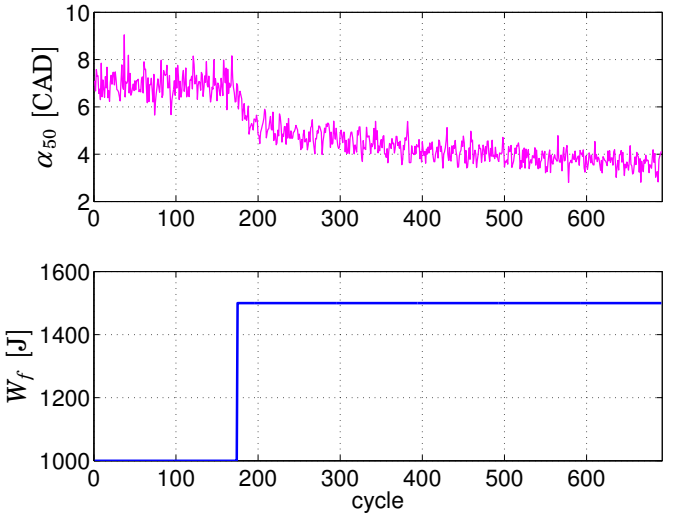

Figure 8.29 Step change in the injected fuel energy and its effect on α_{50} when R_f was 0.5.

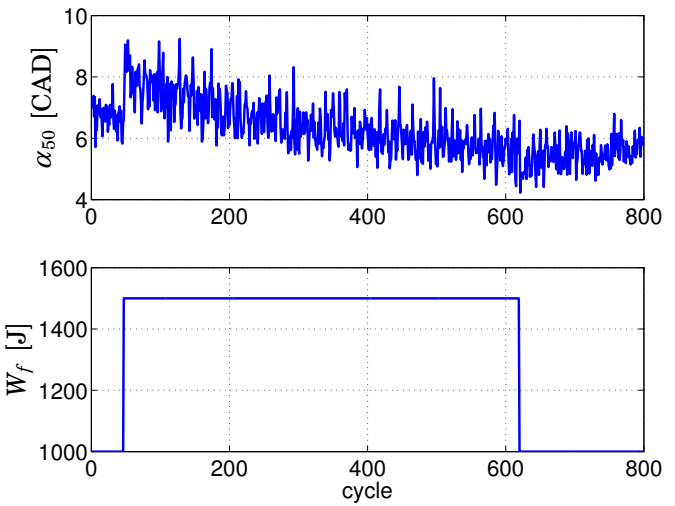

Figure 8.30 Step change in the injected fuel energy and its effect on α_{50} when R_f was 0.9.

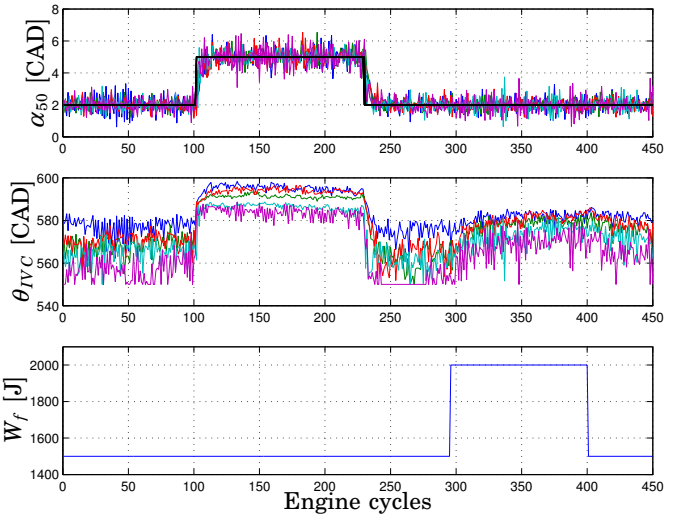

Figure 8.31 PID control of α_{50} using θ_{IVC} for Case 1.

PID

The obtained models in Ch. 7 has been used in the PID design as well as manually tuning. The identified static nonlinearity was used for feed-forward and gain scheduling. Results from the Case 1 experiment, when using a PID controller is shown in Figure 8.31. The PID controller was able to follow the reference value and compensate for the load disturbance. Note the differences between the cylinders.

In Figure 8.32, results from one of the cylinders are shown in order to better illustrate the step response for Case 1. Notice that the amplitude on the control signal was decreased when the combustion phasing was retarded. This effect was due to the nonlinearity between θ_{IVC} and α_{50}. The step response was not symmetric, which is due to the dynamics of the cylinder wall temperature.

Results from the Case 2 experiment, when using a PID controller is shown in Figure 8.33. The PID controller was able to follow the reference value and compensate for the load disturbance, but the bandwidth of the controller was decreased. The PID controller used for Case 2 could not be used for Case 2, as it resulted in large oscillations.

In Figure 8.34, results from one of the cylinders are shown in order to better illustrate the step response for Case 2. Note that the amplitude on the control signal increased in comparison to the amplitude used in

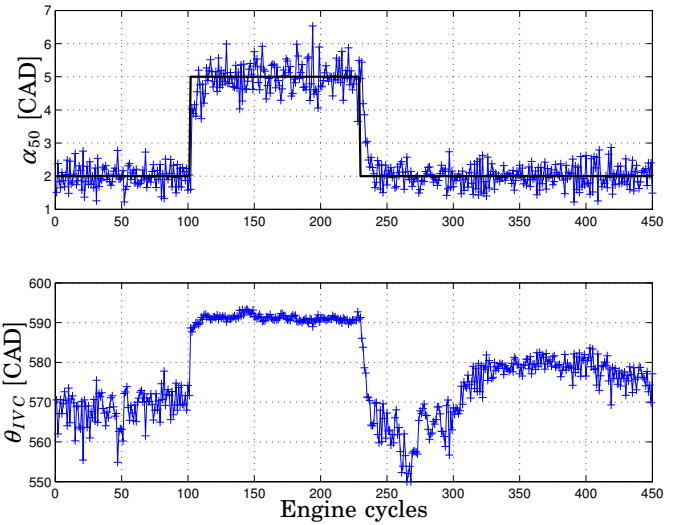

Figure 8.32 PID control of α_{50} using θ_{IVC} for Case 1. Result from cylinder 3.

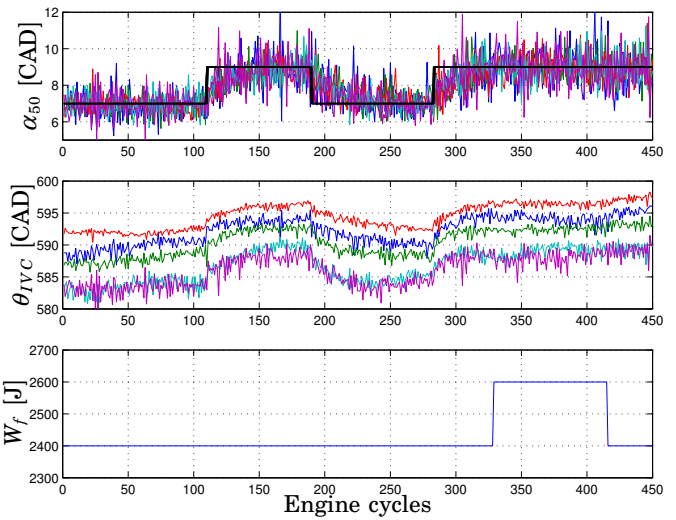

Figure 8.33 PID control of α_{50} using θ_{IVC} for Case 2.

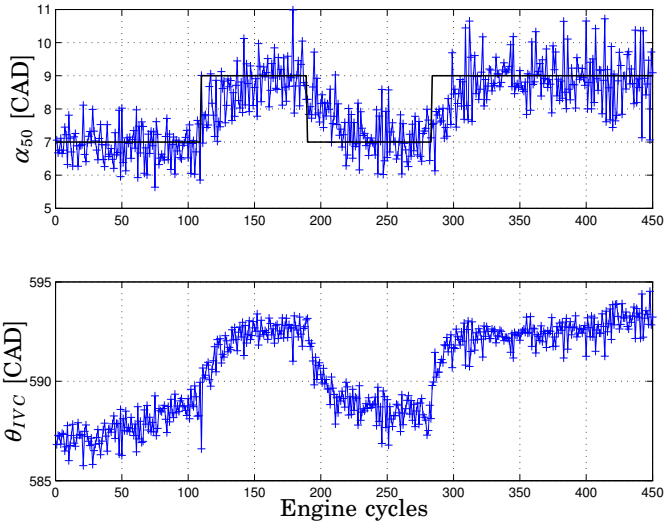

Figure 8.34 PID control of α_{50} using θ_{IVC} for Case 2. Result from cylinder 3.

Case 1. A possible explanation is that the cycle-to-cycle variations were increased as the combustion phasing was retarded. The variance of α_{50} became larger at later phasing.

The identified static nonlinearity could also be used in the PID control in order to linearize the system, and to make a feedforward design and gain scheduling of the controller. In Figure 8.35, step responses in α_{50} are shown. From the figure it can be noted that the reference value was followed and the feedforward worked well.

LQG

In the control design, the identified linear model was used. The same LQG controller was used for both experiment cases. Results from the Case 1 experiment, when using an LQG controller is shown in Figure 8.36. The LQG controller was able to follow the reference value and compensate for the load disturbance. In Figure 8.37, results from one of the cylinders are shown in order to better illustrate the step response for Case 1.

The cycle-to-cycle variations is larger at later timing and this could give rise to oscillations. Results from the Case 2 experiment, when using an LQG controller, where the static nonlinearity was not included in the model and a poor linear model was used in the LQG design, is shown in Figure 8.38. In this experiment, cylinder 3 was initially stable after

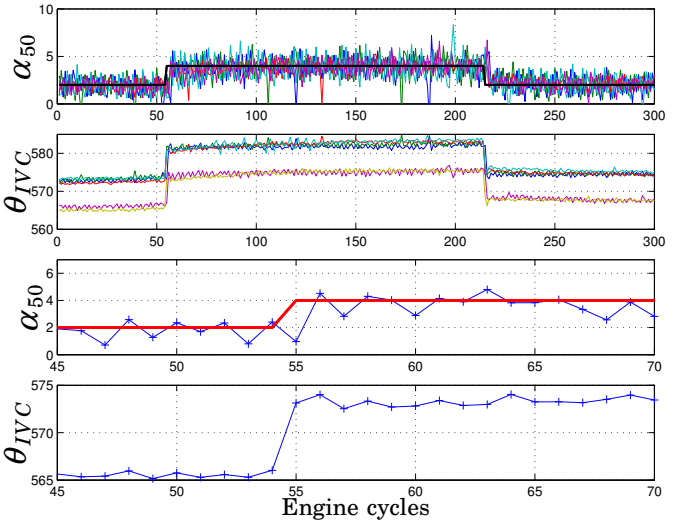

Figure 8.35 PID control of α_{50} using θ_{IVC}. The lower figures shows a closer view of the step change.

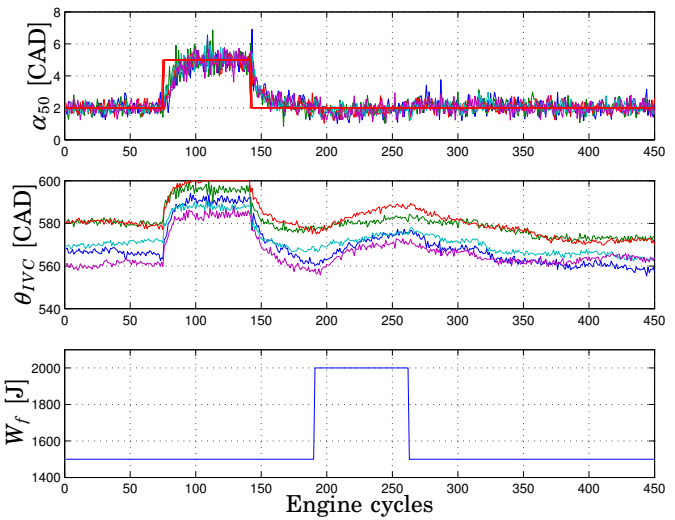

Figure 8.36 LQG control of α_{50} using θ_{IVC} for Case 1.

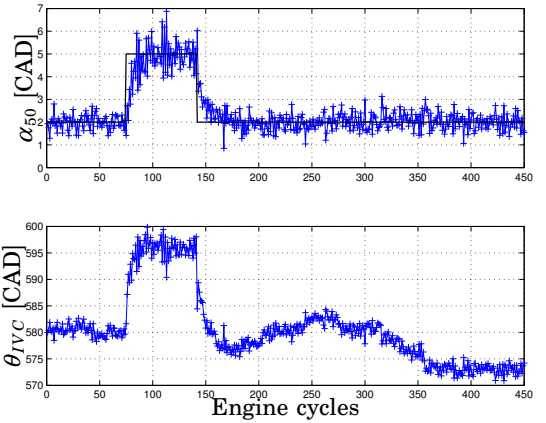

Figure 8.37 LQG control of α_{50} using θ_{IVC} for Case 1. Result from cylinder 3.

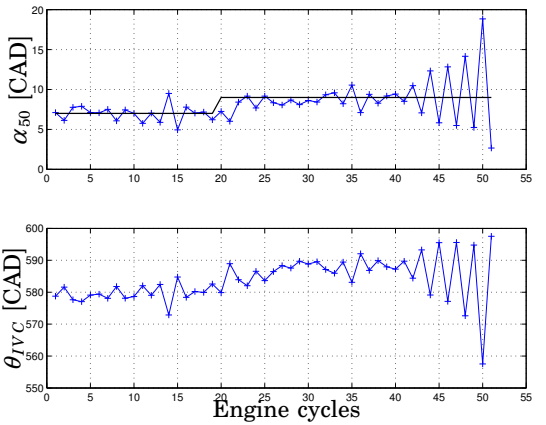

Figure 8.38 LQG control of α_{50} using θ_{IVC} in Case 2. Result from cylinder 3.

the step change. But 20 cycles after the step change the instability was triggered, this without any change of the controllable operation condition. Notice that the amplitude of the control signal increased very quickly and in a few cycles the process becomes unstable. The engine was automatically shut down, as the engine safety limit was exceeded. This example shows the need of accurate models.

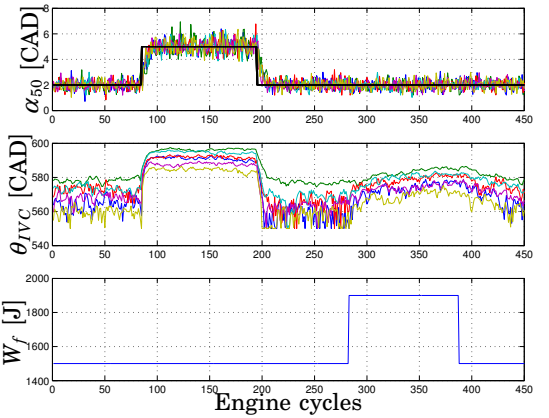

Figure 8.39 MPC control of α_{50} using θ_{IVC} in Case 1.

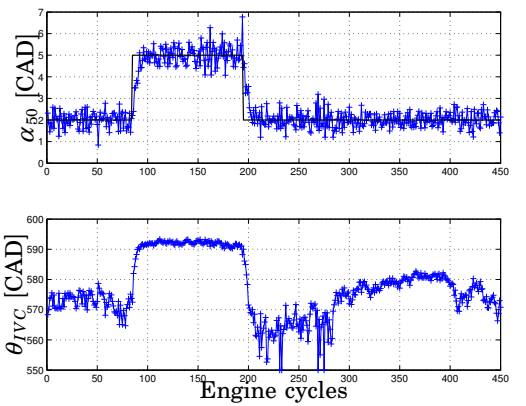

Figure 8.40 MPC control of α_{50} using θ_{IVC} in Case 1. Result from cylinder 3.

MPC

In the control design, the identified linear model was used. The same MPC controller was use in both experiment cases. Results from the Case 1 experiment, when using a MPC controller i shown in Figure 8.39. The MPC controller was able to follow the reference value and compensate for the load disturbance.

In Figure 8.40, results from one of the cylinders are shown in order to better illustrate the step response for Case 1. The step response is achieved in 5-6 cycles.

Results from the Case 2 experiment, when using a MPC controller is

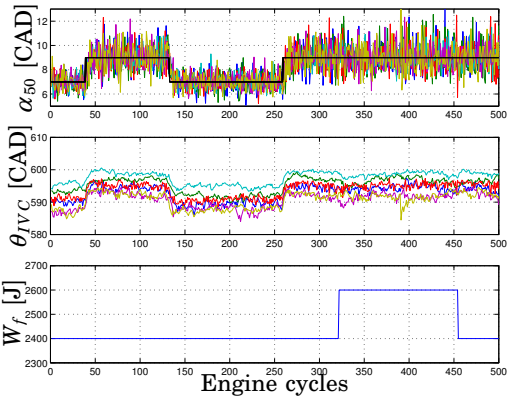

Figure 8.41 MPC control of α_{50} using θ_{IVC} in Case 2.

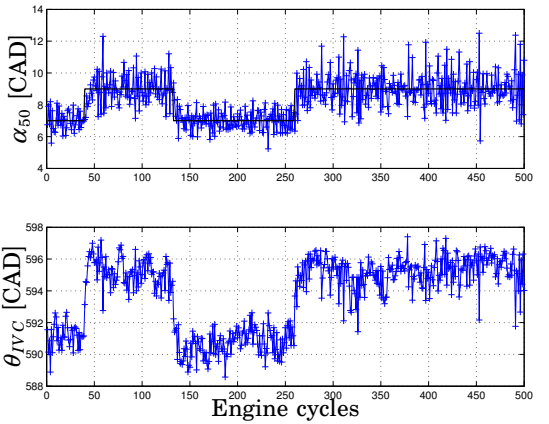

Figure 8.42 MPC control of α_{50} using θ_{IVC} for Case 2. Result from cylinder 3.

shown in Figure 8.41. The MPC controller was able to follow the reference value and compensate for the load disturbance. It can be seen that there are differences between the cylinders.

In Figure 8.42, results from one of the cylinders are shown in order to better illustrate the step response for Case 2. It can be noticed that at late timing the step response is almost symmetric. The combustion phasing effect on the wall temperature decreases at later timing, as the difference in cylinder temperature becomes smaller at step response at late timing.

The cycle-to-cycle variations on a HCCI engine are significant and it is

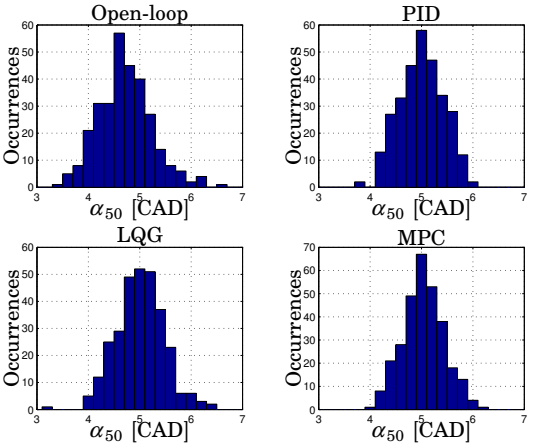

Figure 8.43 Histogram of α_{50} in open loop, LQG control, PID control, MPC control and open loop for one cylinder.

desirable that the controller does not increase these variations. In Figure 8.43, the histogram of the control error when the reference value of α_{50} was 5 CAD and for a open-loop experiment where the α_{50} was close to 5 CAD. The distributions were similar to the normal distribution.

Note that all cases exhibit similar distributions and there was no significant reduction of the variance when using closed-loop control compared to open-loop control. The variances in α_{50} depend on the reference value, and in Table 8.2 the variances for the three controllers and for open-loop experiment are shown. In the open-loop experiments the operating condition was such that similar α_{50} as in controlled was achieved.

It was observed that the method to obtain the desired α_{50} in open-loop did not matter. A similar result was obtained when the inlet temperature was used to obtain the desired α_{50} when θ_{IVC} was used. As already indicated, there was no significant difference in the variance between open-loop and closed-loop.

8.6 Safety limits

The HCCI engine used was operated up to IMEP_n of 14 bar, which is approximately 70% of the full load for the same engine with diesel cycle operation. The HCCI engine can be operated at higher loads, but then there are increased problems with mechanical strain and noise level. In this work, safety limits for automatically shutting down the engine were

Table 8.2 Variances in α_{50} at different reference value for the three controllers.

α_{50}	2 CAD				5 CAD			
#	Open	PID	LQG	MPC	Open	PID	LQG	MPC
1	0.145	0.133	0.132	0.138	0.216	0.276	0.244	0.209
2	0.127	0.132	0.118	0.137	0.216	0.281	0.249	0.225
3	0.116	0.114	0.098	0.098	0.239	0.172	0.236	0.159
4	0.114	0.109	0.076	0.100	0.168	0.154	0.175	0.177
5	0.101	0.128	0.079	0.108	0.179	0.226	0.181	0.228
6	0.142	0.136	0.109	0.115	0.206	0.250	0.261	0.216

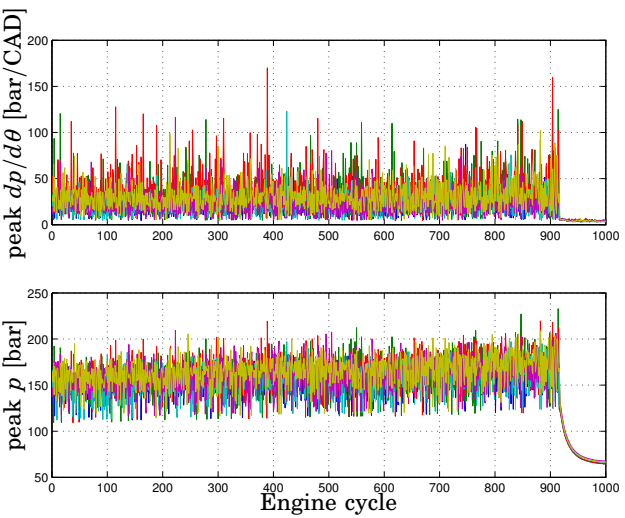

Figure 8.44 Experiment where the engine safety limit was exceeded, resulting in automatic engine shut down.

applied both on the peak pressure and on the peak pressure gradient. The medium of the last three samples was used in the safety limit check. Fig. 8.44 shows results from an experiment where the engine was automatically shut down. An engine needs to have a long lifespan, hence the safety limits. The safety limits could probably be increased without immediate problems, but in the long run the engine and the cylinder pressure transducer could be damaged.

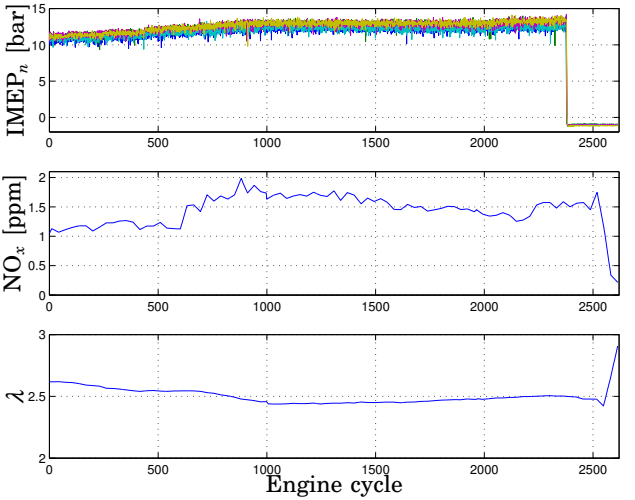

Figure 8.45 NO$_x$ emissions when the HCCI engine operates at high load IMEP$_n \approx$ 13 bar. The engine was shut down around engine cycle 2400.

8.7 Emissions

As previously stated, the main purpose for HCCI is the promise of low NO$_x$ emissions. Fig. 8.45 shows the resulting NO$_x$ emissions when the engine was operated at high load. It can be observed that the concentrations of NO$_x$ emissions are kept below 2 ppm (parts per million) and that the NO$_x$ emissions increased when the load increased. These values can be considered to very low. In experiments where NO$_x$ was measured, the concentrations of NO$_x$ never exceeded 3 ppm. These concentrations could be compared with the concentration of NO$_x$ in SI engines where they often are few thousands ppm before aftertreatment of the emissions, and the concentration of NO$_x$ in CI engines where the concentrations are few hundreds of ppm before aftertreatment of the emissions. For the experiment shown in Fig. 8.45, the HC emissions were around 2500 ppm and the CO emissions were around 1200 ppm. These are not low levels but may be reduced to acceptable levels by a oxidation catalyst.

8.8 Discussion

The models used by the MPC controller were of low order, the MIMO model was of sixth order. There were only four constraints, three on the control variables and one on the output variable $dp/d\theta$. Therefore, the

QP problem has low complexity when the control horizon is short. As the engine had fast dynamics, there was no significant improvement when the prediction horizon was chosen larger than ten samples, and when the control horizon was larger than five samples. As the computational effort of solving the optimization problem was small, longer horizons may however be applied as it would generally increases the robustness.

At the load increased it was noticed that the NO_x emissions increased, and even if the level of the NO_x emissions were very low, it would be interesting to model and control the NO_x emissions. Modeling of the NO_x emissions is difficult and the measurements have long time delays.

There are several commercial and research VVA systems available and they have various degrees of freedom. The VVA system used is a research system aiming for production and only the inlet port could be varied. If the outlet port could also be controlled, the residual gas in the cylinder could be controlled using negative overlap. This will result in that cycle-to-cycle control of the temperature gas mixture could be controlled. An additional benefit is that there is no need for a heater (with the drawback of being a more complex and expensive system). The benefit by only using control by θ_{IVC} is that it requires a less expensive and complex system. In this comparison, a heater has low complexity and cost. The drawback with only using IVC is that at high load, when the combustion phasing must be retarded in order to not damage the engine, late IVC closing may be needed. This results in decreased volumetric efficiency, which is the opposite to what is desired when aiming towards high loads. The dual fuel approach has not this drawback. A benefit with VVA is that there is less dynamics between θ_{IVC} and α_{50} than between R_f and α_{50}, as wall wetting and heat of vaporization does not change with θ_{IVC}.

The PID controller is intuitive and simple controller, if comparison of tuning time needed in the design of the three different control methods were similar.

It was found that dynamic behavior of the cylinder differs significantly and cylinder individual-control design was necessary.

The cancellation of the nonlinearity can give rise to singularities and add sensitivity to the noise. In practice, no such problem were experienced.

In order to have a fast and robust control of the HCCI combustion phasing in the whole operation range, it is probably necessary either to switch or to change the controller, if linear control design methods are to be used. Methods for this is are for example Linear Parameter Varying systems, Hidden Markov Models, gain scheduling or hybrid control. Other approaches are for instance to use nonlinear control based on nonlinear models, or to use adaptive control. Mean Value Engine Model can be used in the control design for internal combustion engines [Hendricks, 1989], and in [Rausen *et al.*, 2004] a Mean Value Model of HCCI was presented.

8.9 Summary and Concluding Remarks

In this chapter, different control strategies, actuators and feedback alternatives for HCCI closed-loop control were demonstrated. Previously, it was reported that VVA can be used to control HCCI combustion. These results were obtained on a one-cylinder engine. The presented VVA results in this chapter, were obtained from a six-cylinder heavy duty engine. Control of a six-cylinder engine is a more difficult control problem compared to control a on-cylinder engine, as the cylinders interacts and more dynamics are added to the system. The interactions are mainly temperature interactions, such as wall temperature and inlet air temperature. VVA systems can have various degrees of freedom, and it was demonstrated that control of IVC was sufficient to cycle-to-cycle control the combustion phasing in a six-cylinder heavy-duty HCCI engine.

The engine was controlled in load ranges up to 14 bar IMEP_n, which corresponds to approximately 70% of max load, and at engine speed up to 1800 rpm. Both dual fuel and VVA can be used to cycle-to-cycle control HCCI combustion and it was found that the HCCI engine could operate at a wider range of operation conditions by IVC, without changing the inlet temperature, than by dual fuel. Model based control, such as LQG and MPC, and PID control was successfully demonstrated to be able to control the HCCI dynamic, both when using VVA or dual fuel as actuator. Of these controllers, MPC was found to give practically robustness in a wider range of operating conditions than LQG and PID controllers. When the LQG, MPC or PID controller was operated at operation condition, which was excited in the data from which the model used in the control design was used, there was no significant difference in the control performance.

Cycle-to-cycle control of α_{50} increased the load control performance. In the performed closed-loop control experiments, a step change in the load did not affect α_{50}, as the cycle-to-cycle controllers were sufficiently fast to reject the effect on α_{50}.

A MPC controller was proposed to solved the problem of control of the load and simultaneous minimization of the fuel consumption and emissions, and satisfying the constraint on $dp/d\theta$ and successful experiment was presented.

At the operating condition of $\lambda \in [2, 2.7]$ it was demonstrated that feedback based on cylinder ion current gave similar control performance as feedback based on cylinder pressure.

9

Concluding Remarks

In this thesis, modeling and control of six-cylinder heavy-duty HCCI engine has been presented. Control of the combustion phasing is necessary in order to generate low emissions and obtain high efficiency. The bandwidth of the controller is a limiting factor in the load and emission control. This thesis presents results where a reference change in combustion phasing was achieved within a few engine cycles.

To practically use an HCCI engine it is desired that the load of the engine can be controlled and the fuel consumption should be minimized. Simultaneously, the emissions must be kept low, and the cylinder peak pressure and peak pressure gradient must be limited. One suggested solution to this problem is to use Model Predictive Control. Successful experiments demonstrating that an MPC controller could solve the problem were performed.

Among the scientific HCCI challenges listed in Sec. 2.10, this thesis has contributed in the following areas:

Deriving dynamic models of HCCI combustion

Results that lower-order dynamic models are sufficient to describe the HCCI dynamics in the load range 2-14 bar IMEP$_n$ were presented. It was shown that system identification can be used as a tool for obtaining dynamic models of the combustion phasing in HCCI. It was also shown that low-order physical models can be used to model the HCCI combustion.

Sensor and actuator studies

It was demonstrated that ion current can be used for feedback control of the combustion phasing in an HCCI engine, for $\lambda \in [2, 2.7]$. An ion current sensor has the benefit of being very cheap and having long lifespan. Comparison of feedback alternatives of HCCI combustion phasing showed that heat release based feedback or mass fraction burned based feedback were most robust in detecting the combustion phasing. Results

where the combustion phasing in a six-cylinder heavy-duty engine was controlled by either a VVA system using the inlet valve or a dual-fuel system was presented.

Control of combustion phasing

Control of HCCI on a cycle-to-cycle basis, where each cylinder was individually controlled, was performed on a six-cylinder heavy duty engine. The engine has been controlled in load ranges up to 14 bar $IMEP_n$ and at engine speed up to 1800 rpm. Model based control, such as LQG and MPC, and PID control was successful demonstrated.

10

Bibliography

Agrell, F., H.-E. Angstrom, B. Eriksson, and J. Wikander (2003): "Transient control of HCCI through combined intake and exhaust valve actuation." SAE Technical Paper 2003-01-3172.

Ahmed, S., T. Tzeuch, P. Amnéus, E. Blurock, H. Soyhan, and F. Mauss (2003): PLANET D4 report, The European Community.

Amnéus, P. (2002): *Homogeneous Ignition – Chemical Kinetic Studies for IC-Engine Applications*. PhD thesis, Division of Combustion Physics, Lund Institute of Technology, Lund University, Lund, Sweden.

Anderson, B. D. and J. B. Moore (1990): *Linear Optimal Control*. Prentice Hall, Englewood Cliffs, New Jersey.

Andersson, I. and L. Eriksson (2000): "Ion sensing for combustion stability control of a spark-ignited, direct- injected engine." SAE Technical Paper 2000-01-0552.

Aoyama, T., Y. Hattori, J. Mizuta, and Y. Sato (1996): "An experimental study on premixed-charge compression ignition gasoline engine." SAE Technical Paper 960081.

Åström, K. J. and B. Wittenmark (1997): *Computer Controlled Systems—Theory and Design*, Third edition. Prentice Hall, Englewood Cliffs, New Jersey.

Babajimopoulos, A., G. A. Lavoie, and D. N. Assanis (2003): "Modelling HCCI combustion with high levels of residual gas fraction - a comparison of two VVA strategies." SAE Technical Paper 2003-01-3220.

Bemporad, A., F. Borelli, and M. Morari (2002): "Model predictive control based on linear programming-the explicit solution." *IEEE Transactions on Automatic Control*, **47**, pp. 1974–1985.

Bengtsson, J. (2001): "Adaptive cruise control and driver modeling." Licentiate thesis ISRN LUTFD2/TFRT--3227--SE. Department of Automatic Control, Lund Institute of Technology, Sweden.

Bengtsson, J., A. Ahlstrand, K. Nilsson, A. Robertsson, M. Olsson, A. Heyden, and R. Johansson (2000): "A robot playing scrabble using visual feedback." In *6th Int. IFAC Symposium on Robot Control (SYROCO 2000)*. Vienna, Austria.

Bengtsson, J., M. Gäfvert, and P. Strandh (2004): "Modeling of hcci engine combustion for control analysis." In *Conference in Decision and Control (CDC 2004)*. Bahamas.

Bengtsson, J., M. Haage, and R. Johansson (2002): "Variable time delays in visual servoing and task execution control." In *2nd IFAC Conference on Mechatronic Systems*. Berkeley.

Bengtsson, J., R. Johansson, and A. Sjögren (2001): "Modeling of drivers longitudinal behavior." In *2001 IEEE/ASME International Conference on Advanced Intelligent Mechatronics (AIM'01)*. Como,Italy.

Bengtsson, J., R. Johansson, and A. Sjögren (2002): "Modeling of driver's longitudinal behavior." In Johansson and Rantzer, Eds., *Nonlinear and Hybrid Systems in Automotive Control*, pp. 41–58. London.

Bengtsson, J. and S. Solyom (2004): "ABS and anti-skid on a LEGO car." Technical Report LUTFD2/TFRT --7609-- SE. Automatic Control, Lund Institute of Technology, Sweden.

Bengtsson, J., P. Strandh, R. Johansson, P. Tunestål, and B. Johansson (2004a): "Control of homogeneous charge compression ignition (HCCI) engine dynamics." In *Proceedings of the American Control Conference*, pp. 4048–4053. Boston, Massachusetts.

Bengtsson, J., P. Strandh, R. Johansson, P. Tunestål, and B. Johansson (2004b): "System identification of homogenous charge compression ignition (HCCI) engine dynamics." In *IFAC Symp. Advances in Automotive Control (AAC04), Salerno, Italy, April 19-23, 2004*.

Bengtsson, J., P. Strandh, R. Johansson, P. Tunestål., and B. Johansson (2005): "Variable valve actuation for timing control of a homogeneous charge compression ignition engine." draft submitted to SAE World Congress 2005, Detroit, USA.

Bengtsson, J., P. Strandh, R. Johansson, P. Tunestål, and B. Johansson (2004): "Closed-loop combustion control of homogeneous charge compression ignition (HCCI) engines dynamics." *International Journal of Adaptive Control and Signal Processing*, **18**, pp. 167–179.

Christensen, M. (2002): *HCCI Combustion — Engine Operation and Emission Characteristics*. PhD thesis, ISRN LUTMDN/TMHP–02/1006-SE, Department of Heat and Power Engineering, Lund Institute of Technology, Lund University, Lund, Sweden.

Christensen, M., P. Einewall, and B. Johansson (1997): "Homogeneous charge compression ignition (HCCI) using isooctane, ethanol and natural gas–a comparison with spark-ignition operation." SAE Technical Paper 972874.

Christensen, M., A. Hultqvis, and B. Johansson (2002): "The effect of combustion chamber geometry on hcci operation." SAE Technical Paper 2002-01-0425.

Christensen, M., A. Hultqvist, and B. Johansson (1999): "Demonstrating the multi fuel capability of a homogeneous charge compression ignition engine with variable compression ratio." SAE Technical Paper 1999-01-3679.

Dec, J. E. and M. Sjöberg (2004): "Isolating the effects of fuel chemistry on combustion phasing in an HCCI engine and the potential of fuel stratification for ignition control." SAE Technical Paper 2004-01-0557.

Draper, C. S. (1938): "Pressure waves accompanying detenotion in the internal combustion engine." *J. Aeronautical Sciences*, **5:6**, pp. 219–226.

dSPACE (2004):. http://www.dspace.com.

Egeland, O. and J. T. Gravdahl (2002): *Modeling and Simulation For Automatic Control*. Marine Cybernetics, Trondheim, Norway.

Eriksson, L., L. Nielsen, and M. Glavenius (1997): "Closed loop ignition control by ionization current interpretation." SAE Technical Paper 970854.

European Federation for Transport and Environment (2004): *Waiting for Euro 5 and Euro 6 New Emission Standards for Passenger Cars, Vans and Lorries*. http://www.t-e.nu.

Fiveland, S., R. Agama, M. Christensen, B. Johansson, J. Hiltner, F. Mauss, and D. Assanis (2001): "Experimental and simulated results detailing the sensitivity of natural gas HCCI engines to fuel composition." SAE Technical Paper 2001-01-3609.

Flierl, R., R. Hofmann, C. Landerl, T. Melcher, and H. Steyer (2001): "Der neue BMW viercylinder-Ottomotor mit valvetronic Teil 1: Konzept und konstruktiver Aufbau." *Motortechnische Zeitschrift*, **No 6**.

Franke, A. (2002): *Characterization of an Electrical Sensor for Combustion Diagnostics*. PhD thesis, ISRN LUTFD/TFCP–80–SE, Department of Physics, Lund Institute of Technology, Lund University, Lund, Sweden.

Gatowski, J. A., E. N. Balles, K. M. Chun, F. E. Nelson, J. A. Ekchian, and J. B. Heywood (1984): "Heat release analysis of engine pressure data." SAE Technical Paper 84135.

Gillbrand, P., H. Johansson, and J. Nytomt (1987): "Method and apparatus for detecting ion current in an internal combustion engine ignition system." Technical Report. U.S. Patent No. 4,648,367.

Griffiths, J. and B. Whitaker (2002): "Thermokinetic interactions leading to knock during homogeneous charge compression ignition." *Combustion and Flame*, **131:4**, pp. 386–399.

Halstead, M., L. Kirsch, and C. Quinn (1977): "The autoignition of hydrocarbon fuels at high temperatures and pressures — fitting of a mathematical model." *Combustion and Flame*, **30**, pp. 45–60.

Haraldsson, G., J. Hyvonen, and P. Tunestål (2004): "HCCI closed-loop combustion control using fast thermal management." SAE Technical Paper 2004-01-0943.

Haraldsson, G., J. Hyvonen, P. Tunestål, and B. Johansson (2002): "Hcci combustion phasing in a multi-cylinder engine using variable compression ratio." SAE Technical Paper 2002-01-2858.

Haverkamp, B. and M. Verhaegen (1997): *SMI Toolbox—State Space Model Identification Software for Multivariable Dynamical Systems*. Dept. Electrical Engineering, Systems- and Control Engineering Group, TU Delft, Delft, Netherlands.

Hendricks, E. (1989): "Mean value modelling of large turbocharged two-stroke diesel engines." SAE Technical Paper 890564.

Heywood, J. B. (1988): *Internal Combustion Engine Fundamentals*. McGraw-Hill, New York.

Ho, B. and R. Kalman (1966): "Effective construction of linear state-variable models from input/output pressure." *Regelungstechnik*, **No 14**, pp. 545–548.

Hultqvist, A., M. Christensen, B. Johansson, A. Franke, M. Richter, and M. Alden (1997): "A study of the homogeneous charge compression ignition combustion process by chemoluminescence imaging." SAE Technical Paper 1999-01-3680.

Hyvönen, J., G. Haraldsson, and J. Bengt (2004): "Balancing cylinder-to-cylinder variations in a multi-cylinder VCR-HCCI engine." SAE Technical Paper 2004-01-1897.

Jeuland, N., X. Montagne, and P. Duret (2004): "New HCCI/CAI combustion process development: Methodolgy for determination of relevant fuel parameters." In *Which Fuels for Low CO_2 Engines?* IFP International Conference.

Johansson, R. (1993): *System Modeling and Identification*. Prentice Hall, Englewood Cliffs, New Jersey.

Juang, J. N. and R. S. Pappa (1985): "An eigensystem realization algorithm for modal parameter identification and model reduction." *Journal of Guidance, Control and Dynamics*, **8**, pp. 620–627.

Keller PAA-21S (2004):. http://www.keller-druck.ch.

Kistler 7061 B (2004):. http://www.kistler.com.

Larimore, W. E. (1990): "Canonical variate analysis in identification, filtering and adaptive control." In *Proc. 29th IEEE Conference on Decision and Control*, pp. 596–604. Honolulu.

Law, D., J. Allen, D. Kemp, G. Kirkpatrick, and T. Copland (2001): "Controlled combustion in an IC-engine with a fully variable valve train." SAE Technical Paper 2001-01-0251.

Linde, L. . (2004):. http://www.leinelinde.se.

Maciejowski, J. (2002): *Predictive Control with Constraints*. Prentice Hall, Pearson Education, England.

Martinez-Frias, J., S. M. Aceves, D. L. Flowers, J. R. Smith, and R. W. Dibble (2000): "HCCI engine control by thermal management." SAE Technical Paper 2000-01-2869.

Milovanovic, N., R. Dowden, R. Chen, and J. W. G. Turner (2004): "Influence of the variable valve timing strategy on the control of a homogeneous charge compression (HCCI) engine." SAE Technical Paper 2004-01-1899.

Najt, P. and D. Foster (1983): "Compression-ignited homogeneous charge combustion." SAE Technical Paper 830264.

Noguch, M., Y. Tanaka, T. Tanaka, and Y. Takeuchi (1979): "A study in gasoline engine combustion by observation of intermediate reactive products during combustion." SAE Technical Paper 790840.

Oakley, A., H. Zhao, and N. Ladommatos (2001): "Experimental studies on controlled auto-ignition (CAI) combustion of gasoline in a 4-stroke engine." SAE Technical Paper 2001-01-1030.

Olsson, J.-O. (2004): *The HCCI Engine - High Load Performance and Control Aspects*. PhD thesis, ISRN LUTMDN/TMPH–04/1019-SE, Department of Heat and Power Engineering, Lund Institute of Technology, Lund University, Lund, Sweden.

Olsson, J.-O., P. Tunestål, G. Haraldsson, and B. Johansson (2001a): "A turbo charged dual fuel HCCI engine." SAE Technical Paper 2001-01-189.

Olsson, J.-O., P. Tunestål, and B. Johansson (2001b): "Closed-loop control of an HCCI engine." SAE Technical Paper 2001-01-1031.

Olsson, J.-O., P. Tunestål, B. Johansson, S. Fiveland, J. R. Agama, and D. N. Assanis (2002a): "Compression ratio influence on maximum load of a natural gas HCCI engine." SAE Technical Paper 2002-01-0111.

Olsson, T., J. Bengtsson, R. Johansson, and H. Malm (2002b): "Force control and visual servoing using planar surface identification." In *IEEE Int. Conference on Robotics and Automation*, pp. 4211–4216. Washington D.C., USA.

Olsson, T., J. Bengtsson, A. Robertsson, and R. Johansson (2003): "Visual position tracking using dual quaternions with hand-eye motion constraints." In *IEEE Int. Conference on Robotics and Automation*, pp. 3491–3496. Taipei, Taiwan.

Onishi, S., S. H. Jo, K. Shoda, P. D. Jo, and S. Kato (1979): "Active thermo—atmosphere combustion (ATAC)–a new combustion process for internal combustion engines." SAE Technical Paper 790501.

Pentronic (2004):. www.pentronic.com/.

Pischinger, M., W. Salber, F. V. D. Staay, H. Baumgarten, and H. Kemper (2000): "Benefits of the electromechanical valve train in vehicle operation." SAE Technical Paper 2000-01-1223.

Rassweiler, G. and L. Withrow (1938): "Motion pictures of engine flames correlated with pressure cars." *SAE Transactions*, **42:5**, pp. 185–204.

Rausen, D. J., A. G. Stefanopoulou, J.-M. Kang, J. A. Eng, and T.-W. Kuo (2004): "A mean-value model for control of homogeneous charge compression ignition (HCCI) engines." In *Proceedings of the American Control Conference*, pp. 125–131.

Reinmann, R. (1998): *Theoretical and Experimental Studies of the Formation of Ionized Gases in Spark Ignition Engines*. PhD thesis, ISRN LUTFD2/TFCP –37–SE, Department of Physics, Lund Institute of Technology, Lund University, Lund, Sweden.

Richter, M., A. Franke, J. Engström, A. Hultqvist, B. Johansson, and M. Alden (2000): "The influence of charge inhomogeneity on the HCCI combustion process." SAE Technical Papers 2000-01-2868.

Roth, K., A. Sobiesiak, L. Robertson, and S. Yates (2002): "In-cylinder pressure measurements with optical fiber and piezoelectric pressure transducers." SAE Technical Paper 2002-01-0745.

Ryan, T. and T. Callahan (1996): "Homogeneous charge compression ignition of diesel fuel." SAE Technical Paper 961160.

Sellnau, M., F. Matekunas, P. Battiston, C.-F. Chang, and D. Lancaster (2000): "Cylinder-pressure-based engine control using pressure- ratio-management and low-cost non-intrusive cylinder pressure sensors." SAE Technical Paper 2000-01-0932.

Shaver, G. M., J. C. Gerdes, P. Jain, P. Caton, and C. Edwards (2003): "Modeling for control of HCCI engines." In *Proceedings of the American Control Conference*, pp. 749–754. Denver, Colorado.

Shaver, G. M., J. C. Gerdes, and M. Roelle (2004): "Physics-based closed-loop control of phasing, peak pressure and work output in HCCI eninges utilizing variable valve actuation." In *Proceedings of the American Control Conference*, pp. 150–155. Boston, Massachusetts.

Shimasaki, Y., M. Kobayashi, H. Sakamoto, M. Ueno, M. Hasegawa, H. Yamaguchi, and T. Suzuki (2004): "Study on engine management system using in-cylinder pressure sensor integrated with spark plug." SAE Technical Paper 2004-01-0519.

Sjöberg, M. and J. Dec (2003): "Combined effects of fuel-type and engine speed on intake temperature requirements and completeness of bulg-gas reactions for HCCI combustion." SAE Technical Paper 2003-01-3173.

Strandh, P., J. Bengtsson, M. Christensen, R. Johansson, A. Vressner, P. Tunestål, and B. Johansson (2003): "Ion current sensing for HCCI combustion feedback." SAE Technical Paper 2003-01-3216.

Strandh, P., J. Bengtsson, R. Johansson, P. Tunestål., and B. Johansson (2004): "Cycle-to-cycle control of a dual-fuel HCCI engine." SAE Technical Paper 2004-01-0941.

Tanaka, S., F. Ayala, and J. Keck (2003a): "A reduced chemical kinetic model for HCCI combustion of primary reference fuels in a rapid compression machine." *Combustion and Flame*, **133**, pp. 467–481.

Tanaka, S., F. Ayala, J. Keck, and J. Heywood (2003b): "Two-stage ignition in HCCI combustion and HCCI control by fuels and additives." *Combustion and Flame*, **132**, pp. 219–239.

Theobald, M., B. Lequesne, and R. Henry (1994): "Control of engine load via electromagnetic valve actuators." SAE Technical Paper 940816.

Thurns, S. R. (1996): *An introduction to combustion*. McGraw-Hill, Singapore.

Tunestål, P. (2001): *Estimation of the In-Cylinder Air/Fuel Ratio of an Internal Combustion Engine by the Use of Pressure Sensors*. PhD thesis, ISRN LUTMDN/TMVK–1025-SE, Department of Heat and Power Engineering, Lund Institute of Technology, Lund University, Lund, Sweden.

U.S. Environmental Protection Agency (2000): *2007 emission standard for Heavy-Duty Truck and Bus Engines*. http://www.epa.gov.

Verhaegen, M. (1994): "Identification of the deterministic part of MIMO state space models." *Automatica*, **30**, pp. 61–74.

Vibe, I. I. (1970): *Brennverlauf und Kreisprozessrechnung*. VEB Verlag Technik Berlin.

Vressner, A., A. Lundin, P. Tunestål, and J. B. (2003): "Pressure oscillations during rapid HCCI combustion." SAE Technical Paper 2003-01-3217.

Vressner, A., P. Strandh, A. Hultqvist, P. Tunestål, and B. Johansson (2004): "Multiple point ion current diagnostics in an HCCI engine." SAE Technical Paper 2004-01-0934.

Woschni, G. (1967): "A universally applicable equation for instantaneous heat transfer coefficient in the internal combustion engine." SAE Technical Paper 670931.

xPC Target (2004):. http://www.mathworks.com/products/xpctarget/.

Yelvington, P. and W. Green (2003): "Prediction of the knock limit and viable operating range for a homogeneous-charge, compression-ignition (HCCI) engine." SAE Technical Paper 2003-01-1092.

A

Appendix

A.1 Air-fuel ratio, λ

The Air-fuel ratio value is relative to the actual measured condition and the stoichiometric condition.

$$\lambda = \frac{\left(\frac{\dot{m}_{air}}{\dot{m}_{fuel}}\right)_{actual}}{\left(\frac{\dot{m}_{air}}{\dot{m}_{fuel}}\right)_{stoich}}$$

where $\dot{m}_{air}$ is the mass flow to the engine and $\dot{m}_{fuel}$ is the injected fuel to the engine.

A.2 Mean Effective Pressure

The indicated work per cycle is obtained by integrating around the curve in a p-V diagram. There are two different definitions of indicated output:

Gross indicated work per cycle, $IMEP_g$. Work delivered to the piston over the compression and expansion strokes only.

$$IMEP_g = \frac{1}{V_D} \oint_{comp}^{expan} pdV \tag{A.1}$$

where V_D is the displacement volume.

Net indicated work per cycle, $IMEP_n$. Work delivered to the piston over the entire four-stroke cycle, intake, compression, expansion and blow-down stroke.

$$IMEP_{net} = \frac{1}{V_D} \oint_{Intake}^{Blow} pdV \tag{A.2}$$

The Fuel Mean Effective Pressure, FuelMEP, is defined as

$$\text{FuelMEP} = \frac{m_f Q_{\text{LVH}}}{V_d} \tag{A.3}$$

where m_f is the mass of fuel supplied per cycle, Q_{LVH} is the lower heating value for the fuel, and V_d is the displacement volume of the engine.

LUND INSTITUTE OF TECHNOLOGY
Lund University

Department of Automatic Control

ISSN 0280 5316
ISRN LUTFD2/TFRT--1070--SE